PZT Sensor Arrays for Integrated Damage Monitoring in Concrete Structures

ARUN NARAYANAN

A Dissertation Submitted to

Indian Institute of Technology Hyderabad

In Partial Fulfillment of the Requirements for

The Degree of Doctor of Philosophy

भारतीय प्रौद्योगिकी संस्थान हैदराबाद
Indian Institute of Technology Hyderabad

Department of Civil Engineering

May, 2018

Declaration

I declare that this written submission represents my ideas in my own words, and where others' ideas or words have been included, I have adequately cited and referenced the original sources. I also declare that I have adhered to all principles of academic honesty and integrity and have not misrepresented or fabricated or falsified any idea/data/fact/source in my submission. I understand that any violation of the above will be a cause for disciplinary action by the Institute and can also evoke penal action from the sources that have thus not been properly cited, or from whom proper permission has not been taken when needed.

(Signature)

(ARUN NARAYANAN)

(CE11P1001)

Approval Sheet

This thesis entitled PZT Sensor Arrays for Integrated Damage Monitoring in Concrete Structures by (Arun Narayanan)is approved for the degree of Doctor of Philosophy from IIT Hyderabad.
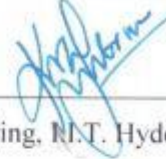
-Prof. Suresh Bhalla (I.I.T. Delhi)-

Examiner 1

-Prof. Manu Santhanam (I.I.T. Madras)-

Examiner 2

-Dr. Anil Agarwal, Department of Civil Engineering, I.I.T. Hyderabad -

Internal Examiner

-Prof. K.V.L. Subramaniam, Department of Civil Engineering, I.I.T. Hyderabad -

Adviser/Guide

-Name and affiliation-

Co-Adviser

-Dr. Saket Asthana, Department of Physics, I.I.T. Hyderabad -

Chairman

Acknowledgements

This is the product of my hard work and perseverance for more than five years. But this wouldn't have become a reality without the seamless encouragement and support of a bunch of people who stood with me during all turmoil and who brought me up from the pit of deep distress on several occasions.

At the outset, I would like to extend my sincere gratitude to my thesis adviser, Prof. K V L Subramaniam. He was the powerful spark who ignited my learning spirit when I started this thesis empty handed. He took the role of a catalyst whenever I was starving with ideas and he sharpened my mind when I became blunt and wandered aimlessly. I have no words to say thanks to him, however he enlightened my research perspective and I can walk into any international research arena with full confidence with the inspiration he instilled on me.

I am indeed thankful to Dr. S Suriya Prakash, Dr. Anil Agarwal and Dr. Viswanath Chinthapenta for giving consent to serve as my Doctoral Committee. They were not passive observers but their positive interventions helped me in giving my thesis a perfect finish. The thesis is the live example of their immaculate observation and objective criticism.

I would like to express my special thanks to Amar, my friend and group mate. He was there with me for all discussions and preparations. Over many cups of tea from Amul, we deliberated a lot on this thesis. He has a powerful way of disagreement and often this has led to petty fights too. However, everything ended over a cup of tea. Thanks my friend for being with me.

I was very lucky to have a vibrant research group, which includes Mehar, Sahith, Jayaprakash, Chiranjeevi, Bhagath and Hanuman for being supportive and encouraging. I am thankful to Mehar, Chiranjeevi and Sahith, they were fully energetic and committed even on holidays.

I would like to thank Pradeep Mishra of Department of electrical engineering for his extended support.

I am happy to say that I have benefitted a lot from Lakshman, Venkatesh, Raju and Gopal, the supporting staff of Structural lab. Their patience and practical knowledge helped me a lot in doing experiments.

Vinay and Koti are two excellent guys who encouraged me when I was down with stress and pressure. Many times I have felt they have an aura of inspiration. Thanks a lot dear friends.

.

Dedicated to

Arya, my life partner, friend and sometimes an inspiring guide. After a hectic day and night, I reach home completely tired and messed up, she welcomed me with her soothing words and smile. That was enough for me to work for another day and night.

Abstract

The broad objective of the work reported here is to provide a fundamental basis for the use of Lead Zirconate Titanate (PZT) patches in damage detection of concrete structures. Damage initiation in concrete structures starts with distributed microcracks, which eventually localize to form cracks. By the time surface manifestation in the form of visible cracking appears there may be significant degradation of the capacity of the structure. Early detection of damage, before visible signs appear on the surface of the structure is essential to initiate early intervention, which can effectively increase the service life of structures. Development of monitoring methodologies involves understanding the underlying phenomena and providing a physical basis for interpreting the observed changes in the parameters which are sensed. PZT is a piezoelectric material, which has a coupled constitutive relationship. In the case of the PZT patches bonded to a concrete structure, any sensing strategy requires developing an understanding of the coupled electromechanical (EM) response of the PZT-concrete system.

The challenges associated with the use of PZT patches for damage monitoring in a concrete substrate include providing the following: a clear understanding of the fundamental response of the PZT patch when bonded to a concrete substrate; interpretation of the coupled response of the PZT patch under load induced damage; and development of an efficient, continuous monitoring methodology to sense a large area of the concrete substrate. Due to a lack of a fundamental basis, the use of PZT patches in concrete structures often involves inferring the measured response using model-based procedures. The work outlined in this thesis addresses the key issue of developing the theoretical basis and providing an experimental validation for PZT-based damage monitoring methodology for concrete structures. A fundamental

understanding of response of the PZT patch when bonded to concrete substrate is developed. The outcome of the work is an integrated local and distributed sensing methodology for concrete structures by combining the electromechanical impedance and stress wave propagation methods using an array of bonded PZT patches.

The work presented in this thesis is focused on using PZT patches bonded to a concrete substrate. A fundamental understanding of the coupled electromechanical behaviour of a PZT patch under an applied electrical excitation in an electrical impedance (EI) measurement, is developed. The influence of the substrate size and its material properties on the frequency dependent EI response of a PZT patch is investigated using concrete substrates of different sizes. The dynamic response of a PZT patch is shown to consist of resonance modes of the PZT patch with superimposed structural response. The resonance behaviour of the PZT patch is shown to be influenced by the material properties of the substrate. The size dependence in the EI response of a PZT patch bonded to a concrete substrate is produced by the dynamic behaviour of the structure. The size of the local zone of the concrete material substrate in the vicinity of the bonded PZT patch, which influences the frequency dependent EI response of the PZT patch is identified. For each resonant mode, a local zone of influence, which is free from the influence of boundary is identified. The dynamic response of the PZT resonant mode is influenced by the elastic material properties and damping within the zone of influence. The structural effects of the concrete substrate produced by the finite size of the specimen are separated from the material effects produced by the material properties and the material damping in the coupled EM response of the bonded PZT patch. The influence of size of the concrete substrate on the coupled impedance response of the PZT is identified with peaks of

structural resonance, which are superimposed on the resonant peaks of the bonded PZT patch

The EI response of the PZT patch when bonded to concrete for detecting load-induced damage from distributed microcrack to localized cracks within the zone of influence of the PZT patch is investigated. Using an approach which combines an understanding of the coupled EM constitutive behaviour of PZT with experimental validation, a methodology is developed to decouple the effects of stress and damage in the substrate on the coupled EM response of a PZT patch. The features in the EI signature of a bonded PZT patch associated with stress and damage are identified. An increasing level of distributed damage in the concrete substrate produces a decrease in the magnitude and the frequency of the resonant peak of the bonded PZT patch. The substrate stress produces a counter acting effect in the EI spectrum of the bonded PZT patch. A measurement procedure for the use of bonded PZT patches for continuous monitoring of stress-induced damage in the form of distributed microcracks in a structure under loading is developed.

An integrated methodology for damage monitoring in concrete structures is developed by combining the EI method for local sensing and the stress wave propagation-based method in a distributed sensing mode. An array of surface mounted PZT sensors are deployed on a concrete beam. The EI measurements from individual PZT sensors are used for detecting damage within the local zone of influence. PZT sensor pairs are used as actuators and sensors for distributed monitoring using stress wave propagation. A stress-induced crack is introduced in a controlled manner. It is detected very accurately from the full-field displacement measurement obtained using digital image correlation. The crack opening profile in concrete produced by the fracture is established from the surface displacement measurements. From the measurements of bonded PZTs, the localized crack is detected in the zone of influence by EI.

The change in compliance of the material medium due to a localized crack is small and it is reflected in the smaller change in the measured EI when compared to distributed damage. Stress wave based measurements sensitively detect crack openings on the order of 10µm. The material discontinuity produced by a closed crack, after removal of the stress is also detected. A damage matrix is developed for stress wave based method which is independent of transmission path to assess the severity of damage produced by the crack in a concrete structure.

Nomenclature

l	Length of the PZT
b	Width of the PZT
t	Thickness of the PZT
S	Strain vector
T	Stress vector
C_E	Elasticity matrix
d^T	Piezoelectric coefficients
E	Applied electric field vector
D	Electric displacement vector
ε_T	Dielectric permittivity
e	Relative permittivity
ν	Poisson's ratio of the PZT
ρ	Density of the PZT
δ	Dielectric loss factor of the PZT
ζ	Damping ratio of the PZT
Q_m	Mechanical quality factor
Y	Admittance
$\bar{Y}$	Complex admittance of the PZT
Z_A	Mechanical impedance of the PZT
Z_S	Mechanical impedance of the substrate
$\bar{f}$	Centroidal frequency of the resonance peak
$\bar{f}_c$	Centroidal frequency at Loading or Unloading states
$\bar{f}_0$	Base line centroidal frequency
Y_{Ci}	Baseline value of conductance
Y_{CB}	Value of conductance at Loading or Unloading states
Y_C	conductance signature

Y_{CN} *Normalized conductance signature*

Y'_{CN} *Centroid of the normalized conductance signature*

I *Current*

V *Applied voltage*

I_Z *Current density along the poling direction of the PZT*

$\overline{C_E}$ *Complex elasticity matrix*

$\overline{\varepsilon_T}$ *Complex dielectric permittivity*

j $\sqrt{-1}$

η_s *Isotropic loss factor of the PZT*

η *Isotropic loss factor of the concrete cube*

$(TOF)_0$ *TOF at zero CMOD level*

$(TOF)_d$ *TOF at different CMOD level*

r_s *Received signal*

a_s *Actuating signal*

l_{ea} *Signal losses due to epoxy at concrete-beam interfaces for actuator*

l_{es} *Signal losses due to epoxy at concrete-beam interfaces for sensor*

l_{sp} *Signal losses due to path*

$*$ *Convolution operator*

$r_s(f)_0$ *Sensor signal at zero CMOD level*

$r_s(f)_d$ *Sensor signal at different CMOD levels*

L_d *Signal losses due to crack*

x_i *Conductance at zero CMOD level*

y_i *Conductance at different CMOD levels*

N *Total number of frequencies*

Contents

List of Figures

xviii

List of Tables

Chapter 1

Introduction

1.1   Motivation and introduction

Assessment of the integrity of a structure and its constituent parts requires reliable non-destructive evaluation (NDE) procedures and continuous monitoring of structural parameters to determine the intensity and location of the damage. This involves sensors, data acquisition and signal processing tools. The performance characteristics of the structure depend upon the level of damage produced by the combination of load-induced stress and internal stress. Often the damage, particularly in the incipient stages is not directly visible and by the time signs of distress appear on the surface of the structure, significant damage would have accrued in the structure. Aging and deterioration of the existing infrastructure leads to a high cost of maintenance if corrective measures and remedial action are initiated when visible signs of distress appear on the surface of the structure. Continuous monitoring and assessment of structural performance assures an as-needed maintenance practice reducing the need for expensive scheduled maintenance.

Typically, methods for damage detection have relied on applying a low frequency excitation to a structure and observing its dynamic characteristics. Major drawbacks of the global method of damage detection are that it works

well only if the damage is substantial, and the exact location and extent of damage are hard to infer. Localized damage is hard to detect with a level of certainty by the global method. The detection of damage using the global schemes, which rely on inferring damage from the measured response of the entire structure, requires accurate models which represent the dynamic response of the structure. Developing accurate representation of the structural response is challenging for large civil structures. The model uncertainty coupled with the loss in sensitivity to local effects in a global system parameter have limited the application of the vibration-based global methods in concrete structures.

In concrete structures, damage can occur due to load or environmental effects. The damage in concrete is identified with cracking and it can take a localized form or it can result in distributed cracking. Tensile cracking in concrete is very localized and occurs due to several factors such as overloads and internal stress development due to restrained shrinkage and thermal effects. Damage due to environmental distress on concrete associated with alkali-silica reaction or freeze-thaw degradation takes the form of distributed patterns of cracks. Damage in concrete initiates in the form of microcracks. The microcracks coalesce to produce cracks. Often, by the time a surface manifestation of damage is visible, there is a substantial loss in capacity. Therefore, for concrete structures effective monitoring methods, which can help identify the location and extent of damage are essential for initiating timely repairs.

Damage monitoring of civil structures relies on sensing, which can be done on a local or a distributed basis. Local monitoring provides information about the state of the material in the immediate vicinity of the sensor. Distributed sensing provides information about the presence and extent of damage in a structure or a part as a whole. Successful application of the distributed methodology requires substantial instrumentation, which makes it expensive.

Effective implementation of large scale monitoring requires inexpensive sensors, which can be used for combined local and distributed sensing. Low-cost sensors, which can provide integrated local and distributed sensing would enable continuous monitoring of the health of the structure.

The use of Lead Zirconate Titanate (PZT) patches is becoming popular in health monitoring of structures because of their low cost and the potential for integrated monitoring. PZT is a piezoelectric material which has the ability to produce surface charges when strained and strain when electrically excited. The electrical measurements from a PZT patch have been used to infer about the local stiffness of the structure. Changes in the electrical impedance (EI) of the PZT due to the elastic restraint by the surrounding medium provides the basis for the electrical impedance-based measurements. Successful applications of PZT sensors have been limited to light metallic and composite structures, primarily in aerospace applications. Vibration based techniques, high frequency wave based and piezoelectric based electro mechanical impedance methods have been developed for detecting microcracks in metallic and thin structural elements. PZT patches can be used as emitters for sending stress waves, receivers for collecting stress waves, monitoring of the stiffness of the surrounding medium in the single electromechanical impedance mode and as vibration sensors. Therefore, PZT patches provide the potential for developing local and distributed sensing capability.

There are few studies available on the application of surface mounted piezoelectric patches for monitoring of concrete structures. The changes in the EI response of the surface mounted PZT patches bonded to concrete are not fully understood. Understanding of the coupled response of the PZT provides the basis for establishing an EI-based monitoring methodology. The coupled dynamic response of a PZT patch required for interpreting the measured electrical response is yet not fully studied. The effects of geometry, substrate

3

size and material properties on the coupled impedance behaviour of the PZT patch bonded to a concrete structure are still not understood. Most concrete structures support substantial load in the form of self-weight and therefore, the substrate stress is present. Further damage is induced by the substrate stress and there is a change in the stress level after damage. The influence of substrate stress on the EI response of a PZT has not been studied. Wave propagation methods typically rely on using ultrasonic bulk or guided waves for evaluating the structure. The effective utilization of the bonded PZT patches, which are bonded as an array, includes using them for stress-wave based monitoring. Changes in the characteristics of the stress waves, which are usually detected using a through transmission or a surface reflection measurement, are related to the elastic material properties of the material medium. Most of the wave-based techniques are not amenable for continuous monitoring of the structure and will be tedious if the area of examination is inaccessible and the accessories involved in the above methods are more.

In this thesis an integrated local and distributed sensing methodology for concrete structures by combining the EI and stress wave propagation methods using an array of bonded PZT patches is developed. The research presented here deals with developing the fundamental basis, which is required for interpretation of the EI and stress wave propagation measurements are developed through a combined experimental and numerical approach. A study of the influence of the material properties and substrate size on the EI response of a PZT patch bonded to a concrete substrate is conducted. The learnings from this study translate to identifying the local zone, identified as the zone of influence, monitored by the PZT patch. The influence of the change in the substrate compliance induced by stress-induced damage in concrete on the measured EI of a PZT patch bonded to concrete substrate within the zone of influence is determined. The influence of substrate stress on the measured EI

4

response of a bonded PZT patch is established from a physical understanding of the coupled electromechanical constitutive response of the PZT material. A theoretical framework is developed to decouple the effect of stress and damage from the EI response of the bonded PZT. Finally, the concept of an array of PZT sensors for continuous monitoring of concrete structures, which combines local monitoring with distributed sensing, is developed. Surface mounted PZT patches are used for continuous local monitoring of local material properties in the immediate vicinity of the patch. Information from the multiple PZT patches distributed over a structural element is used for assessing uniformity in property. The array of bonded PZT patches are used as actuator and receiver pairs for monitoring using stress-wave propagation. A frequency domain based damage index which is independent of wave transmission paths is developed to interpret the stress wave data collected from different actuator and receiver pairs of PZT.

1.2   Objectives and scope of work

The objective of the work is to develop a fundamental basis for combined local and distributed monitoring of damage in concrete structures using a surface mounted PZT sensor array. Specific objectives, which contribute to an understanding of the underlying effects on the measured response of a PZT patch in EI measurements and the effective implementation of the stress-wave propagation technique include:

(a) To develop an understanding of the dynamic response of a PZT patch bonded to a concrete substrate and the influence of the local material properties and the substrate size on the mechanical impedance to the motion of the PZT;

(b) To determine the influence of damage and substrate stress on the material compliance and its impact on the coupled electromechanical response of a bonded PZT patch in an EI measurement;

5

(c) To develop a methodology for accurate measurement of stress wave attenuation produced by a physical discontinuity in the medium introduced by a stress-induced crack;

(d) To develop the concept of using an array of surface mounted sensors for global and local monitoring of concrete structure using combined EI and wave propagation methods.

1.3   Outline of the thesis

A brief description of the work presented in different chapters is given below

Chapter 2 gives the review of literature related to the presented research, including experimental methods and theoretical modeling used to study the damage assessment in concrete structures using EI method and wave propagation method (PZT in actuator/receiver (AR) pairs) using surface mounted PZT patches.

Chapter 3 emphases on the influence of substrate size on the coupled dynamic electromechanical response of a PZT (Lead Zirconate Titanate) patch bonded to a concrete substrate. For each resonant mode of the bonded PZT patch a finite zone of influence, where there is an influence of the boundary on the resonant behaviour of the bonded PZT patch, is identified. For a substrate size smaller than the zone of influence of a resonant mode of the PZT patch, the coupled dynamic response of the PZT patch would include the influence of the geometry of the specimen given by the dynamic structural response.

Chapter 4 presents the influence of damage and substrate stress on the electromechanical impedance of the PZT bonded to concrete structures with in the zone of influence of the PZT. The effect of stress and microcrack damage is decoupled using the normalized conductance signatures of the bonded PZT. It is identified that, for distributed microcracking, the counteracting influences of increasing level of damage and increasing stress on the resonant peak result in no shift in frequency for measurements under applied load.

Chapter 5 presents the development of a sensing methodology which combines EI, wave propagation methodologies for detecting damage in concrete. Surface mounted PZT patches are used for continuous local monitoring of concrete and obtaining the information related to damage in the vicinity of the patch. Additionally, the PZT sensor array is used for monitoring damage in the actuator-receiver (AR) mode. A new damage index known as attenuation factor is introduced for the wave propagation technique. The attenuation factor is shown to be an effective damage index for detecting the severity of discontinuity produced by a crack.

Chapter 6 presents the major findings and future directions of research which arise from this study.

Chapter 2

Literature Review and Theoretical Background

2.1   Introduction

Piezoelectric elements are commonly used in developing smart structural systems. Piezoelectric effect refers to the property when a poled piezoelectric ceramic is mechanically strained it becomes electrically polarized, producing an electric charge on the surface of the material. When an alternating current is applied to a Lead Zirconate Titanate (PZT) patch, it produces mechanical vibration of the PZT. When bonded to a substrate, the vibratory motion of the PZT patch results in stress waves in the material. The resistance to the free motion of the PZT patch provided by the substrate, which is referred to as the mechanical impedance of the substrate, has an influence on the vibratory signature of the PZT patch. This also influences the electrical impedance of the PZT patch and forms the basis of the electrical impedance-based measurements. Impedance-based measurements of a bonded PZT patch to a substrate provide an effective way for monitoring changes in the material stiffness (or compliance). The major advantage of piezoelectric materials is that the coupled electromechanical response of a PZT patch allows it to sense

changes in stress in the substrate. This forms the basis for using piezo elements as actuator and receiver pairs in stress wave transmission based measurements. The use of PZT patches in electrical impedance (EI) based measurements and through transmission-based measurements in concrete is reviewed in this section. The development of the electrical impedance (EI) technique and the significant contributions of researchers in providing a theoretical basis for relating the impedance measurements with the properties of the PZT material and the substrate are summarized. The progression in through transmission based measurements using surface bonded ultrasonic transducers or PZT patches to assess the damage in concrete structures is reviewed.

2.2   EI-based Measurements

2.2.1   Theoretical formulation

The coupled electromechanical constitutive equation describes the behaviour of the piezoelectric material. The relationships between mechanical strain and mechanical, electrical charge and electrical potential and their inter-relations. The constitutive equations describing the piezoelectric property consider the total strain in the transducer as a sum of mechanical strain induced by the mechanical stress and the actuation strain caused by the applied electric voltage. The constitutive relation for a PZT is given as [1, 2].

$$S_k = \bar{s}^E{}_{km}T_m +\ d_{jk}E_j \tag{2.1}$$

$$D_i = \bar{\varepsilon}^T{}_{ij}E_j + d_{im}T_m \tag{2.2}$$

where vector D_i of size (3 × 1) is the electric displacement (Coulomb/m²), S_k is the strain vector (6 × 1), E_j is the applied electric field vector (3 × 1) (Volt/m) and T_m is the stress vector (6 × 1) (N/m²), $\bar{s}^E{}_{km}$ is complex dielectric constant of size (3 × 3) (Farad/m),. $\bar{s}^E{}_{km}$ is complex compliance of size (6 × 6) (m²/N), the piezoelectric coefficient d_{jk} (6 × 3) (m/Volt) is the strain per unit field at constant stress and d_{im} (3 x 6) (Coulomb/N) is the electric displacement per unit stress at constant electric field.

For 1-D motion, which considers only uniaxial strain (along one in-plane direction) and electric potential applied in the perpendicular direction the constitutive relations can be simplified as,

$$S_2 = \bar{s}^E{}_{22} T_2 + d_{32} E \tag{2.3}$$

$$D_3 = \bar{\varepsilon}^T{}_{33} E + d_{32} T_2 \tag{2.4}$$

Electrical impedance is a measure of opposition to alternating current for a unit applied electrical potential. When a PZT patch is excited with an alternating current of variable frequency ranging between 10 kHz and 500 kHz, there is a relative phase change between current and voltage and the extracted electrical impedance will be complex in nature. Typical admittance (inverse of impedance) and conductance responses (real part of admittance) of the free PZT of size 20mm x 20mm x 1mm are shown in Fig. 2.1. The distinct resonance modes of the PZT patch can be identified in the measured frequency responses.

(a)   (b)
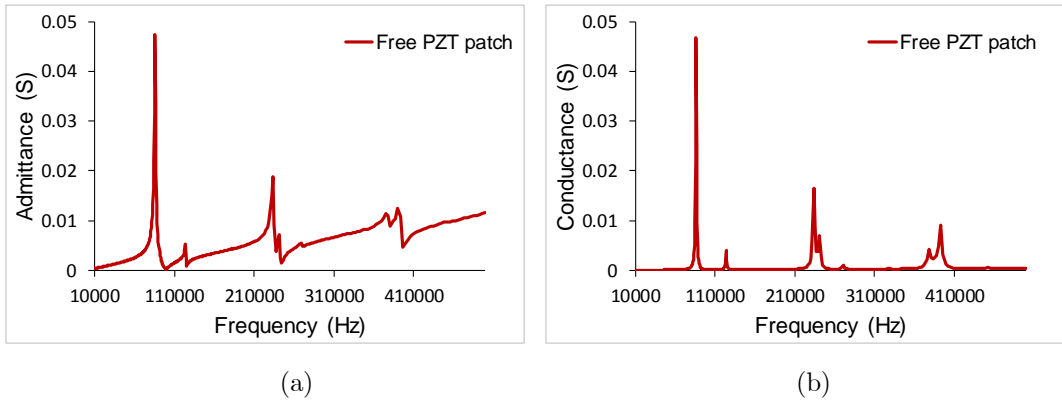
Figure 2.1: Free response of PZT (a) admittance (b) conductance

Mechanical impedance (inverse of compliance) is defined as the ratio of applied force to the velocity of motion. For an elastic substrate, the driving point impedance, which is the dynamic point response of medium, is dependent on elastic properties of the material. The driving point impedance of the substrate medium influences the mechanical response of a PZT patch bonded to the

substrate. The electrical impedance signature of a PZT bonded to a substrate, depends upon the effective mechanical impedance of the PZT patch and the mechanical substrate. Monitoring the electrical impedance of a bonded PZT patch therefore provides information about the substrate.

The first systematic attempt to derive the electrical impedance of the PZT which is mechanically connected to a structure was made by Liang et al. [3]. The effective mechanical impedance was derived considering the model shown in Fig. 2.2, which idealizes the PZT patch as 1-D element coupled to a structure which is idealized as a single degree of freedom system. The motion is restricted in one direction (only in y-direction in the coordinates shown in Fig. 2.2). In this arrangement, for an applied input potential, the PZT patch functions like an actuator moving along its axis. The motion of the interface subjected to continuity conditions is governed by the combined mechanical impedance of the structure and the PZT. The mechanical impedance of the PZT actuator was derived in terms of the elastic properties of the PZT material and the dimensions of the patch. To derive the admittance of the coupled system, one of the constitutive relation of PZT patch and structure was coupled with their equilibrium, compatibility conditions and the equation of motion. The formulation for total admittance of the system was derived in terms of the mechanical impedances of the PZT patch and mechanical impedance of structure.

The electrical impedance of the PZT bonded to a structure was obtained as function of the constitutive parameters of the PZT material and the mechanical impedances of the PZT and structure as

$$\therefore \ \bar{Y} = \frac{i\omega w l}{h}\left(\frac{Z_A d_{32}^2 \bar{Y}_{22}^E}{(Z_A + Z)}\frac{tan(kl)}{kl} + \bar{\varepsilon}^T_{\ 33} - d_{32}^2 E\bar{Y}_{22}^E\right) \tag{2.5}$$

where Z is the impedance of the structure and Z_A is the impedance of the PZT actuator, where $\bar{Y}$ is the complex admittance of the PZT. w, l and h are the

width, half-length and the thickness of the PZT patch, respectively. E is the applied electric field. $\bar{\varepsilon}^{T}_{33}$ is complex dielectric constant at constant stress, $\bar{\varepsilon}^{T}_{33} = \varepsilon^{T}_{33}(1 - \delta i)$, δ=dielectric loss factor. $\bar{Y}^{E}_{22}$ is the complex Young's modulus of PZT at constant electric field, which is given as $\bar{Y}^{E}_{22} = Y^{E}_{22}(1 + i\eta)$, where Y^{E}_{22} is the Young's modulus of the PZT and η is the mechanical loss factor. d_{32} is the piezoelectric strain constant, k is the wave number which is calculated by $k = \omega\sqrt{\frac{\rho_p}{\bar{Y}^{E}_{22}}}$, ρ_p is the density of the PZT material, ω is the circular frequency of the applied electric field for actuation and i is $\sqrt{-1}$.

$$\therefore Z_A = \frac{K_A(1+i\eta)}{i\omega}\frac{kl}{tan(kl)} \tag{2.6}$$

where K_A is the static stiffness of PZT.

Structural mechanical impedance
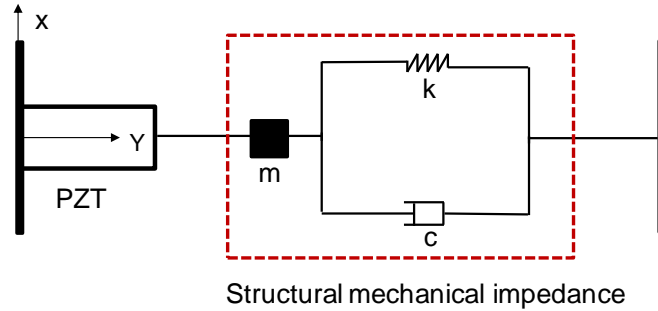
Figure 2.2: Schematic representation of the idealization for obtaining the impedance of the PZT coupled with a structure [3]

Zhou et al. [4] extended the Liang's [3] one-dimensional (1D) impedance model to two-dimensional (2D) by considering PZT in plane stress condition. From planar forces and velocities in two directions, the direct and cross structural mechanical impedance elements were derived (Fig. 2.3) by applying boundary conditions and equilibrium conditions along two directions, the coupled admittance of the PZT is calculated. The coupled admittance equation of the PZT consisted of four mechanical impedance parameters. The model was

shown to be more accurate than one-dimensional (1D) impedance model and experimentally verified for simply supported thin plate.
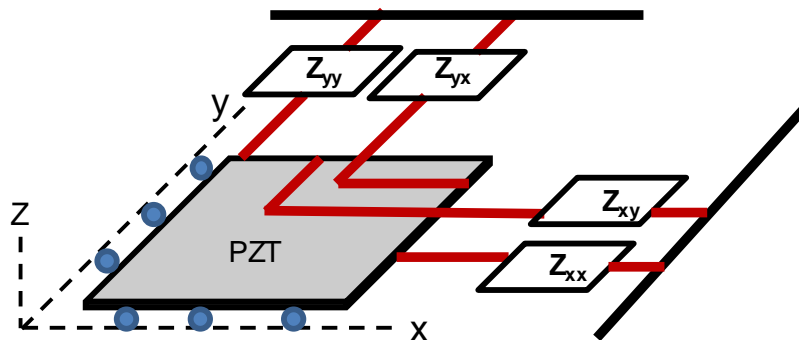
Figure 2.3: Schematic representation of the idealization for two dimensional PZT-Structure interaction [4]

Giurgiutiu and Rogers [5] derived an electro mechanical impedance model for thin plate like structures based on one-dimensional (1D) impedance model. Structural response of the host structure was included as structural dynamic stiffness in the formulation. Structural dynamic stiffness of the structure was calculated by replacing PZT response as force and moments acting on the host structure. A numerical model of a composite beam with simulated damage were used show the change in point -wise structural impedance of pristine and damaged structure.

One-dimensional (1D) impedance model which was composed of one spring mass damper idealization (1DOF) further updated to two degrees of freedom (2 DOF) impedance model by introducing one more spring mass damper for bonding layer as shown in the Fig. 2.5 [6]. The coupled electrical admittance for the bonded PZT was derived by applying equilibrium at the interface between the PZT patch and bonding layer and the interface between the bonding layer and host structure. A coefficient 'α' introduced as a multiplier to the structural mechanical impedance in the coupled impedance model which was a function of dynamic stiffness of the structure (k_s) and bonding layer (k_b)

, $\alpha = \left[\dfrac{1}{(1+\frac{k_s}{k_b})}\right]$. The effect of bonding layer on coupled electrical admittance was numerically studied using 'α' and shown that with decrease in bonding quality, a PZT-driven system would show decrease in resonant frequencies.

The 1-D approximation of the PZT is suited for describing the wave response in a PZT bar where the motion of the PZT patch is unconstrained in the in-plane transverse direction. Therefore, it is not suited for describing the motion of a square or a rectangular patch, where the in-plane motions along two perpendicular in-plane directions of the patch and the electric field in a direction perpendicular must be considered. The mechanical impedance of the PZT actuator was derived assuming only in-plane behaviour of the PZT subjected to spatially uniform and harmonic electric field and the symmetry conditions which affect the motion of the edges of the PZT [7]. This is shown graphically in Fig. 2.4. The effective 1D model is based on a 2-dimensional impedance of the PZT patch replaced the concept of cross impedance model by "effective impedance". The two dimensional deformation of PZT is included in the model as the ratio of change in surface area (δA) to perimeter (P_o) which is a one dimensional parameter. The admittance of the bonded PZT patch was derived by updating PZT constitutive equations with mechanical equilibrium equations which is calculated by applying boundary conditions and force equilibrium conditions. The effective mechanical impedance of structure was extracted from the admittance signature of a PZT patch bonded to the surface of the structure and used as a damage indicator of the structure. The results of the proposed model were validated using finite element analysis. The effective 1-D motion considers in-plane motion of the PZT subjected to an electric potential in a plane perpendicular to the plane of motion. The out-of-plane motion and any influence of out-plane motion on the in-plane behaviour is ignored in this model. The in-plane direction is considered to be a plane of

14

isotropy. It does however provide a realistic representation of the polarization response of the PZT which is a square. Further, considering symmetry, displacements at the active boundaries of $\frac{1}{4}$ of the patch (the boundaries along the nodal axes are "inactive" boundaries) an effective 1-D formulation was developed considering in terms of the ratio of the change in the area to perimeter of the PZT given as,

$$u_{\text{eff}} = \frac{\delta A}{P_o} = \frac{u_{1o}l + u_{2o}l + u_{1o}u_{2o}}{2l} \approx \frac{u_{1o} + u_{2o}}{2} \tag{2.7}$$

The effective mechanical impedance of the PZT in terms of the effective 1-D displacement parameter (u_{eff}) was derived as,

$$Z_{a,\text{eff}} = \frac{2\kappa lh\overline{Y^E}}{i\omega(\tan \kappa l)(1-\nu)} \tag{2.8}$$

The admittance $\overline{Y}$, which is the ratio of current to voltage, of the PZT bonded to the elastic substrate is derived as,

$$\overline{Y} = \frac{4\omega i l^2}{h}\left[\bar{\varepsilon}^T{}_{33} - \frac{2d_{31}^2\overline{Y^E}}{(1-\nu)} + \frac{2d_{31}^2\overline{Y^E}Z_{a,eff}}{(1-\nu)(Z_{s,eff}+Z_{a,eff})}\left(\frac{\tan \kappa l}{\kappa l}\right)\right] \tag{2.9}$$

Where $Z_{a,\text{eff}}$ and $Z_{s,eff}$ are effective mechanical impedance of the PZT and the substrate, respectively refers to the of the substrate to effective 1-D motion. ν is the Poisson's ratio of the piezoelectric material. d_{31} is the piezoelectric strain constant. $\overline{Y^E}$ is the complex Young's modulus of PZT at constant electric field, which is given as $\overline{Y^E} = Y^E(1 + i\eta)$, where Y^E is the Young's modulus of the PZT and η is the mechanical loss factor. k is the wave number which is calculated by $k = \omega\sqrt{\frac{\rho_p(1-\nu^2)}{Y^E}}$, ρ_p is the density of the PZT material
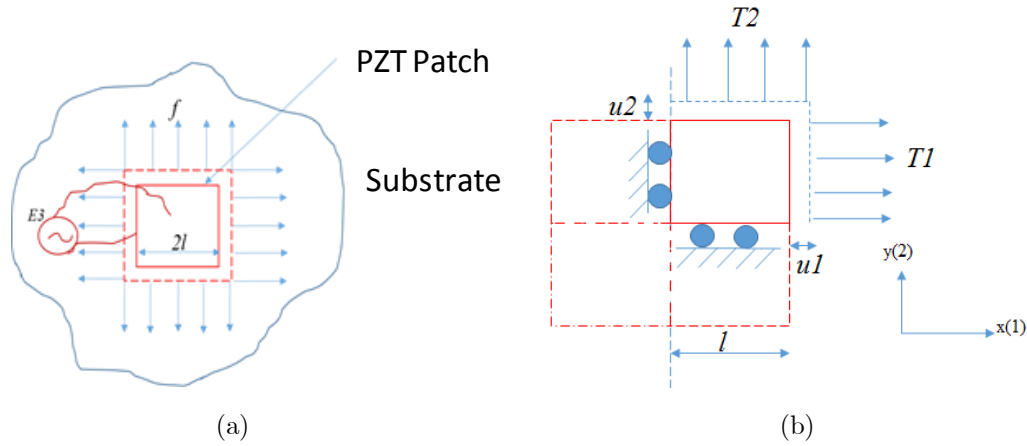
Figure 2.4: (a) PZT patch bonded to a structure (b) Stresses and displacements on patch [7]

The effective 1-D formulation was used to study the damage in structures by idealizing the mechanical impedance of the structure using spring (k), viscous damper (C) and mass (m) elements. The change in mechanical impedance due to material damage changes the spring constant and the damping. The frequency of the resonance mode mainly depends on the spring and mass element and the admittance of resonance mode mainly depends on the damper system. So from the impedance signature the value of k, C and m can be extracted. Comparing the value of k, C and m the structure can be analyzed. The extended effective impedance model of PZT-structure interaction by incorporating shear lag effect in to the model [8]. The effect of bonding layers on PZT- structure interaction was studied. Based on the study, the PZT patch should be bonded to the structure using an adhesive of high shear modulus and smallest practicable thickness.

16
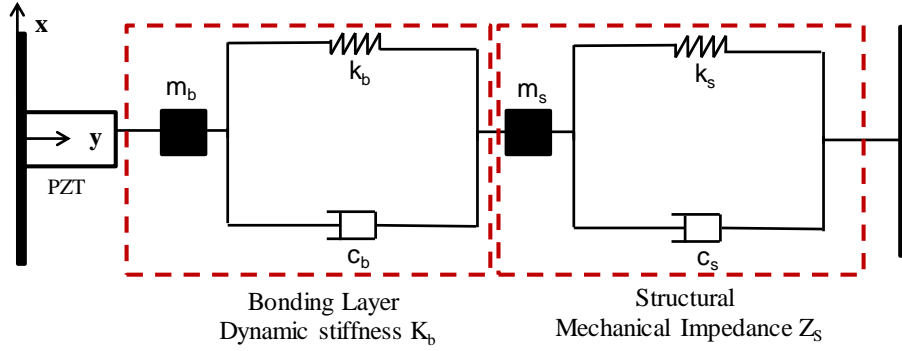
Figure 2.5: Analytical model for PZT-Structure interaction via bonding layer [6]

A 1D and a 2D generic impedance-based model for predicting the electromechanical impedance of one dimensional and two-dimensional structure-piezoceramic interacting systems was developed [9]. The vibration of a PZT patch is first analyzed for different boundary conditions with assumption that the dimension of the host structure is much larger than that of the PZT patch and PZT patches are not close to the boundary. The effect of the host structure is then represented by its force impedance, which is obtained by a semi analytical method. EM impedance of a 2D system was also derived using cross impedance elements for all four edges. The generic model was experimentally verified.

Annamdas and Soh [10] proposed a three dimensional (3D) semi analytical generic electromechanical impedance model (no constraints on thickness, shape, or size on the PZT) including both longitudinal (thickness) and extensional actuations of the PZT. A 3D PZT-Structure interaction model is derived using generalized stress-strain relationships and applying boundary conditions and solved by numerical methods. The impedance of the host structure was calculated as sum of direct and cross impedances which were calculated from normal and shear stresses of the PZT upon actuation. The model was experimentally validated using PZT surface bonded on an aluminum plate.

A simplified 1-dimensional impedance model including shear lag effect into electromechanical admittance was formulated [11]. The formulation is then extended to an effective 1D model based on a 2-dimensional impedance of the PZT. The extracted structural impedance from the measured conductance (real part of admittance) and susceptance (imaginary part of admittance) signature using new formulation is shown to be more accurate.

A new impedance measurement technique based on a dual PZT transducer is developed theoretically and numerically verified [12]. The new technique utilizes two separate but concentric PZT segments within a single dual PZT for independent excitation and sensing (Fig. 2.6). It is shown that the dual PZT measures the EM impedance signals from massive structures with a high signal-to-noise ratio (SNR) and good repeatability.
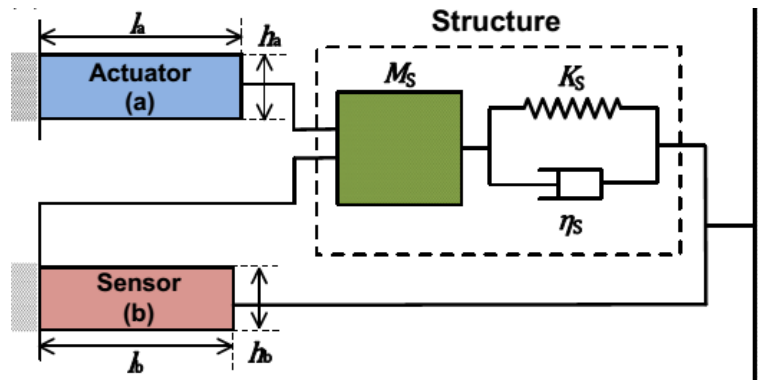
Figure 2.6: Schematic representation of dual PZT impedance model [12]

Wang et al. [13] developed 3D electromechanical (EM) impedance model based on the 2D model and by using concept of effective mechanical impedance. The structural mechanical impedance was extracted from the measured EM admittance signatures. Changes in the mechanical impedance of the host structure was shown to be more sensitive to changes in the compressive strength of the concrete cube than changes based on EM impedance. Wang et al. [14] further extended the concept of effective mechanical impedance for developing 3D EM impedance model for dual PZT transducer and validated

experimentally by embedding dual-PZT transducers in cement cubes and also by finite element modelling. 3D effective impedance model is shown to be more accurate when compared with 1D and 2D and more close to actual circumstances.

A 1D EM impedance model was developed and experimentally verified to study the effect of axial load on EI signature of bonded PZT on bar like structures [15]. The model used 1D beam dynamic governing equation for longitudinal vibration and nonlinear piezoelectric constitutive equations for deriving the coupled response of the PZT. It is concluded from the study that the resonance peak shifts towards lower frequencies as the applied stress varies from tension to compression and the stress-induced conductance resonance shifts associated to flexural vibrational modes are independent of the excitation frequency.

2.2.2   Application of EM impedance-based technique

Ayres et al. [16] studied the application of EM impedance technique to monitor the damage using the 1-D model proposed by Liang et al. [3]. A quarter scale deck truss bridge joint was used to study the damage due to loose bolts. The electrical admittance of PZT placed at different location in the truss member was compared with the corresponding admittance pristine state. A vertical shift in the admittance measurements was observed for small damage (loosening of two bolts) while distinct change in the admittance measurements in the form of distinct peak and valleys was observed for larger damage (loosening of fourteen bolts). The level of damage was quantified using root mean squared error (RMSE) of admittance. The localized damage was found to be sensitively detected by the application of high frequency impedance measurements.

EM impedance technique was used to monitor the crack growth in spot welded lap-shear structural joint specimen under fatigue load [17]. Root mean square

19

(RMS) change of real part of impedance were used as damage index. Change in stiffness of the specimen due to fatigue loading is shown to be correlated with the change in the RMS of the real part of impedance of the PZT.

Park et al. [18] extended application of EM impedance technique of structural health monitoring using the 1-D model proposed by Liang et al. [3] to real time damage detection of the masonry wall reinforced externally with fiber reinforced polymer sheets (composite reinforced wall). The wall was loaded diagonally and the joint failure between the cement blocks of the wall was monitored. The influence of boundary condition and temperature effect on the measured impedance was also investigated. The capability and robustness of technology was demonstrated by consistent repetition of tests. The influence of dielectric constant which is sensitive to temperature changes on the imaginary part of the impedance makes analysis based on imaginary part of the impedance unreliable. The real part of impedance was shown to be more reliable for monitoring damage.

Soh et al. [19] tested the impedance approach during the destructive load test of a prototype scaled laboratory sized reinforced concrete bridge. The conductance signatures recoded from the PZTs located near the load-induced crack showed higher change compare to PZTs located farther away from the crack (Fig. 2.7). Root mean square deviation (RMSD) was used as damage index. Unstable and non-repetitive readings were shown to be a result of weakening bond between PZT and concrete beam or PZT break down.

(a)   (b)
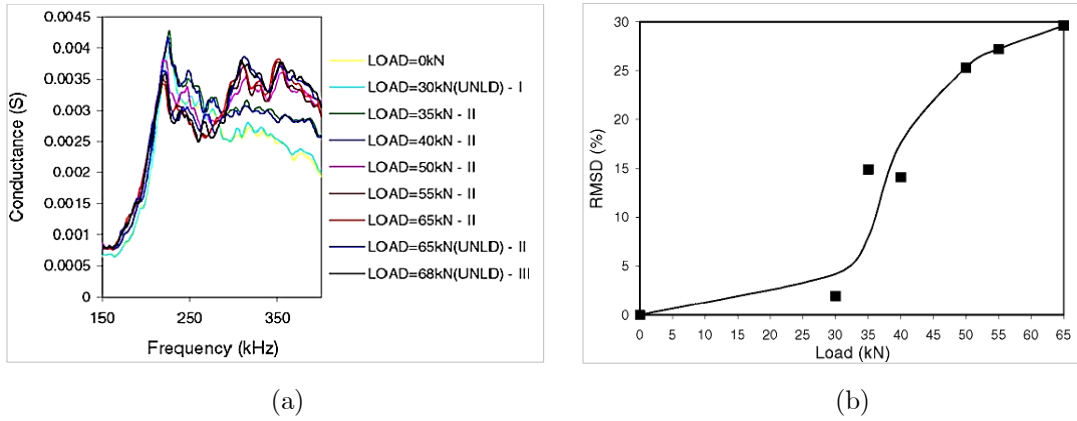
Figure 2.7: (a) Conductance signatures of PZT patch at various load levels (b)
Variation of RMSD (%) with load [19]

Ong et al. [20] numerically investigated the effect of axial load on EM
admittance signature of the bonded PZT. It was shown that the shift in
resonance frequency of the bonded PZT is linearly related to the magnitude of
applied load.

Tseng and Naidu [21] investigated the effect of frequency range on the
detection of incipient damage in metallic structures using the EM impedance
technique. PZT patch was bonded to the upper surface of a thin aluminum
strip specimen and damage was simulated on the strip by drilling 5 mm
diameter holes sequentially, with a spacing of 50 mm. Impedance signatures
were taken at two frequency ranges of 100–150kHz and 400–450 kHz after
drilling each hole. Signature acquired for the undamaged and damaged states
were evaluated using RMSD, mean absolute percentage deviation (MAPD),
covariance (Cov) and correlation coefficient (CC). Based on the study, higher
frequency ranges are found to be more sensitive in characterizing damage. The
RMSD and MAPD indices were found to be more suitable for characterizing
growth and the location of damage, whereas the increase in damage size at a
fixed location was more effectively monitored by covariance and CC.

A new method for damage diagnosis was introduced using mechanical
impedance extracted from the electro-mechanical admittance signatures of

21

piezoelectric-ceramic (PZT) patches surface bonded to the structure using the EM impedance technique [22]. Damage was induced on a laboratory sized RC (reinforced concrete) portal frame mounted with PZT patches by different levels of base vibrations. The passive (parameters depends on the PZT patch) and active (parameters depends on the structure) components are separated from 1D coupled EM equation using coupled experimental EM response. Real and imaginary part of the active component extracted were used for damage evaluation. A damage index based on extracted complex mechanical impedance was also used for assessing damage. It is shown that damage index based on new analysis technique can be used for sensitive evaluation of damage.

The effectiveness of surface mounted PZTs to monitor damage progression in concrete using EM impedance technique was studied experimentally and numerically [23]. Cracks were simulated on a laboratory sized specimen of 500 mm in length by machine cut of 5 mm in depth with a spacing of 50 mm. Calculated RMSD index from the conductance measurements was correlated to the crack location in order to locate the crack. The results obtained were also verified numerically.

Soh and Bhalla [24] examined the damage progression in concrete structure using EM impedance technique introducing new damage index based on equivalent mechanical parameters of the substrate. A concrete cube of size 150mm surface mounted with PZT patch tested under compressive load and EM signatures were taken at regular load intervals. The coupled EM signatures at no load state were used to extract mechanical impedance of the cube using effective 1D formulation and fitted with a parallel spring-damper (k, c) system in small frequency range (60-100 kHz). The k, c parameters extracted at different load levels were used to assess the damage in concrete. It is concluded that proposed damage index based on mechanical impedance

was shown to be better for characterizing damage (incipient to severe) when compared to the conventional statistical methods.

Park et al. [25] developed a procedure for damage detection using root mean square deviation (RMSD) in the impedance signatures of the PZT patches. Two frequency ranges were selected, one is 1 to 5 MHz (high frequency range) for the thickness modes of the PZT patch, and the other is 20 to 500 kHz (low frequency range) for the lateral modes of the PZT patch. It was shown the lateral mode impedance has larger sensing area (more than 30 cm) as compared with the cases which use the thickness mode-impedance in the PZT patch for progressive surface damage in a concrete beam.

Lim et al. [26] used EM admittance response, initially for structural identification then identified parameters were used for damage characterization using 1D and effective 1D impedance models. The real and imaginary part of measured extracted mechanical impedance for a narrow frequency range from surface mounted PZTs were compared with the behaviour of different combinations of spring-mass-damper (k, m, c) system and equivalent mechanical system for the structure is identified (Fig. 2.8). The extracted k, m, c from the admittance response for damaged states were used as damage index. It is shown from the study that proposed damage index were shown to be better for characterizing damage (incipient to severe) when compared to the conventional RMSD.

(a)   (b)
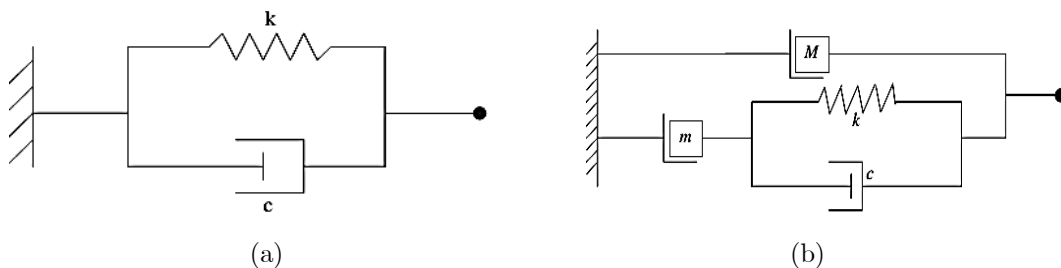
Figure 2.8: Equivalent mechanical system identified for (a) Concrete cube (90-100 kHz) (b) Aluminum beam (55-60 kHz) [26]

Annamdas et al. [27] experimentally investigated the influence of loading on EM admittance signatures. PZTs were bonded to the bottom of laboratory sized aluminum beam specimens and tested under simply supported boundary condition with increment loading. It is observed that the susceptance signature (imaginary part of admittance) is a better indicator of influence of stress than the conductance of the PZT.

Identification of damage severity and location was done using root mean square deviation (RMSD) to associate the damage level with the changes in the EM admittance signature at both low (30-100 kHz) and high frequency (200-400 kHz) ranges and dividing them into sub frequency intervals. The results of RMSD values obtained from PZTs bonded to a concrete structure show that damage close to the PZT changes the RMSD at high frequency range significantly, while the damage far away from the PZT changes the RMSD at low frequency range significantly [28].

Wang et al. [29] studied crack propagation in 2.7x.15x.25 m RC beam using EM technique with surface mounted distributed PZT patches. Five PZT patches were bonded to the soffit of the simply supported beam near the midpoint, load points and support points. The electric admittance corresponding to the frequency bands of 30-50 kHz were taken under different levels of loading. It is concluded that surface mounted distributed PZT was found to be effective in RC concrete structures to monitor the cracking load and crack propagation by analyzing qualitative changes in piezoelectric admittance.

A sensitivity analysis using different frequency ranges of surface bonded PZTs to monitor crack depth change in concrete was studied [30]. Damage was artificially induced on specimen at different depths by machine cut. One PZT was bonded 20mm and other was at 60 mm away from the notch. EM impedance was taken at frequency ranges of 20–70 kHz, 80–260 kHz and 600

kHz–2.4 MHz at each crack depth increment. It is shown that 20–70 kHz, 80–260 kHz frequency ranges (planar vibration frequencies) are insensitive to crack depth change while thickness vibration frequencies (600 kHz–2.4 MHz) are shown to be an effective frequency range for monitor crack depth change. Park et al. [31] applied wireless EM impedance method to detect the debonding of Carbon fiber reinforced polymer (CFRP) laminated concrete structures. Debonding condition was artificially simulated by partially bonding CFRP sheet. The impedance signals were measured over the frequency range of 1–3 kHz. Debonding conditions were evaluated using the *1-CC* (cross correlation) method as a statistical method. Bases on the study, the irregular resonance peak shift was observed with different levels of debonding and *1-CC* method can be used effectively used to diagnose the debonding condition of CFRP laminated concrete structures.

The effect of axial load on the impedance signature of the PZT coupled to a thin aluminum beam was studied [32]. An analytical model was developed to simulate the interaction between the PZT patch and uniform beam structure in the presence of axial loading. It is found that the tensile stress will induce stiffening effect, resulting in an increase in natural frequency as well as resonance frequency of peaks in the admittance signature spectrum.

The damage locations and severities of damage of a plain concrete beam was determined by measuring the electrical admittance signals of surface mounted PZT in different frequency ranges. Damages were artificially induced on the beam. A cross-correlation (CC) coefficient based damage matrix was introduced to measure the location and severity of the damage and had shown that the CC index value decreases gradually with the damage severity increasing [33].

Ribolla et al. [34] extended the EM impedance method to biomedical applications by monitoring the effectiveness of dental implant using wafer type

surface mounted PZT patch. The curing of the sealer, which connects the implant and the bone was monitored by bonding a PZT patch to the side of an abutment secured to the implant. It is concluded that the RMS and the RMSD index can be used to assess the healing stage since change in conductance and peak frequency of the conductance peak strongly depend on the conductance of the free PZT and are minimally influenced by the location within the same bone.

Annamdas et al. [35] used EM impedance technique and DIC (digital image correlation) based techniques to study the fatigue growth in high strength steel. It is shown that frequency shift of the conductance signature can be used effectively to monitor fatigue growth in steel while DIC images can be used to separate strain coalesce stage and crack propagation stage.

EM impedance technique was applied to monitor damage in rock in dry as well as saturated conditions [36]. Small PZT patches of size 0.5x0.5x0.2 mm^3 were surface mounted to cylindrical specimens. Based on the investigation, the frequency range of interest of the conductance spectrum should contain resonance peaks and the RMSD index was shown to be directly related to damage level in rocks under dry and saturated/moist underground conditions.

Ai et al. [37] investigated the load-induced structural tension/compression stress and damage using surface mounted PZT patches on a full scaled concrete beam. The effect of tension/compression stress and stress-induced damage were evaluated by analyzing the electrical admittance signatures of the bonded PZT. Frequency range containing the resonance peak were used for analysis. Based on the study, the resonance frequency and amplitude increased for PZT conductance response under compressive stress and resonance frequency and amplitude decreased for PZT conductance response under tensile stress. The change in frequency shift and amplitude can be correlated to the stress level and used as effective stress-monitoring indices.

2.3   Wave propagation based damage detection in concrete

The crack growth in concrete cylinders of different mix-proportions under uniaxial compression and cyclic compression loads were monitored using longitudinal ultrasonic waves [38]. Commercially available ultrasonic transducer pair of 700 kHz were placed in the axial direction and 500 kHz ,150 kHz transducer pair were used in the lateral direction. Results showed that, ultrasonic attenuation can be used effectively to monitor the crack growth in concrete and usage of excitation frequency more than 250 kHz for concrete will be inefficient as this frequency would undergo a large amount of attenuation. The results also showed that prediction of fatigue life using linear damage accumulation may lead to erroneous results since damage accumulation as measured by pulse attenuation during cyclic loading was found to be nonlinear. Berthaud [39] extended the study to investigate the effect of compressive stress and damage on ultrasonic wave propagation in concrete. The configuration of the ultrasonic transducers is shown in Fig. 2.9. The study has carried out in two stages, the behaviour of stress on wave propagation was studied by applying three different load values when the specimen was in elastic zone. The effect of damage on wave characteristic was studied by loading the specimen in load steps up to failure. Based on the study, it was shown that there was decrease in velocity spectrum and increase in amplitude of the received wave in stress only stage and vice versa in stress-damage state of study. It is deduced that the coupled effect of stress and damage should be considered for interpreting wave propagation results when the concrete specimen is under load since even in undamaged state, the specimen is micro cracked and the waves are also expected to be sensitive to stress even in damaged state.
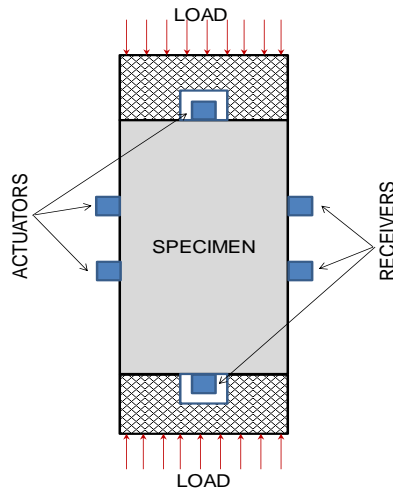
Figure 2.9: Schematic representation of test set up [39]

Selleck et al. [40] investigated the efficiency of ultrasonic wave propagation technique to evaluate distributed cracking in concrete structures. Distributed cracking in prismatic concrete specimens was induced by freeze-thaw cycling and salt-scaling. A through transmission measurement was conducted using immersion type ultrasonic transducer pair of 500 kHz center frequency. Changes in attenuation, pulse velocity, and peak frequency of the ultrasonic waves were correlated to the change in the specimen due to the distributed damage. It was found that ultrasonic pulse velocity is very insensitive to changes caused by distributed micro cracking while the wave amplitude and peak frequency were found to be sensitive indicators to evaluate the distributed damage in concrete.

Freezing and thawing deterioration in concrete was studied using ultrasonic waves [41]. A through transmission ultrasonic measurements was conducted at 54kHz pulse using pulsar/receiver set up. It was concluded that the signal energy of ultrasonic waves is a more sensitive measure for detection of freezing and thawing damage than ultrasonic wave velocity.

Yeih and Huang [42] examined the applicability of ultrasonic wave propagation measurements to evaluate the corrosion damage of reinforced concrete members. The direct pitch-catch method was used to obtain the ultrasonic

28

signals. The wave amplitude decayed as the corrosion of the rebars caused some deterioration in the concrete. There was a linear relationship between open circuit potential and wave amplitude attenuation.

Nogueira and William [43] investigated the efficiency of longitudinal and transverse ultrasonic waves for assessing microcrack growth and degradation of elastic properties in concrete specimens of different mix proportions under uniaxial compression. The specimens were subjected to monotonic axial loading until failure. Changes in peak to peak amplitude of the wave with the increase of stress was correlated to the microcrack growth. The peak-to-peak amplitude of the longitudinal wave showed mixed trend while transverse wave did not show much variability in amplitude trend (Fig. 2.10). It was concluded that the change in peak–to-peak amplitude of the transverse waves provided a measure to monitor microcrack growth than the longitudinal waves.

(a)   (b)
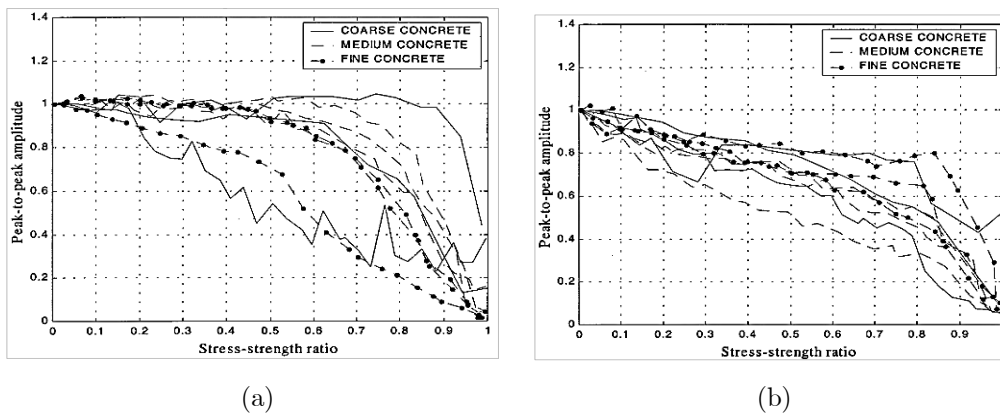
Figure 2.10: Decrease of peak-to-peak amplitude with increase in stress for (a) Longitudinal wave (b) Transverse wave [43]

Jung et al. [44] examined the possibility of using ultrasonic guided waves to detect the internal defect in reinforced concrete beams. Three types of defects honeycomb, Plexiglas inclusion. and cracks were artificially induced in the beam. The lamb wave signal attenuation parameter was more sensitive to damage than ultrasonic through transmission measurements.

Chaix et al. [45] investigated the possibility of using back scattered ultrasonic waves for monitor damage evolution in concrete. Cylindrical concrete specimens a 110 mm diameter and 210 mm length was used in the study. Damage were induced in the specimen by thermal loading at different temperatures between 80 and 200^0c. Ultrasonic transducers of 500 kHz,1 MHz 2.5 MHz center frequency were used for the study. Ultrasonic backscattered signals were recorded at different spatial positions for different thermal states. It is shown from the study that the backscattered wave attenuation coefficient increases with damage growth and hence can be used as a measure of damage in concrete. It is also concluded that transducer frequency should be optimized for maximum penetration and scattering for effective use of the method.

A new nondestructive method called actively modulated acoustic was introduced for analyzing damage progression in concrete. Experiments were carried out on cylindrical concrete specimens in through transmission mode under compression test [46]. An amplified continuous sinusoidal signal of 100 kHz was used for exciting the transducer and a low-frequency stress wave by using tuned impact hammer was used to modulate the received signal. A frequency domain analysis was carried out to analyze the signal along with wave attenuation and pulse velocity. Based on study, actively modulated acoustic method is shown to be sensitive to incremental damage and can be used for assessing level of damage in concrete structures.

Stauffer et al. [47] compared the effectiveness of a nonlinear ultrasonic testing method with established ASTM testing methods such as pulse velocity, resonance in detecting early damage in concrete. The investigation was based on the theory that when the fundamental ultrasonic frequency interacts with a material, harmonics are generated. As damage increases, the magnitude of the nonlinear interaction increases, causing a greater portion of the fundamental frequency to be converted to higher harmonics. Concrete prism

specimens equipped with ultrasonic transducers on the side faces for through transmission mode were tested under different levels of compression loading. Transducers with a center frequency of 50 kHz were used as transmitter while transducers with a center frequency of 150 kHz were used as receivers. The study concluded that the ratio of amplitude of third harmonics to cubic power of first harmonic can be used as a sensitive parameter for detecting early damage when compared with ASTM methods.

The repair effectiveness of RC bridge deck was studied using a combination of Rayleigh surface waves and longitudinal waves [48]. Through thickness cracks of the bridge deck were repaired using epoxy injection. A total of ten transducers were used in equal numbers on top and bottom of the deck. Rayleigh waves were used to check the repair condition of the material into the shallow layer near the surface while longitudinal waves used for the area inside the structure. The effectiveness of the repair was analyzed using change in longitudinal velocity and phase velocity of the longitudinal and Rayleigh waves respectively. It is shown that combination of Rayleigh waves and longitudinal waves is effective than using single method to check the repair condition.

Sun et al. [49] examined the possibility of using surface mounted piezoceramic patches for wave propagation based damage evaluation studies in concrete structures. Three circular PZT patches were surface mounted to the concrete prism as shown in Fig. 2.11. PZT1 worked as the transmitter, PZT2 and 3 as the receiver. PZT1 was excited with five cycle Hanning windowed signal of frequency 120 kHz. The concrete prism was loaded up to half of the design load and the received signals were collected at regular load interval. The procedure repeated to study the effect of internal microcracking. The change in amplitude of first, second and third wave packets of the received signal (PZT 3) were taken for assessing damage in the specimen (Fig. 2.11). The

change in amplitude for first wave packet decreased continuously while changes in the amplitudes for second and third wave packets showed increases in value at early stages of loading. It was concluded from the study that surface mounted PZTs can be effectively used for wave propagation studies in concrete and effect of stress, debonding of surface mounted PZT should be carefully studied for interpreting the wave measurements and the change in amplitude of the wave packets can be used as a sensitive measure for assessing internal microcracking.
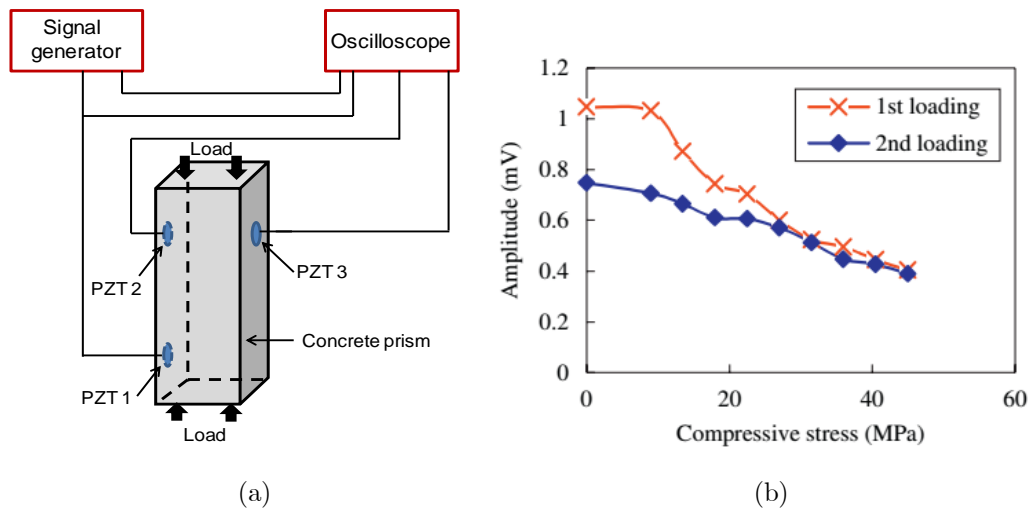
Figure 2.11: (a) schematic diagram of test set up (b) Variation of amplitude of the first wave packet [49]

The through-the-thickness ultrasonic wave measurements were carried out on mortar cubes with vinyl inclusions of 1%, 5% and 10% for simulate different degrees of distributed damage [50]. An electric spike with duration of 2µs was used as an excitation signal for piezoelectric broadband transducers with response up to 1MHz. The ultrasonic measurements were analyzed using wavelet transform. As the degree of damage increased, the frequency content of the received signal decreased and the distribution of signal energy was increased. There was an increase in dispersion of frequency content with an

increase in the damage. It is also concluded that pulse velocity was not sensitive even for material with 10% of artificial damage.

The sensitivity of linear and nonlinear analysis tools of received ultrasonic signal from through transmission measurement to evaluate the damage progression in concrete cylinder was compared under compressive loading [51]. The study showed that nonlinear analysis method like Scaling Subtraction Method, which is a nonlinear parameter was found to be a sensitive parameter for damage characterization in concrete when compared with linear parameters like pulse velocity and wave attenuation.

Zhu and He [52] experimentally investigated the effect of excitation frequency and amplitude to estimate the interior local damage of concrete when using surface mounted PZT actuator/sensor based wave propagation method. Surface mounted PZTs were excited by a harmonic sine wave of frequencies of 1, 2, 5, 10, 20, 30, 50 kHz having amplitudes ranging from 15 V to 75 V with increment of 15 V by the arbitrary waveform generator and the power amplifier. The results obtained were analyzed using relative voltage attenuation coefficient (output voltage to input voltage). Based on the study, amplitudes of excitation voltage only affect the intensity of sensor signals and of actuator sensor distance. It was also concluded that higher frequency under goes higher attenuation in concrete.

Efficiency of PZT surface mounted sensor based wave propagation to detect the damage in concrete structures were studied [53]. A 5-cycle Hanning-windowed tone burst at 50 and 200 kHz central frequencies with a peak-to-peak voltage of 60 V was used to excite the PZT. Cracking was induced in the concrete beam by subjecting to four-point bending and the sensor signals were acquired. From the study, it was concluded that PZT surface mounted sensor based wave propagation technique can be applied to monitor the damage in

concrete and also showed that wave magnitude and delay in the arrival time of longitudinal waves are sensitive measures to detect the damage in concrete. Rucka and Wilde [54] studied damage evolution in reinforced concrete element subjected to tensile loading by wave propagation studies using surface mounted PZT transducers. A pair of PZTs were surface mounted on the concrete element and tensile force was applied through corrugated steel rod as shown in the Fig. 2.12. A 4-cycle Hanning-windowed tone burst at 96 kHz of central frequency was used as excitation signal. Signals were measured at each 15 seconds and each signal was assigned ordinal number 'n' during the incrementally increased loading. The measured signals were analyzed using power spectral density (PSD) and were plotted in the form of maps (Fig. 2.12b). It was deduced that frequency components decreased at early stages of cracking while lower frequencies decreased at a later stage of damage.

<div align="center">(a)   (b)</div>
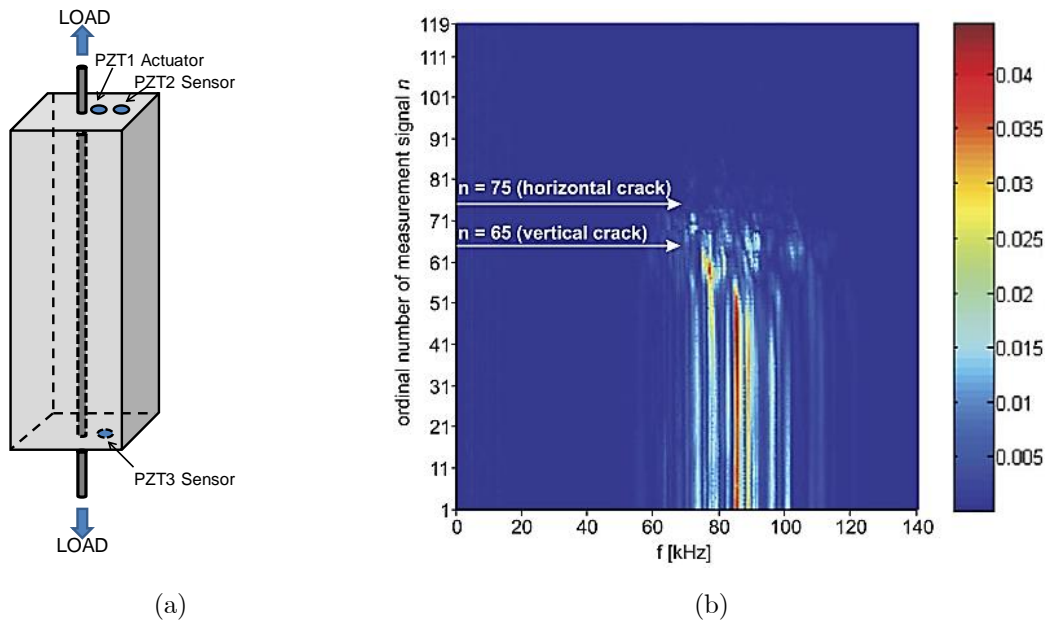
Figure 2.12: (a) schematic diagram of test set up (b) Power spectral density maps of signal received by PZT 3 [54]

Sensitivity of ultrasonic waves to distinguish damage phases (structural cracking to yielding of reinforcing bars) in the concrete slabs during bending

test was studied [55]. Ultrasonic transducers of 250-kHz central frequency were placed on the same face and generated signals were detected from the other pair of transducers on the opposite side. According to the study, the robust methods for monitoring stress changes in concrete such as velocity variations and time shift methods are not applicable because the ductility property of reinforced concrete distorts acoustic waves and changes the waveform. It is concluded that wave energy approach to time-domain and frequency-domain signals can be sensitively used to assess the stress evolution and cracking propagation in the reinforced concrete elements. It is also shown that ultrasonic waves are capable of detecting initial structural crack and bars yielding phases.

Divsholi and Yang [56] used surface-bonded PZT patches in a concrete beam to monitor the damage growth by wave propagation technique. Five surface-bonded PZT patches were installed on one side surface of the beam of size 220x40x20 cm. One PZT was bonded at the center of the beam, two PZTs were bonded in alignment with two loading points, and remaining two PZTs near the two ends of the beam. The beam was tested under four-point bending. The PZTs were excited individually and signals were collected at regular loading intervals. Based on the study, it is showed that a large area can be monitored efficiently in concrete by using wave propagation technique using surface mounted PZTs. It is also concluded that distances greater than 70 cm were unsuitable for damage monitoring purposes in concrete. Percentage change in wave energy can be used as damage index for monitoring crack development in the beam.

Chen et al. [57] attempted to correlate the both linear and nonlinear damage parameters of the ultrasonic wave signal with the change of crack opening in cement-based materials. Artificial notches of five different widths were used to simulate cracks in concrete. An amplified tone burst signal of 100 cycles at 22

kHz was used to actuate the piezoelectric transducer. Piezoelectric transducers with center frequency of 25 kHz and 50 kHz were used as actuator and sensor, respectively in the through transmission mode and the signals were collected for the different notch widths. Pulse velocity and second harmonic amplitude based damage index were used as linear and non-linear analysis parameter respectively for analysis. Damage index based on nonlinear parameter, second harmonic amplitude was found to be very sensitive to the presence of a notch, about an order of magnitude larger than the pulse velocity for the growing crack width. Nonlinear parameter showed an exponential increase with respect to the crack width and was proposed for the damage diagnostics of cement-based materials.

Sensitivity of amplitude and phase measurements of continuous pulsed single frequency ultrasonic signals to detect the concrete damage was investigated [58]. Measurements were performed in the unloaded stage on a concrete slab subjected to incremental damage level with piezoelectric transducers of center frequency 47 kHz. The amplitude and phase measurements are shown to be good indicators of damage in a reinforced concrete slab.

Ju et al. [59] nondestructively evaluated the damage induced by alkali-silica reaction (ASR) in concrete using wave mixing technique. The experiment was conducted on concrete prism made with highly reactive coarse aggregate. Six pairs of ultrasonic transducers were used in through transmission mode. The ASR affected specimens were tested using three individual excitation frequencies 0.1 MHz, 0.25 MHz, 0.35 MHz and using mixing wave frequencies of 0.25 MHz, 0.35 MHz. The collected signals were analyzed using wave speed, wave attenuation for normal waves and acoustic nonlinearity parameter measurement for mixed wave and results were compared. It was concluded that changes in the linear parameters of the concrete (wave speed and attenuation) are not sufficient to be effective for quantitative non-destructive

evaluation purposes. The acoustic nonlinearity showed an increasing trend with ASR damage and provided better correlation with the degradation of compressive strength due to ASR.

2.4   Summary and Overview

A clear understanding of the coupled EI response of a PZT patch bonded to a concrete substrate is still evolving. Concrete structural elements typically have a large mass and therefore structural modes of vibration have low frequencies. The energy requirements for exciting structural modes in concrete structures are high. While in previous studies, some low frequency peaks in the EI response of PZT patches bonded to concrete cubes have been reported, the exact nature of these peaks was not clearly established. The influence of the boundary in finite-sized concrete specimens is not fully understood. Considering the high material damping of concrete, information on the finite zone of influence beyond which the influence of the boundary may be insignificant is not yet available. The contributions of the material of the substrate and the structural motion to the mechanical impedance in the EI response of the PZT bonded to a concrete substrate is not fully decoupled.

Several studies on the use of bonded PZT patches for detecting damage in structures using the EI measurements are reported in the literature. Most of the studies have been conducted using artificial damage and are predominantly in steel or composites. Studies of damage in concrete using EI-based measurements of PZTs have been conducted using embedded defects and machine cuts. In concrete, the influence of artificial damage on the mechanical impedance experienced by the PZT is not identical to that of load-induced damage. Stress induced damage occurs in the form of microcracks, which coalesce to form discrete cracks in the material medium. The level of discontinuity in concrete depends upon the level of stress in the substrate. Upon unloading, the cracks close. This aspect of combined crack opening and

stress is not captured when artificial damage is used. Distributed damage in concrete results from microcracks in the material medium, which also produce an increase in the material damping in addition to an increase in the material compliance. While a few experimental studies on the influence of load induced damage have also been reported, a fundamental understanding of the influence of the material damping and damage on the EI response of a PZT bonded to a concrete substrate is still not available. Load-induced damage in concrete is associated with an increase in the stress in the material. For a PZT placed in a stress field, its EI response includes the influence of the stress in the substrate, in addition to the effect of increase in the level of damage in the material. The use of EI -based monitoring of concrete structures requires identifying changes in the impedance signature due to an increment in the level of damage and a change in the applied stress, which is currently not fully understood.

Through transmission of elastic waves have been used to assess the damage in concrete structures using surface bonded ultrasonic transducers or PZT patches. Ultrasonic transducers (transmitter and receiver) were temporarily adhered to the surface of the concrete using couplant and the effect of load induced distributed cracking in concrete was studied using through transmission measurement of ultrasonic waves. Majority of the studies relied on the change in attenuation and pulse velocity of the ultrasonic waves to quantify the damage. Most of the through transmission measurements use ultrasonic transducers as actuator-receiver pairs, to scan a large area of the structure the ultrasonic transducer pairs to be relocated and it results in slow measurements. Concrete structures often encounter uneven surfaces, and it is difficult to attain effective coupling between transducer and the surface. Measurements are shown to be extremely sensitive to the contact between the transducer and the concrete surface, which is very difficult to maintain using

38

typical couplant. Partial contact results in scattering of the waves and noisy signals.

Few studies have been reported on through transmission studies using surface mounted PZT pairs for damage detection in concrete structures. Most of the studies used a single PZT pair on laboratory sized specimen to evaluate the effect of the damage on the elastic wave characteristics. Wave velocity and change in energy of the received signal were used to evaluate the presence and degree of damage. It is shown that change in energy of the received wave is a sensitive parameter to quantify the damage. The effect of transmission path and other losses which influence the energy of the received signal has not been addressed in any of the experimental studies. A single PZT pair often limits the applicability of the technique to small portion of the structure while distributed crack often happens in concrete structures. A systematic study to evaluate the sensitivity of the PZT pair to different levels discrete discontinuity due to a stress induced crack has not been studied.

Chapter 3

Understanding the Coupled Electro-mechanical Response of a PZT Patch Bonded to Concrete: Influence of Substrate Size

3.1   Introduction

PZT patches are increasingly being used in health monitoring schemes and in developing damage detection strategies for structural components. The use of a PZT patch to infer about the level of damage in the substrate requires interpreting the coupled electrical impedance (EI) response of the PZT patch bonded to the substrate. When a PZT patch is bonded to a substrate, the dynamic motion of the PZT patch in response to an applied electrical potential depends on the dynamic mechanical impedance to its motion provided by the substrate. Most experimental studies on the coupled EM response of PZT patches bonded to a concrete substrate involve using laboratory-sized specimens [16, 60-65]. Application of these results to real structures requires a careful evaluation of the influence of geometry and size of the specimen on the dynamic mechanical impedance provided to the motion of the PZT patch.

40

Separating the influence of the geometry and the finite size of the substrate from the mechanical impedance of the substrate material is essential for developing EI-based damage detection procedures suitable for structural applications.

The electrical admittance (or impedance) spectrum of a PZT patch, which is obtained by varying the frequency of the electrical input depends on the coupled EI response of the PZT patch to the given electrical input. The mechanical motion of the PZT is influenced by the dynamic restraint to its motion from the substrate. Most approaches for predicting the dynamic response of a coupled PZT patch subjected to a given electrical input idealize the dynamic restraint as the mechanical impedance of the substrate derived from a single or a multi-degree of freedom system [3, 6, 7, 9, 12, 14, 34]. This method provides a reasonable approximation for the coupled EI response of a PZT bonded to a structure where the energy supplied by the motion of the PZT patch is sufficient to excite structural motion or to represent the dynamic impedance of the substrate over a narrow range of frequencies. The approach of representing resistance to the motion of the PZT patch using the dynamic impedance derived from distinct structural modes associated with a known pattern of structural motion has been applied successfully to thin, light plate-like structures made of aluminum and composites, typically used in aerospace applications [6, 8, 66-72].

A clear understanding of the coupled EI response of a PZT patch bonded to a concrete substrate is still evolving. Concrete structural elements typically have a large mass and therefore structural modes of vibration have low frequencies. The energy requirements for exciting structural modes in concrete structures are high. While in previous studies, some low-frequency peaks in the EM response of PZT patches bonded to concrete cubes have been reported, the exact nature of these peaks was not clearly established [24, 73]. The influence

41

of the boundary in finite-sized concrete specimens is not fully understood. Considering the high material damping of concrete, information on the finite zone of influence beyond which the influence of the boundary may be insignificant is not yet available. The contributions of the material of the substrate and the structural motion to the mechanical impedance in the EI response of the PZT bonded to a concrete substrate is not fully decoupled.

The objective of this study is to understand the influence of the finite size of a concrete substrate on the electrical impedance measurement of a bonded PZT. The approach followed includes experimentation using different sized concrete cubes and a calibrated numerical model for evaluating the full range of variables including PZT patch size. The experimental investigation establishes the fundamental issue of scaling of response with size. The numerical simulation is performed to provide additional insight into understanding the influence of size of PZT relative to the concrete substrate. From the measured electrical response of PZT patches bonded to concrete cubes of different sizes, the baseline response contributed by the mechanical impedance of the material, is extracted. The influence of the finite boundary is shown to be associated with structural resonance modes of the finite sized specimen, which overlap with the baseline resonant response of the bonded PZT patch. From an analysis using the calibrated numerical model, the resonant modes of the bonded PZT patch are evaluated for different sizes of PZT patch. Smaller PZT patches are shown to have resonant modes at higher frequencies in the bonded configuration. A finite-sized zone of influence is identified with each resonant mode of the bonded PZT patch. The zone of influence is smaller for resonant modes of higher frequency. For a size of specimen smaller than the zone of influence of the resonant mode, the structural modes are superimposed on the resonant mode of the PZT patch.

3.2   Background

In a piezoelectric material, the application of an electrical field results in mechanical strain in the material due to the coupled electro-mechanical constitutive relations. The constitutive relation for a PZT is given as [1, 2, 74]

$$S = \frac{T}{C_E} + d^T E \tag{3.1}$$

$$D = dT + \varepsilon_T E \tag{3.2}$$

where vector D of size *(3 × 1)* is the electric displacement *(Coulomb/m²)*, S is the strain vector *(6 × 1)*, E is the applied electric field vector *(3 × 1) (Volt/m)* and T is the stress vector *(6 × 1) (N/m²)*, ε_T of size *(3 × 3) (Farad/m)* is the Dielectric permittivity, C_E is the elasticity matrix of size *(6 × 6)* (N/ m²), the piezoelectric coefficient, d^T *(6 × 3) (m/Volt)* is the strain per unit field at constant stress and d *(3 × 6) (Coulomb/N)* defines electric displacement per unit stress at constant electric field. From the constitutive relation of piezoelectric material, it can be seen that there is a coupling between electrical displacement and applied stress through piezoelectric strain coefficient. Change in the applied stress will reflect a change in electrical displacement of the PZT, and thus the conductance of the PZT.

3.3   Experimental program

The influence of the finite specimen size on the coupled EI response of a PZT patch bonded to a concrete substrate was evaluated using concrete cubes of sizes equal to 40 mm, 70 mm, 100 mm, 150 mm, 200 mm and 250 mm. All the specimens were made from the same batch of concrete and cured under water for 90 days. The elastic properties of concrete measured using three 150 mm cubes are given in Table 3.1. The average compressive strength of concrete measured from the 150 mm cubes was 63 MPa.

Table 3.1: Properties of the concrete and epoxy

Properties	Concrete	Epoxy
Density (kg/m³)	2380	1250
Young's modulus (GPa)	40	2
Poisson's ratio	0.2	0.36

Square PZT patches of 20 mm size and 1 mm thickness were used in the study. The PZT is composed of the two chemical elements lead (Pb) and zirconium (Zr) combined with the chemical compound titanate. The powders of the component metal oxides are mixed in specific proportions then heated to attains a dense crystalline structure. The electrodes are applied to the appropriate surfaces and poled at high electric field and temperature. The PZT material properties are given in Table 3.2. The electrical admittance measurements were performed on the PZT patches using a 6500B series impedance analyser of Wayne Kerr make which has a frequency range of 20Hz to 20MHz with frequency step size of 0.1mHz and a measurement accuracy of ±0.05%. In a typical electrical admittance measurement, the electrical admittance of the PZT patch was measured at an applied voltage of 1 V and frequencies varying in the range between 10 kHz and 500 kHz. Measurements were performed at 800 discrete frequencies at a frequency interval of 613.2Hz. Conductance (real part of admittance) response of the free PZT patch was extracted from the electrical admittance measurements before attaching it to the concrete cube. Typical conductance responses of free PZT patches (before attaching to the concrete substrate), as a function of the frequency of applied electrical input are shown in Fig. 3.1a. The resonant behaviour obtained from PZT patches used in the experimental study were nominally comparable.

Resonant modes of the free PZT patch can be identified with peaks in the conductance spectra (identified as f_1 through f_6 over the frequency range between 10 kHz and 500 kHz). Each PZT patch was bonded to the centre of

one face of a concrete cube using a two-component epoxy. The epoxy was allowed to cure for one day before initiating measurements. A block of mass 1 kg (9.81 N) was placed on the bonded PZT patches during the curing time to maintain the similar thickness of epoxy among the specimens. The properties of the hardened epoxy are given in Table 3.1. A schematic figure and a photograph of the experimental test setup for electrical admittance measurements from a PZT patch bonded to a concrete cube, are shown in Fig.3.2. The conductance signature derived from an electrical admittance measurement of a PZT patch bonded to a 250 mm concrete cube is shown in Fig. 3.1b. Resonant modes of the bonded PZT patch are identified with peaks in the conductance response (identified as b_1 through b_6 over the frequency range between 10 kHz and 500 kHz). In the electrical admittance response obtained from the PZT patch bonded to the concrete cube, the amplitudes of the resonant frequencies of the PZT patch are significantly smaller than the resonant peak amplitudes in the free condition. There is also a distinct baseline shift which increases with an increase in frequency. Closely spaced local peaks can be identified in the EI response of the bonded PZT patch which is shown in the subplot in Fig. 3.1b.
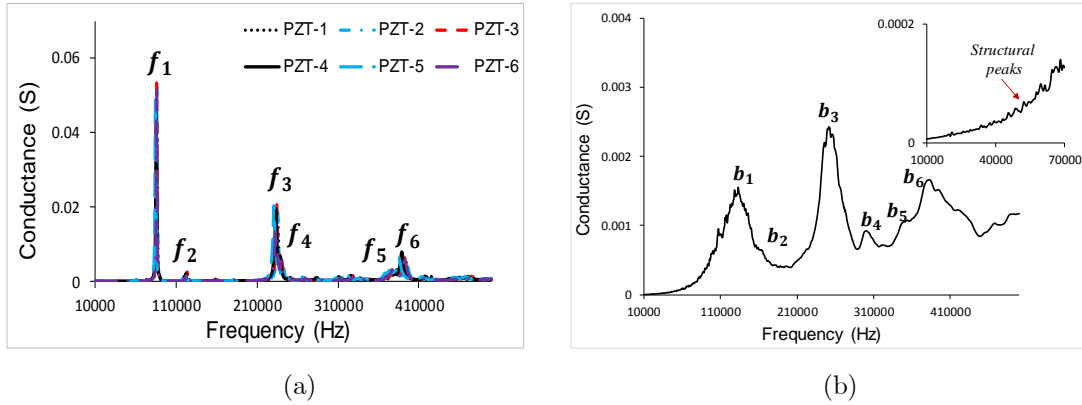
Figure 3.1: The conductance signature from electrical admittance measurement of PZT patches: (a) in the free state; (b) in the coupled response obtained from 250 mm concrete cubes.
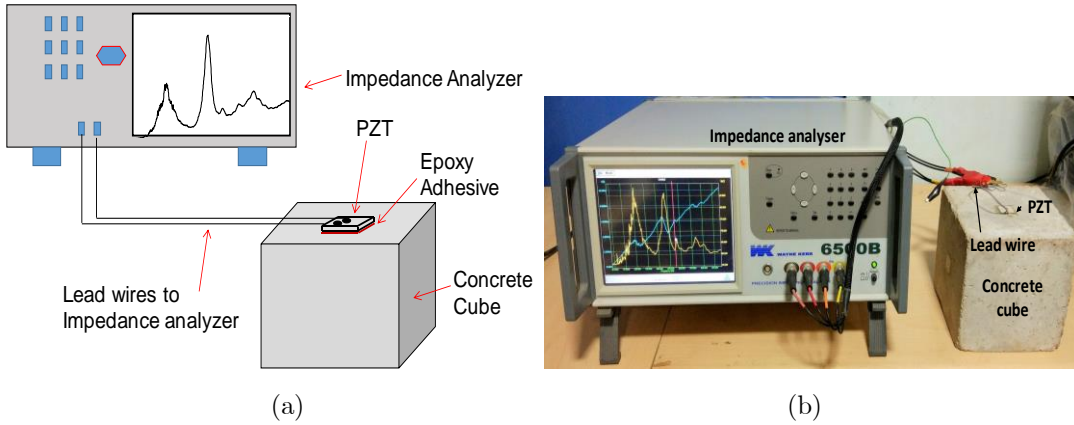
Figure 3.2: Experimental set-up for electrical admittance measurements from PZT patches: (a) Schematic representation; (b) Photograph.

The electrical admittance signatures acquired from PZT patches bonded to the different sized cubes are plotted in Fig. 3.3. The conductance spectra recorded from PZT patches bonded to 40 mm, 70 mm and 100 mm cubes are shown in Fig. 3.3a. There are several closely-spaced, narrow, local peaks in the conductance spectrum, which appear to be superimposed over broad peaks of the bonded PZT patch. These local resonance peaks are dominant in the 40 mm cube and extend over the entire range of frequencies used in the measurement. The local peaks diminish in amplitude with increasing size of the cube. The local peaks diminish more rapidly at higher frequencies. Comparing the spectra recorded from the 40 mm cube and the 70 mm cube,

46

the local peaks are not visible on the broad peak identified with b_6 in the conductance spectrum. There is a convergence in the broad peak, b_6 in the spectrum of the PZT patch bonded to the 100 mm cube. This trend continues with increasing size of the cubes up to 250 mm as seen in Fig. 3.3b. At 250 mm there appears to be a convergence in all the broad peaks identified with b_1 to b_6, in the conductance spectrum of the bonded PZT patch. For the 250 mm cube, the closely spaced local peaks appear at frequencies smaller than the center frequency of the first broad peak, b_1 of the bonded PZT patch and are of very small magnitude when compared with the magnitudes of peaks from the 40 mm and the 70 mm cubes.
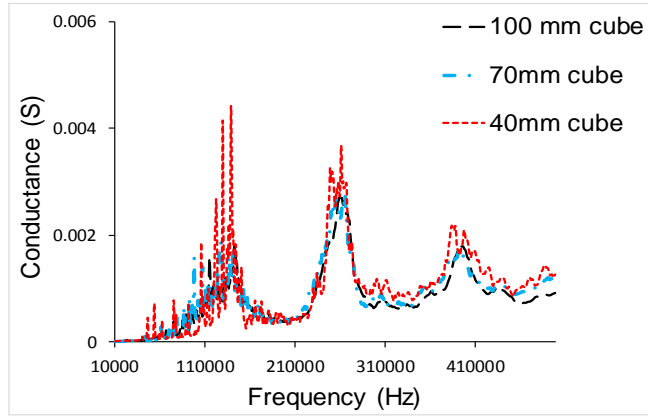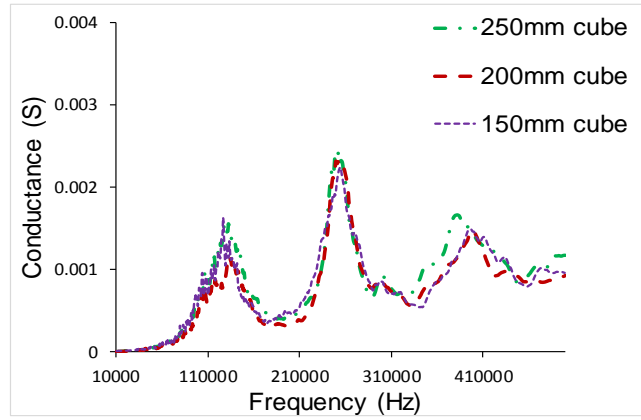
Figure 3.3: Experimental conductance plot for coupled PZT with different substrate sizes: (a) cubes ranging from 40 mm to 100 mm; and (b) cubes ranging from 150 mm to 250 mm.

On increasing the size of the cube, the resonant frequencies of the bonded PZT patch exhibit a convergent behaviour; the resonant peak becomes better defined and there is no further change in the center frequencies and amplitudes of the resonant peaks. The broad peaks in the conductance spectrum are identified with the resonant behaviour of the PZT patch as influenced by the substrate material properties. The closely spaced local peaks, which are superimposed on the broad peaks are associated with the finite size of the substrate and clearly show a dependence on the size of the cube. The closely-spaced narrow peaks are influenced by the boundaries in the finite sized specimens and are identified as structural modes of vibration of the cube. The

range of frequencies over which the narrow, closely-spaced structural peaks occur, increases with a decrease in the size of the cube. For the small size of the cube, the structural modes overlap with all the resonant modes of the bonded PZT patch. With increasing size of the cube, the effect of boundary decreases and the local peaks tend to decrease in magnitude at higher frequencies.

From the electrical admittance response of a bonded PZT patch, a finite zone of influence beyond which the influence of the boundary is insignificant can be identified for each resonant mode of the PZT patch. For the PZT patch used in the study, the zone of influence for the broad peak, b_6 appears to be around 100 mm and for the broad peak identified as b_3 it appears to be smaller than 150 mm. The peak associated with the first resonant mode of the bonded PZT, b_1 shows convergence for concrete cube of size 250 mm. The low-frequency resonant modes of the bonded PZT patch have a larger zone of influence. For the 20 mm square PZT patch of 1 mm thickness, beyond 250 mm, the overlap of structural modes is limited to frequencies lower than the first resonant mode of bonded PZT patch. The underlying response obtained upon convergence as indicated by the spectrum recorded from the 250 mm cube is therefore associated with the resonant modes of the bonded PZT, which is influenced by the dynamic impedance of substrate material free from the influence of the finite size of the domain.

3.4   Identification of resonance modes in bonded PZT patch

In the conductance response of the PZT bonded to concrete cubes of different sizes apart from the closely-spaced structural peaks, the broad peaks are also identified in all the responses. To identify the nature of broad peaks, a numerical study has been carried considering the PZT patch bonded to a half-space (elastic space with no boundaries). The response of a PZT patch bonded to a half-space was simulated to identify the electrical conductance response

of the PZT patch associated with the material, free from the effects of boundaries in a finite sized specimen. The numerical simulations were performed using the Structural Mechanics Module available in COMSOL™ Multiphysics. A half space model was created using a concrete cube with a perfectly matched layer (PML) available in the COMSOL™ Multiphysics. The PML provides perfect acoustic impedance match, and eliminates reflection of waves at the boundary. A finite sized cube with a PML therefore simulates the response of an elastic half-space. The material properties used for numerical simulation of the PZT, concrete and epoxy is same as used in section 3.5.1 of the chapter. The thickness of the epoxy layer is assumed as 0.1mm. A comparison of conductance response obtained from numerical simulation for PZT bonded to a 150 mm cube and to the concrete half-space is shown in Fig. 3.4. The conductance response of the PZT bonded to the 150 mm cube shows closely spaced structural peaks of the specimen superimposed on broad peaks while in the response of the PZT bonded to concrete half space, the broad peaks are free from the closely spaced local peaks. For the PZT bonded to concrete half-space, there is no influence of geometry of the substrate on the PZT conductance response, the broad peaks present in the conductance spectrum is solely due to the resonance behaviour of PZT. It can be concluded from the study that the closely spaced local peak are resonance peaks of the finite substrate while the broad peaks are resonance peaks of the PZT.
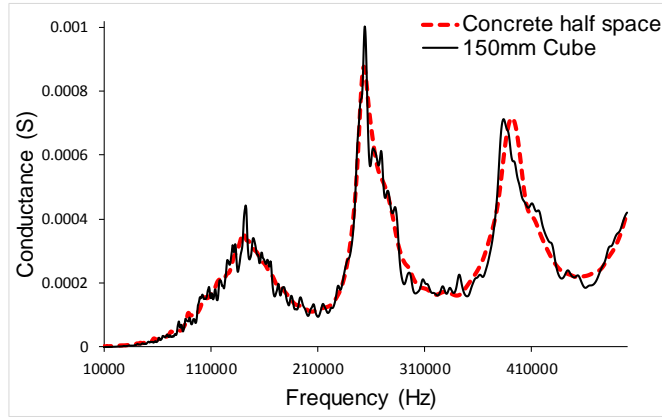
Figure 3.4: Comparison of conductance response obtained from numerical simulation for PZT bonded to 150mm cube and to concrete half space

3.5   Extraction of structural resonance response

The experimental study using different substrate sizes with the 20 mm square PZT patches proves that the effect of finite size structure can be identified with structural peaks, which are superimposed on the resonant peaks of the bonded PZT patch. A baseline detection algorithm was used to separate the closely-spaced structural peaks present in the electrical conductance response of the bonded PZT patch. An end-weighted algorithm was used for baseline separation, to extract the broad baseline function associated with the bonded PZT resonance [75, 76]. This method creates a baseline using the end-points of the spectrum. The adjacent average smoothing method was used to reduce the influence of local noise. A simple linear interpolation was used to generate the baseline. The baseline identified from the EM response spectrum of the 40 mm cube is shown in Fig. 3.5a. The extracted baseline signatures of the bonded PZT patch from the coupled conductance responses of the PZT patches bonded to 40 mm, 100 mm and 150 mm cubes are shown in Fig. 3.5b. The extracted baseline signatures of bonded PZT patches corresponding to different sized concrete cubes are similar to the spectra obtained directly from larger sized cubes shown in Fig. 3.3b. Due to the presence of intense structural peaks in the lower frequency range for smaller cubes, an accurate detection of

51

the first peak is difficult. While the convergent behaviour is clearly identified with increasing size of the concrete cube, the exact magnitude and the central frequency of the first peak in the electrical conductance response of the bonded PZT bonded to smaller sized cubes are not accurately established through the baseline analysis. This is indicated by a slight mismatch observed in the first peak of the bonded PZT bonded to a 40 mm concrete cube.

(a)   (b)
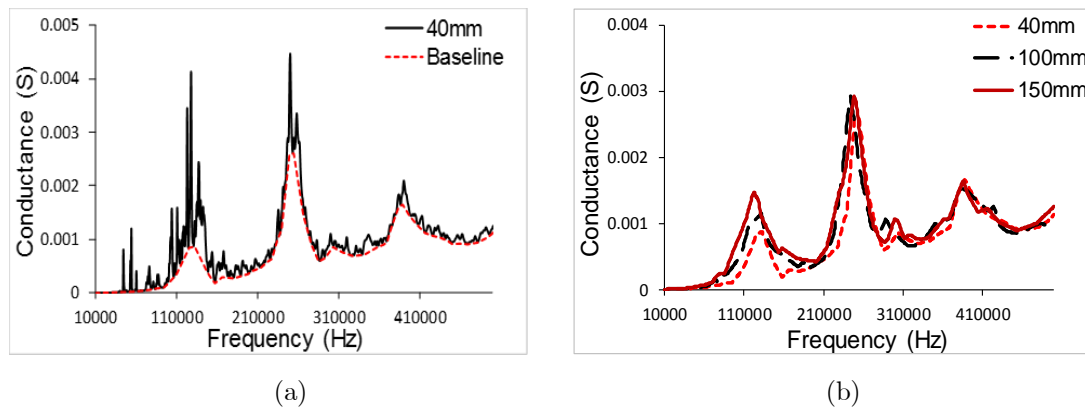
Figure 3.5: Conductance response of a 20 mm square PZT patch of 1 mm thickness (a) Total conductance spectrum and the extracted baseline response for the 40 mm concrete cube (b) A comparison of the extracted baseline responses of the bonded PZT resonance peaks from 40 mm, 100 mm and 150 mm concrete cubes.

The structural peaks, which are separated from the electrical conductance response of the bonded PZT patches bonded to different substrate sizes using the baseline detection algorithm are shown in Fig. 3.6. As the size of the substrate increases, the structural modes identified with the finite sized cube diminish in amplitude. There is a larger relative decrease in amplitude at higher frequencies. There are a significant number of the structural modes close to the first mode of the bonded PZT patch. The amplitudes of the structural peaks close to the first resonant peak of the bonded PZT diminish drastically as the size of the cube increases larger than 200 mm.
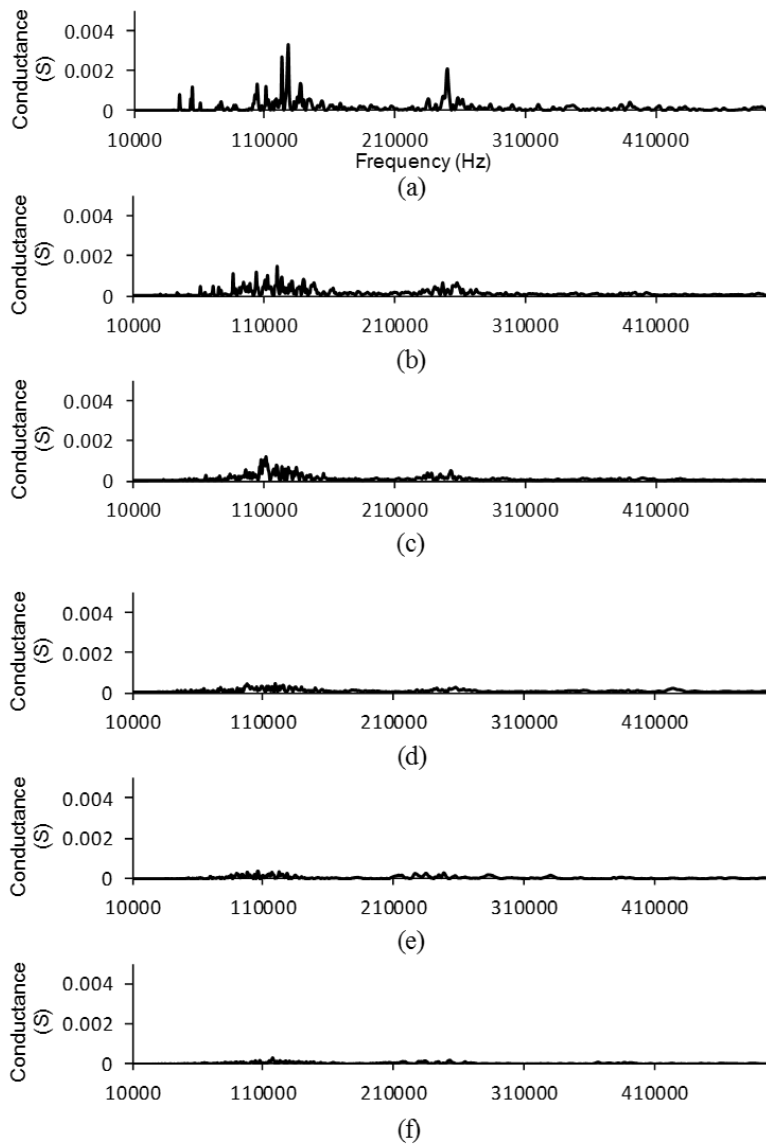
Figure 3.6: The structural peaks extracted from the electrical conductance spectrum of a PZT patch bonded to concrete cube of different sizes: (a) 40mm cube; (b) 70mm cube; (c) 100mm cube; (d) 150mm cube; (e) 200mm cube; (f) 250mm cube.

3.6 Numerical analysis of the EI response of PZT patch

A numerical simulation of the coupled EI response was performed to understand the relative influence of the substrate size and size of the PZT patch on the measured electrical response of a bonded PZT patch. A calibrated 3-dimensional numerical model was developed for the 20 mm square patch used in the experimental program using the Structural Mechanics Module

53

available in COMSOL™ Multiphysics. Free and coupled behaviour of the PZT patch was obtained from a 3-dimensional numerical simulation. A discretized model of the PZT patch with nominal dimensions of width, b = 20 mm, length, l = 20 mm and thickness, t = 1 mm was modeled in the Piezoelectric devices physics interface in the Structural Mechanics Module of COMSOL, which combines the solid mechanics and the piezoelectric interfaces to model piezoelectric materials. The piezoelectric coupling can be in stress-charge or strain-charge form [74]. The PZT material properties provided by the PZT vendor (Sparkler Ceramics) were used in the numerical analysis and are given in Table 3.2. The constitutive relations of the PZT material, in notation used in COMSOL™ Multiphysics are given equation in 3.1 and 3.2.

Table 3.2: Material properties of the PZT

Properties	Values			
Elasticity matrix (Pa)	$C_E = \begin{bmatrix} 1.20 \times 10^{11} & 7.51 \times 10^{10} & 7.50 \times 10^{10} & 0 & 0 & 0 \\ 7.51 \times 10^{10} & 1.20 \times 10^{11} & 7.50 \times 10^{10} & 0 & 0 & 0 \\ 7.50 \times 10^{10} & 7.50 \times 10^{10} & 1.10 \times 10^{11} & 0 & 0 & 0 \\ 0 & 0 & 0 & 2.10 \times 10^{10} & 0 & 0 \\ 0 & 0 & 0 & 0 & 2.10 \times 10^{10} & 0 \\ 0 & 0 & 0 & 0 & 0 & 2.25 \times 10^{10} \end{bmatrix} Pa$			
Piezoelectric Constants (C/N)	$d = \begin{bmatrix} 0 & 0 & 0 & 0 & 5.84 \times 10^{-10} & 0 \\ 0 & 0 & 0 & 5.84 \times 10^{-10} & 0 & 0 \\ -1.71 \times 10^{-10} & -1.71 \times 10^{-10} & 3.74 \times 10^{-10} & 0 & 0 & 0 \end{bmatrix} C/N$			
Relative permittivity	$e = \begin{bmatrix} 1730 & 0 & 0 \\ 0 & 1730 & 0 \\ 0 & 0 & 1700 \end{bmatrix}$			
Poisson's ratio (ν)	Density, ρ (kg/m³)	Dielectric loss factor (δ)	Damping ratio (ζ)	Mechanical quality factor (Q_m)
0.35	7700	0.02	0.006	75

In the numerical analysis, the 20 mm square faces were treated as equipotential surfaces and a potential of 1 V was applied to the opposite faces of the PZT patch. The analysis was performed with a frequency interval of 613.2 Hz with varying frequencies between 10 kHz and 500 kHz. The admittance, which is a complex number consisting of real and imaginary parts, was determined as the ratio of the current to the applied voltage as

Admittance, $Y = \frac{I}{V}$ (3.3)

where I is the current and V is the applied voltage. The electric current flowing in the PZT was determined from the surface integration of current density extracted from the equipotential surface.

$I = \iint I_Z \, dA$ (3.4)

where I_z is the current density component along the poling direction.

The results of the analysis for a free PZT patch are shown in the plots of admittance and conductance as a function of frequency, in Figs. 3.7a and b, respectively. Distinct resonant modes of vibration can be identified by the local maxima in the conductance spectrum of the PZT patch. The results indicate that numerical model under-predicts the resonant frequencies while the. magnitudes of admittance and conductance are over predicted. Significantly, the difference between the predicted and experimental resonant frequencies increases at higher modes while the difference in the magnitudes appears to decrease at higher modes.
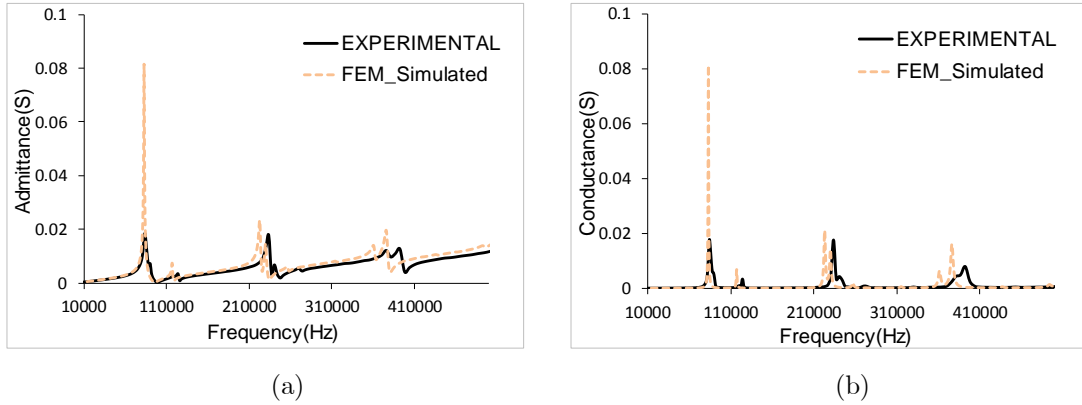
Figure 3.7: Comparison of experimental and simulated electrical impedance response of a free PZT patch (a) Admittance (b) Conductance

A better prediction of the EM response signature was obtained by updating the constitutive material properties of the PZT given by the supplier. The values of the material constants in the constitutive relationship of the PZT were assumed to be the median values applicable to a large population. The elastic properties of the PZT was considered to vary in the range of 5% - 20% of the nominal values, according to the range of variability expected in the properties [7, 77]. A parametric study was performed in order to ascertain the influence of the different properties on the resonant signature of the PZT. The influence of increasing the elastic constants, the dielectric and the piezoelectric constants by 5% on the first resonant mode in conductance spectrum of a free PZT patch is shown in the Figs. 3.8a and b. It can be seen that increasing the axial components C_{E11}, C_{E22} and C_{E33} of the elasticity matrix values result in a rightward shift of the first resonance frequency while shear components C_{E44}, C_{E66} and C_{E66} has very negligible effect on the signature. Increase of dielectric and the piezoelectric constants properties produced a minor change in the magnitude of the peak as shown in the figures.
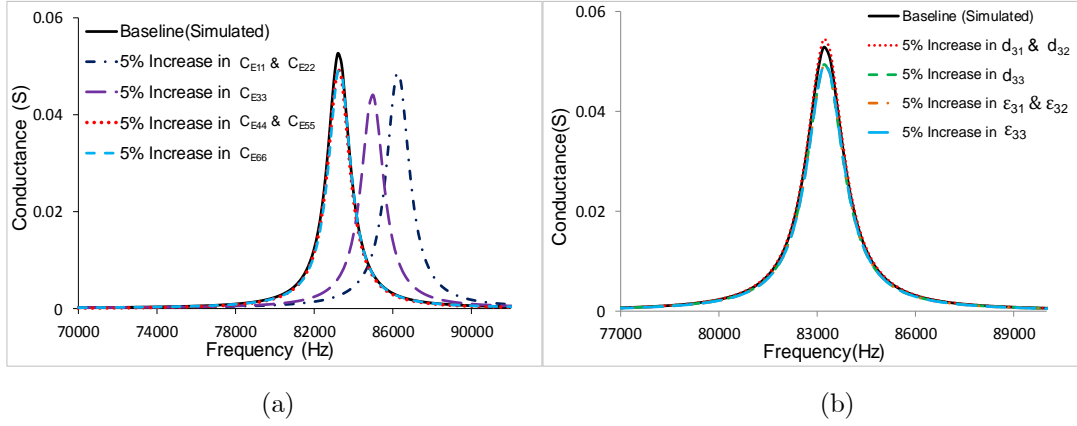
Figure 3.8: Effect of PZT properties on the first resonant peak in the electrical conductance measurement of a free PZT patch (a) changes produced by varying $C_{E11}, C_{E22}, C_{E33}, C_{E44}, C_{E55}, C_{E66}$ (b) changes produced by varying d_{31}, d_{32}, d_{33}, ε_{31}, ε_{32} and ε_{33}.

The frequency shifts in the resonant modes can be accommodated within small variations of the elastic material properties. The change in the magnitude of the admittance, however, could only be achieved with a significant decrease in the mechanical quality factor (Q_m) which in turn increases the damping of the PZT material and an increase in dielectric loss factors. The loss factor damping, which introduces complex material properties to add damping to the model was found suitable for the frequency dependence of material damping over an extended range of frequencies [69,70]. In order to define dissipation in the piezoelectric material for a harmonic analysis, all material properties in the constitutive relations were defined as complex-valued matrices where the imaginary part defines the dissipative function of the material. The loss in the mechanical parameter was introduced in the form of an isotropic loss factor (η_s) in the elasticity matrix of the constitutive equation such that, $\overline{C_E} = C_E(1 + j\eta_s)$ while dielectric matrix becomes $\overline{\varepsilon_T} = \varepsilon_T(1 - j\eta_s)$, where $\overline{C_E}$ and $\overline{\varepsilon_T}$ are the complex elastic modulus and the complex dielectric permittivity of the PZT, respectively. The isotropic loss factor (η_s) can be calculated as $\eta_s = 2\zeta$ for light damping.

The axial components of the elasticity matrix, dielectric loss factor, and damping ratio were updated in an iterative manner to obtain a match with the experimental response. Figs. 3.9a and b show a comparison of the experimental and predicted admittance and conductance response, respectively of the free PZT patch with updated values of the properties of the PZT. It can be seen that the predicted conductance and admittance signature match well in both magnitude and resonant frequency. The updated values of the properties of the PZT, which provide the best match with the experimental response are given in Table 3.3.

(a)   (b)
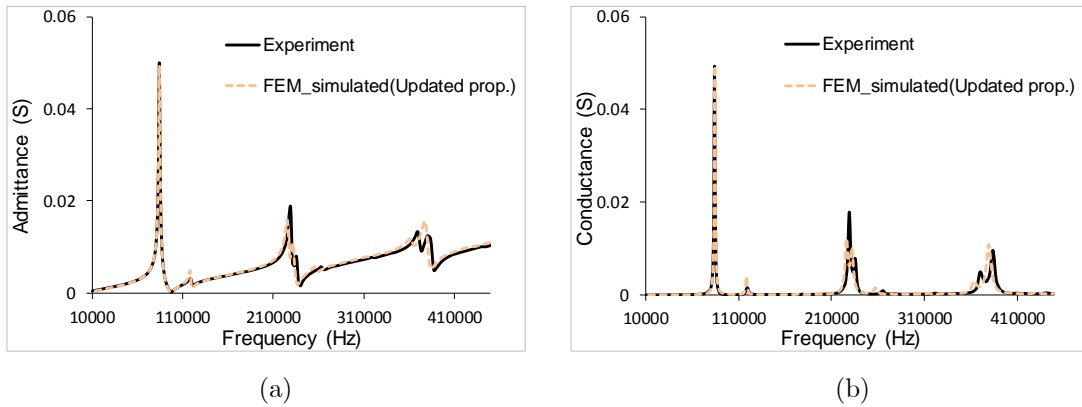
Figure 3.9: Comparison of the EM response of a free PZT patch obtained from numerical analysis with updated material properties of the PZT material and the experimental response: (a) admittance; and (b) conductance

Table 3.3: Updated elastic, dielectric and piezoelectric properties of the PZT

Parameter	Value	Updated value
C_{E11} & C_{E22}	1.20×10^{11}	1.24×10^{11}
C_{E33}	1.11×10^{11}	1.09×10^{11}
δ	.02	.012
ζ	.006	.00845
Mechanical quality factor (Q_m)	75	60

3.6.1   Modelling PZT-structure Interaction

The PZT-structure interaction was evaluated using a numerical simulation of the EI response of a PZT patch bonded to 40 mm cube. A numerical model of the PZT patch bonded to a concrete cube was developed in COMSOL™ Multiphysics (Fig. 3.10). The epoxy thickness was assumed to be equal to 0.1 mm and its isotropic loss factor was taken as 0.05. The properties of epoxy are given in Table 3.1. The properties of the concrete are taken as in Table 3.1. The isotropic loss factor (η) of concrete was assumed to be 0.03. Considering symmetries, a one fourth model of the PZT coupled to concrete cube was developed. Similar to the analysis of the free PZT, the 20 mm x 20 mm faces were treated as equipotential surfaces and a potential of 1 V was applied across the opposite faces of the PZT patch. The frequency of the voltage excitation was varied from 10 kHz to 500 kHz and the analysis was performed with a frequency interval of 613.2 Hz. The updated properties of the PZT given in Table 3.3 were used in the simulation.
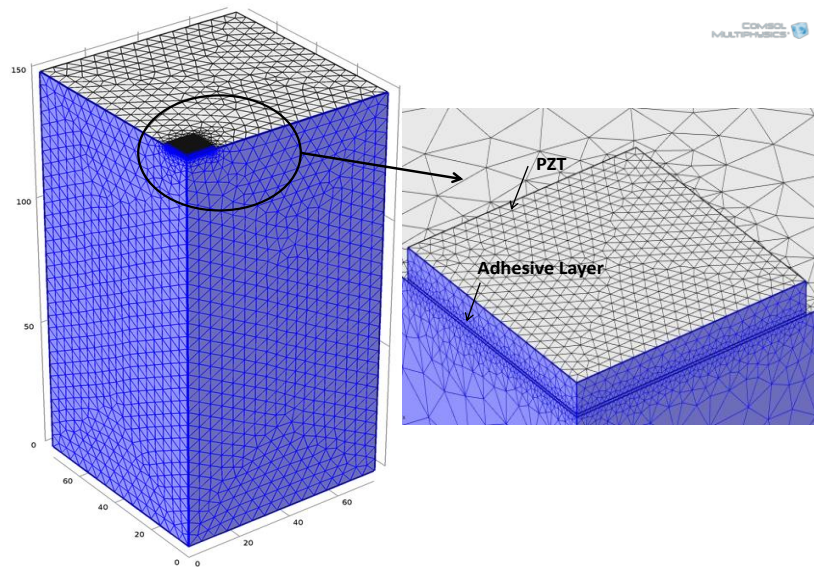
Figure 3.10: The finite element (FE) model for simulating impedance response of PZT bonded to a cube in COMSOL

Figure 3.11a shows a comparison of conductance plot obtained from experiments and numerical simulation. Numerical simulation provides a good prediction of resonance frequencies. While the numerical analysis slightly under predicts the resonance frequencies, there is a large difference in the predicted amplitude. The differences in the magnitudes of the predicted and the experimental resonant peaks values are attributed to several factors such as damping of the substrate and epoxy, the thickness and the stiffness of the epoxy layer. The exact values of damping for the two materials and the stiffness of the epoxy are not known precisely [78].

From simulations, the following were recorded. Changes in the thickness and the stiffness of the epoxy produced changes in the magnitude of the resonant peak accompanied with a frequency shift. The influence of these parameters is more on the frequency content than the magnitude of the peak. An increase in the material damping of epoxy produced a decrease in both the frequency and the amplitude of resonant peak. The influence of damping is more on the amplitude of resonant peak than the resonant frequency. An increase in the substrate damping was found to have a significant influence on decreasing the amplitude of the local peaks present at low frequencies.

The thickness and the elastic modulus of the epoxy layer and the isotropic loss factors of the epoxy and the concrete substrate were changed iteratively to match the experimental response. The final values of the parameters which produced a close match with the experimental result are shown in Table 3.4. A comparison of the conductance response of the coupled PZT patch calculated using updated properties is shown in Fig. 3.11b. It can be seen that the numerical model with updated values of parameters gives a very good prediction of the electrical conductance response of the PZT patch bonded to a concrete cube.

Table 3.4: Updated parameters of the epoxy and concrete substrate used in numerical simulation

Parameter	Value	Updated value
Thickness of epoxy layer	0.1 mm	0.05 mm
Loss factor damping of epoxy	0.05	0.02
Loss factor damping of substrate	0.03	0.017
Young's modulus of the epoxy	2 GPa	4 GPa

(a)   (b)
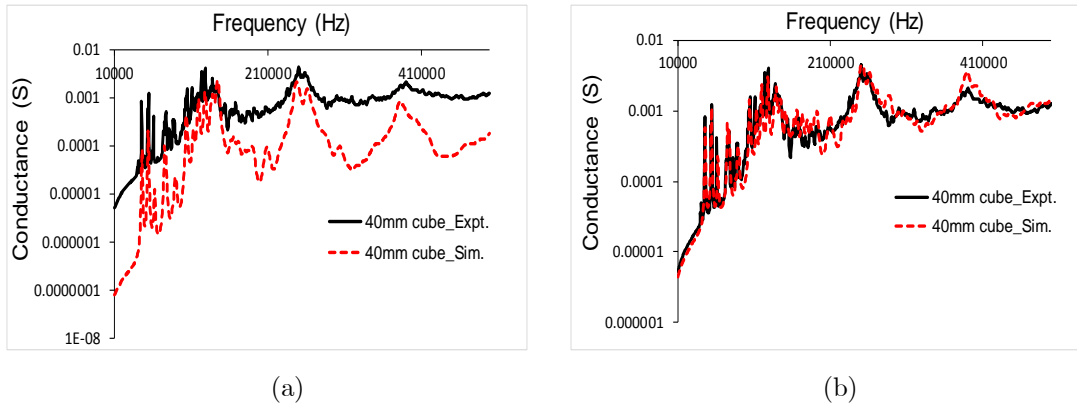
Figure 3.11: Comparison of electrical conductance response of a PZT patch bonded to a 40 mm concrete cube: (a) Without correction; (b) With updated material constants

The calibrated model for the coupled EI response of a PZT patch bonded to a 40 mm cube was extended to evaluate the influence of finite size of substrate on the coupled EM response of PZT patches of different size. The responses of 10 mm and 5 mm square PZT patches of 1 mm thickness were evaluated. The updated material parameters, from the previous analysis were used in the numerical simulations. The electrical conductance signatures of the free PZT patches of different sizes are shown in Fig. 3.12a. There are increases in the resonant frequencies of the free PZT patches with a decrease in its size. As a reference, the frequency of the first resonant mode of the 20 mm, the 10 mm and the 5 mm square PZT patches are equal to 84.16 kHz, 168 kHz, and 334.22 kHz, respectively. The coupled EI response of a bonded PZT patch was

61

evaluated from the electrical conductance measurements over a range of frequencies. The electrical conductance signatures of the PZT patches of different sizes bonded to the 40mm cube are shown in Fig. 3.12b. On decreasing the size of the PZT patch, the resonant peaks identified in the conductance response of the PZT patches bonded to the concrete cube also show an upward shift in the resonant frequencies and the local resonance peaks identified with the structural vibration modes of the finite sized substrate become less prominent. The narrow, closely-spaced peaks are prominently identified over all the broad resonant peaks in the response of the 20 mm PZT patch bonded to the concrete cube. For the 10 mm patch, the closely spaced peaks overlap with the first peak in the electrical conductance spectrum of the bonded PZT patch. The closely spaced structural modes are not evident in the coupled electrical conductance response of the 5 mm PZT patch.

(a)   (b)
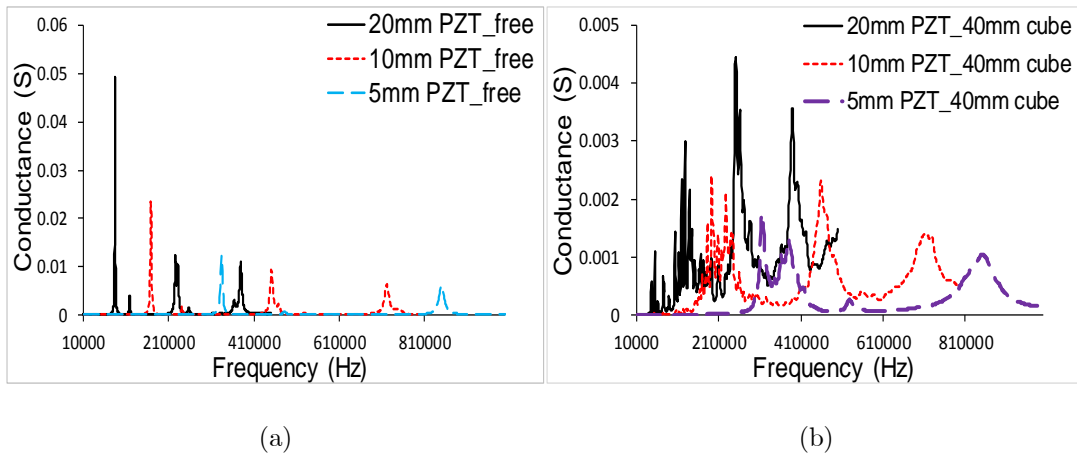
Figure 3.12: The electrical conductance response of PZT patches obtained using the calibrated numerical model with updated material properties: (a) Free response of PZT patches of different sizes (b) Response of PZT patches of different sizes bonded to 40 mm concrete cube.

3.6.2   Analysis of Structural Modes

The low-frequency electrical conductance responses of the square PZT patches of different sizes bonded to the 40 mm concrete cube between 10 kHz and 100 kHz are shown in Fig. 3.13. The resonant frequencies obtained from both

the 20 mm and the 10 mm patches are identical, indicating the same structural modes are excited over the given range of frequencies. While the 10 mm PZT patch excites the structural modes, the amplitudes of the structural peaks are lower when compared with the 20 mm PZT patch. For 5 mm square PZT patch (Fig. 3.13b), the structural modes while present are very small in amplitude when compared with the 20 mm and the 10 mm patches. The existence of the structural peaks in the response of the 5 mm PZT patch bonded to the concrete cube is shown using enlarged ordinate axis in the Fig. 3.13b. The resonant frequencies from the 5 mm patch are obtained at identical frequencies as the other two patches. The exact match in the resonant frequencies in the responses from the PZT patches of different sizes confirms that the closely spaced peaks identified in the EI response of a bonded PZT patch are due to the structural resonance of the finite sized cube.
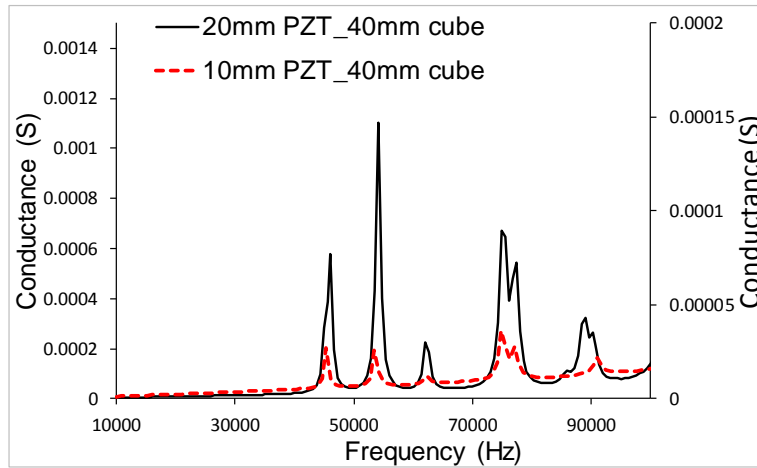
(a)
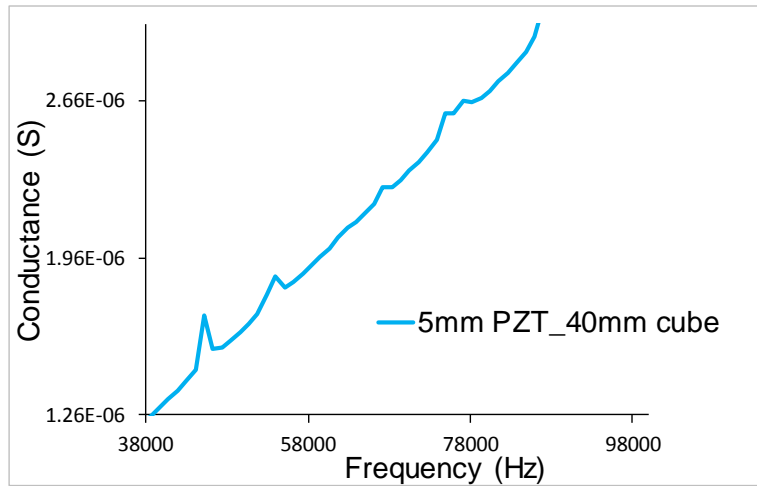
(b)

Figure 3.13: Low-frequency response of the PZTs of different sizes bonded to a 40 mm concrete cube (a) 20mm,10mm PZT patch (b) 5mm PZT patch

The structural resonance modes are produced by standing patterns of waves in the substrate produced by the dynamic motion of the PZT. Considering the large material damping of concrete, the structural modes are heavily damped as the size of the substrate increases. This is confirmed by the results of the structural modes extracted from the conductance response of the bonded PZT. Due to the high material damping of concrete, the high-frequency structural modes of cubes are also more highly damped than the low-frequency modes. As the energy available for the PZT is centered on its resonant modes, the shift in the resonance peaks to higher frequency due to a decrease in PZT size

64

results in less energy in the low-frequency range which overlaps with the structural modes. So the energy of the bonded PZT available to excite the low frequency structural modes of the 40 mm cube decreases as the size of the PZT decreases. From Fig. 13, it can be concluded that the first resonant mode of the PZT for the 20 mm and 10 mm PZT patches overlap with the range of frequencies of the structural modes of vibration of the cube; several structural modes overlap with the modes of vibration of the PZT. The first resonant mode of the 5 mm PZT patch is significantly higher than the structural modes of vibration of the cube. The energy available to drive the structural modes is therefore very small at frequencies removed from the resonant frequency of the PZT. The influence of the structural modes is therefore not significant in the case of 5 mm PZT patch.

3.7   Findings

For a PZT patch bonded to a concrete substrate, the influence of the size of the substrate is seen in the form of local peaks of structural resonance, which are superimposed on the baseline EI response of the bonded PZT patch. For the cubes of concrete used in this study, the local peaks which are identified as the structural peaks of the concrete substrate, are closely spaced and are superimposed over the resonant peaks of the bonded PZT patch. As the size of the substrate increases, the structural peaks are heavily damped and diminish in amplitude relative to the resonant amplitude of the bonded PZT patch. The resonant peaks of the PZT patch show convergence on increasing the size of the substrate.

For each resonant mode of the bonded PZT patch, a finite zone of influence where there is an influence of the boundary on the resonant behaviour of the bonded PZT patch, is identified. The zone of influence represents the volume of substrate material, which influences the dynamic EI response of the bonded

65

PZT patch. The zone of influence is larger for lower frequency modes. The zone of influence decreases in size with an increase in the resonant frequency of the PZT patch. The zone of influence for a given mode of the bonded PZT depends on its resonant frequency, which in turn would depend on the dimensions of the PZT and the material properties of the substrate. If the size of the substrate is larger than the zone of influence at a given frequency of measurement, the dynamic response of the PZT patch would depend only on the material properties of the concrete medium. The coupled dynamic response of the PZT patch within the zone of influence of a given resonant mode will contain the superimposed influence of the structural response. For a substrate size smaller than the zone of influence of a resonant mode of the PZT patch, the coupled dynamic response of the PZT patch would include the resonant modes of the substrate superimposed on the resonant response of the bonded PZT patch.

Chapter 4

Sensing of Damage and Substrate Stress in Concrete using Electro-Mechanical Impedance Measurements of bonded PZT Patches

4.1   Introduction

Signs of distress in concrete are often associated with visible cracking. Since concrete is a brittle material, which is weak in tension, cracking is the manifestation of damage in the material which results from tensile stress in the material. Stress induced damage in concrete could result from load application or due to effects such as restrained shrinkage and thermal contraction. Damage initiation is stress-induced and takes place in the form of distributed microcracks, which eventually coalesce to form localized cracks. Damage produces an increase in compliance of the material, which results in an increase in the strain in the material. By the time surface manifestation in the form of visible cracking appears there may be significant degradation of the capacity of the structure. Early detection of damage is essential to initiate early intervention measures, which can effectively increase the service life of a

structure. Methods to detect incipient damage in the form of microcracks are required to provide effective methods of monitoring structural health and service life performance of structures.

Electrical Impedance (EI)-based measurements of PZT patches bonded to a concrete substrate provide an effective way for monitoring incipient damage in the material. Studies of damage in concrete using EI-based measurements of PZT patches have been conducted using embedded defects and machine cuts [23, 26, 33, 79]. In these studies, electrical impedance measurements were conducted for increasing level of artificial damage. The influence of artificial damage on the mechanical impedance of the substrate experienced by the PZT is not identical to that of load-induced damage. In concrete structures, the evolution of material level damage from distributed microcracks to localization in the form of visible cracking is also associated with a change in the level of strain in the material medium and an accompanied increase in the material compliance [80, 81]. Experimental studies on the influence of load induced damage on the response of bonded PZT patches have also been reported [18, 19, 28]. In these tests, the response of PZT patches were continuously monitored for monotonically increasing load. The PZT patch was placed in a stress field and therefore the measured response from the PZT patch in such experiments includes the influence of the stress in the substrate and an increase in the level of damage in the material. The influence of load induced damage in compression without the influence of applied stress was investigated using specimens unloaded from a specific load level. In measurements performed in the unloaded state, the level of material damage was evaluated using change in the equivalent stiffness extracted from identified equivalent system model, which is derived from the drive point mechanical impedance within a narrow frequency range from the EI response [24]. In the unloaded state, microcrack

damage was shown to produce a decrease in the frequency of the resonant peaks of the PZT patch in the EI measurement.

Some studies on the influence of stress in the substrate on the response of a bonded PZT patch have been reported. Most of these studies have been performed on metallic substrates using small specimen and the influence of stress was evaluated using structural modes in the EI response of the PZT patch. For increasing strain in the substrate, frequency shifts and amplitude changes in the conductance response of the PZT have been reported [20, 27, 32, 82]. The susceptance part of the measured admittance spectrum in an EI measurement of the bonded PZT, associated with the structural modes, is shown to be more sensitive than real part of the admittance for monitoring stress in the substrate [27]. The effect of axial stress on the conductance signature of the coupled PZT was studied using Aluminium specimen and a compensation technique using effective frequency shift (EFS) by cross-correlation analysis was applied to conductance spectrum to compensate the effect of loading for the accurate estimation of damage [82]. The individual effect of load and damage on the structural peaks was decoupled by considering the influence of stress obtained from a pristine specimen as a correction for the specimen with damage in the form of an artificial cut at the corresponding stress level. Decoupling approach is not directly possible in concrete structures, since increasing stress level in the substrate is often associated with an increase in the level of damage. Further, considering the energy requirements for exciting structural modes, the use of these modes in concrete elements may not be feasible.

Embedded PZT smart aggregates were used to observe the effect of stress at various levels by observing the changes in embedded PZT resonance peaks [62, 83]. It has been reported that the embedded smart aggregates are insensitive to the stress since the local stress in the material is different from the applied

stress field. There were no systematic trends observed in the impedance resonance peak and the interpretations were very subjective. In embedded smart aggregates, there are several intervening effects which do not allow the delineation of inference of strain and damage in the substrate.

In concrete structures, an increase in the applied stress is often linked with an increment of damage. Increments in damage level and applied stress produce a change in the substrate strain. The increase in the level of damage has also been shown to produce a change in the substrate compliance. Therefore, a PZT patch coupled to a concrete substrate potentially experiences a change in the imposed strain and a change in the substrate compliance due to a changes applied load. Practical application of the impedance-based measurements to detect incipient damage in concrete structures requires an understanding of the influence of level of damage and substrate strain on the response of a PZT patch bonded to the substrate. The use of EI-based monitoring of concrete structures requires identifying changes in the impedance signature due to changes in damage and substrate strain. Further, the influence of both phenomena on the observed impedance response of a bonded PZT patch need to be separated. In this chapter an experimental investigation of concrete subjected to incremental levels of damage and stress are reported. The level of damage in concrete is increased in a controlled manner using progressively incremental loading. The level of substrate strain associated with applied stress and material damage are obtained using digital image correlation. The influence of damage and strain in the concrete substrate on the EI response of a bonded PZT patch are identified.

4.2 Background

For a PZT patch bonded to a substrate subjected to an applied electrical input, the motion of the interface subjected to continuity conditions is governed by the combined mechanical impedance of the structure and the PZT. The constrained motion in turn produces a change in the measured electrical impedance. The first systematic attempt to derive the electrical impedance of the PZT which is mechanically connected to a structure using a 1D idealization of the system was developed by Liang et al. [3]. Subsequent improvements in modelling the PZT response have included the effective 1-D model of the PZT and varying levels of idealization of the structural impedance [6, 7, 9]. Most of the available analytical solutions are applicable for 1 or 2-D idealizations of the PZT, substrate or both. Typically the complex electrical admittance of the PZT patch ($\bar{Y}$) for a given electrical input at a frequency can be represented as

$$\bar{Y} = \bar{Y}(Z_A, Z_S, \omega, l_i, E) \tag{4.1}$$

Where Z_A And Z_S are the mechanical impedance of the PZT and substrate respectively. l_i, represent the dimensions of patch and E is the electric field applied for actuation. Such equations have been derived assuming the mean strain in the PZT is zero. Damage in the material produces a change in its mechanical compliance, and the associated change in the substrate impedance (Z_S) results in a change the electrical admittance (inverse of impedance) of the PZT patch ($\bar{Y}$). Change in the mean strain of PZT on account of change in substrate stress is not considered.

A change in the substrate stress would produce a change in the imposed strain on the PZT patch. The strain in the substrate for a given stress depends on the mechanical compliance of the material which is related to the level of damage in the material. The strain experienced by a PZT patch bonded to a concrete substrate would therefore depend upon the magnitude of stress and

71

the level of material damage. Considering the coupled electro-mechanical constitutive relations of the PZT, the imposed strain on the PZT would produce a change in its EI signature.

4.3 Materials and Methods

An experimental program was conducted for measuring the impedance of PZT patches bonded to concrete cubes made with two different grades of concrete. 150 mm concrete cubes were used in the test program. Three cubes from each concrete batch were tested to determine the elastic properties and compressive strength of concrete. The material properties of the Normal strength concrete (NSC) and High strength concrete (HSC) are listed in Table 4.1. The material properties of the PZT are given in Table 3.2.

Table 4.1: Properties of materials

Type	Avg. compressive Strength (MPa)	Avg. Young's Modulus (GPa)	Density (kg/m^3)	Poisson's ratio
High strength concrete	75 (Std. dev. 3.35)	44	2370	0.2
Normal strength concrete	49 (std. dev. 3)	35	2300	0.2
Epoxy	-	2	1250	0.36

EI measurements were performed on a PZT patch bonded to a concrete substrate for different levels of compressive stress in the substrate and compression stress-induced damage in the material. From an EI measurement, the frequency dependent electrical admittance of the PZT is analysed using the conductance spectrum. A square PZT patch of 1 mm thickness, and 20 mm length was bonded to the centre of one of the face of 150 mm concrete cube for experimental study (Fig. 4.2a). A two-component epoxy adhesive was used to bond the PZT patch to concrete cube. Admittance signatures were collected

from the PZT patches in the free-state before attaching to concrete cubes. In a typical admittance measurement, the frequency was varied between 1 kHz and 0.5 MHz at an applied voltage of 1 V and data was collected at 800 discrete frequencies (Fig. 4.2c). Average of five measurements were collected to minimize the influence of random noise. The electrical admittance signature of the PZT patch was collected at different loaded and unloaded levels by subjecting the concrete cube to cyclic compressive loading. The poled direction of the PZT was kept normal to direction of loading.

The conductance signatures derived from the EI measurements on the PZT patches bonded to NSC and HSC cubes are shown in Fig. 4.1b. The conductance signature of the PZT in the free-state is also shown in the Fig. 4.1a with its resonant modes marked for reference. The PZT resonant modes are identified by the peaks in the response of the free PZT patch. Comparing the responses of the free and the bonded PZT patches, it can be seen that the dominant PZT resonant modes are clearly identified in the response of the bonded PZT at frequencies close to the resonant frequencies of the free PZT patch (previously discussed in section 3.2 of Chapter 3). In the EI response of bonded PZT patch there is an increasing trend in the background conductance with increasing frequency.

The low frequency response contains closely spaced peak (shown in the inset in Fig. 4.1b) and are identified with the structural modes of the cube. The structural modes in the response of the bonded PZT are found to be overlapping with the first resonance mode of the PZT in the conductance spectrum of the bonded PZT. The first resonant peak of the bonded PZT is not well defined in HSC when compared with NSC cube because of the significant overlap of structural modes. The higher material stiffness of HSC produces structural resonant modes at higher frequencies than the NSC. The third peak in the bonded PZT response is produced by two closely spaced

modes and the relative magnitudes of the two modes are different for the two grades of concrete; while in the stiffer HSC, the lower frequency mode has higher amplitude, the higher frequency mode has relatively higher magnitude in NSC. Objective identification and comparative evaluation of the influence of damage, free from the influence of boundary effects and baseline material compliance in HSC and NSC would not be possible using the first and third peaks in the conductance spectra of bonded PZT patch. The second peak in the impedance response of the bonded PZT patch was selected for evaluation since it is consistently well defined in both HSC ad NSC cubes and is associated with a single resonant mode. The influence of substrate impedance on the response of second peak in the impedance response of bonded PZT patch is obtained by comparing with the third resonant peak of free PZT patch. The centre frequency of the third peak of the free PZT patch is 236 kHz and the second peak in the conductance spectrum of the bonded PZT patch is centred on 256 kHz. Considering the free PZT patch to be the limit case of a substrate material with no impedance, an increase in material impedance is associated with a decrease in amplitude and an increase in the frequency of the resonant peak.
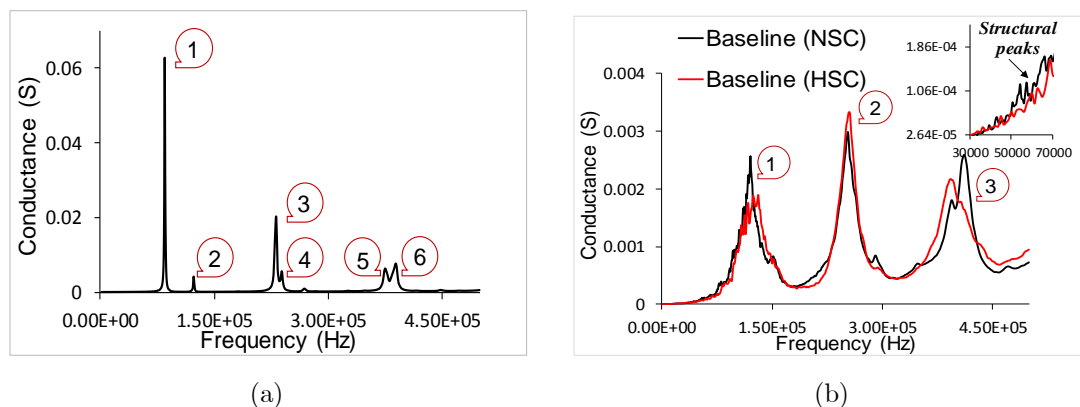
Figure 4.1: The conductance spectrum obtained from the EI measurement: (a) free PZT patch; (b) PZT patch bonded to concrete cubes

In the test program, the compressive stress in the substrate was incremented in a controlled manner using a computer controlled servo-hydraulic testing machine. To ensure uniform contact with the platens of the test machine, the concrete cubes were levelled using a capping compound. The concrete cubes were subjected to cyclic compressive loading where the load amplitude was increased in increments of 10% of the average compressive strength in every cycle as shown in Fig. 4.2b. The loaded and unloaded states in the loading program are referred to as L and U states, respectively. The load in the L states is given as a fraction of the average compressive strength (Fig. 4.2b). In the loading program, the load was cycled between a fixed lower load level and an increasing upper load level at a constant rate of 2 kN/s. The load was held constant at the upper and lower load levels for a duration of 120 seconds. EI measurements were performed at the top and bottom of the loading cycle, when the applied load on the specimen was held constant. The specimens were loaded to failure from the 0.9U state. During the entire loading procedure, deformations were measured using two linear variable differential transformers (LVDTs) over a gauge length of 55 mm. The LVDTs were mounted on opposite faces of the cubes and the average of the two LVDTs was used to measure the deformation of concrete.

(a)

(b)

(c)

76
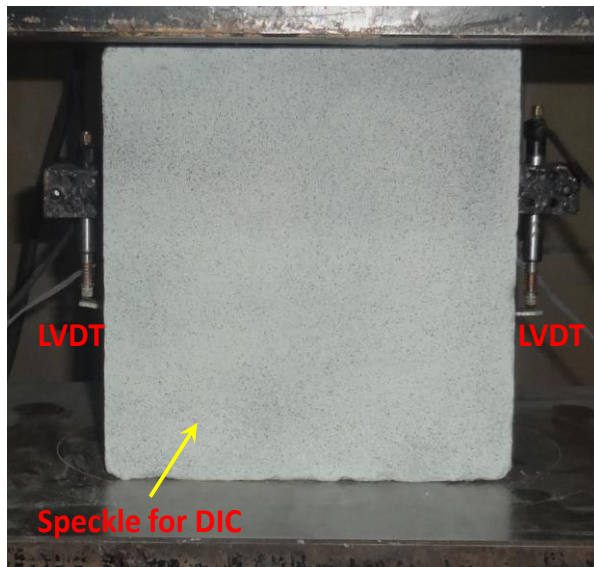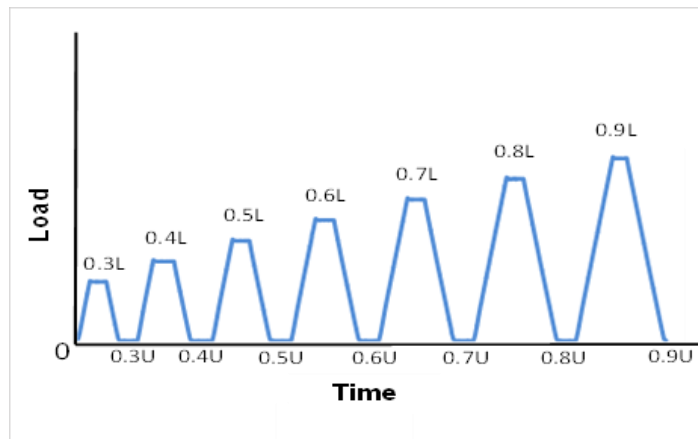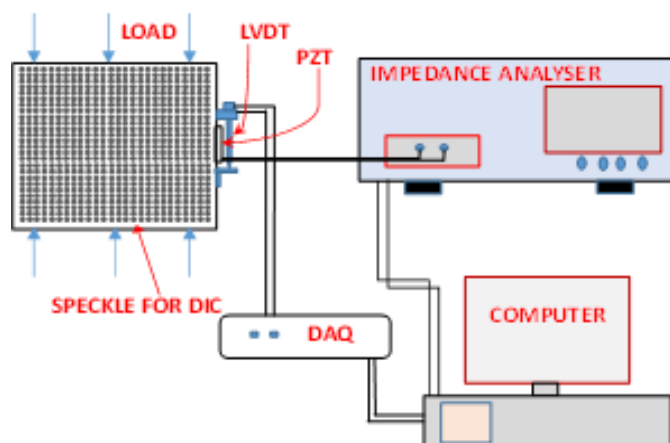
(d)

Figure 4.2: Compression testing of concrete (a) Specimen with LVDT and PZT patch (b) Applied loading history (c) Test setup for EI measurements; and (d) DIC measurement

The surface displacements on the surface of the concrete cube during the loading procedure were determined using a full-field optical technique based on digital image analysis called Digital Image Correlation (DIC). In preparation for the use of DIC technique, a sprayed- on speckle pattern was created on the surface of the specimen. Digital images of the specimen were captured using a camera of 5 mega-pixel resolution which was fitted with a 50 mm lens. The camera was placed at a distance of 1 m from the specimen surface. Uniform light intensity was ensured across the surface of the cube using normal white light (Fig. 4.2d).

The speckle pattern represents a random pattern, which gives a unique distribution of pixel grey level values. Cross-correlation of the pixel grey levels between the image of the deformed specimen and the image of the specimen in the reference configuration is used to determine the 2-dimensional displacement field on the surface of the specimen. In a given image, the pixel

gray-levels in each subset associated with the random sprayed-on pattern gives a unique gray-level pattern, which differs from gray-level distribution in another subset. In the analysis, positions within the deformed image were mapped on to positions within the reference subsets using second-order, two-dimensional shape functions. Spatial domain cross-correlation was performed to establish correspondence between matching subsets in images of the reference and deformed states. Quintic B-spline interpolation of the gray values was used to achieve sub-pixel accuracy. Correlations are performed over small subsets of size equal to 32x32 pixels. The cross correlation analysis of the digital images was performed using the VIC-2D^{TM} software [84]. Surface displacements at each loading stage were calculated at each subset centre, by evaluating the shape functions and their partial derivatives at the subset centre. Strains were computed from the gradients of the displacements. For the setup used in this study, the random error in the measured displacement is in the range of 0.002 pixels. A conservative estimate of the resolution in strain obtained from the digital correlation was 5$\mu\epsilon$ [85, 86].

Prior to initiating the loading program, load was cycled between 25% and 5% of the average compressive strength. The loading was initiated from a seating load 10 kN (approximately 1% of the average compressive strength). For use of image analysis, a reference image corresponding to the unloaded state for computing strains was taken while the specimen was under seating load, before starting the loading program. Baseline EI signatures were also recorded prior to starting the loading program.

4.4   Experimental Results

Typical cyclic stress-strain responses obtained from NSC and HSC cubes using deformation measured by surface mounted LVDTs are shown in Fig. 4.3a. The progressive decrease in mechanical stiffness and continued accumulation of plastic strain are evident with each additional cycle of loading. The secant

compliance calculated between the top and bottom of each unloading cycle is shown in Fig. 4.3b. It can be seen that there is an incremental decrease in stiffness with increasing load amplitude. In HSC, for load amplitude exceeding 0.4L (40% of the average compressive strength), there is an almost linear decrease in stiffness with incremental load. There is an decrease in stiffness with increasing load in NSC where the rate of change is increasingly higher for each additional load level. The plastic strains and hysteresis loops in HSC are significantly smaller indicating a significantly lower level of energy dissipation associated with damage when compared with NSC.

(a)   (b)
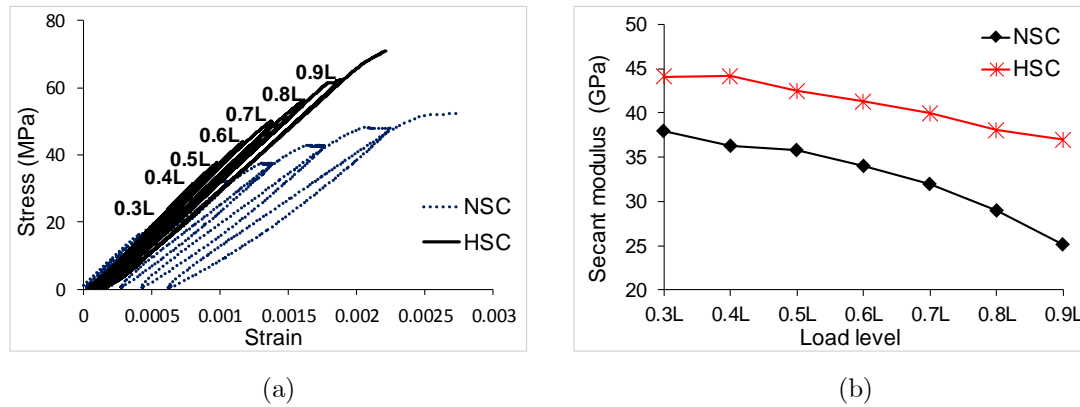
Figure 4.3: (a) Stress-Strain responses of concrete cubes (b) Secant stiffness as a function of load level

Contours of horizontal strain (ε_{xx}) obtained using DIC for both NSC and HSC cubes in the 0.4L, 0.7L and 0.9L states, are shown in Fig. 4.4. The formation of cracks is identified with the localization of strain. From the strain contours, in NSC, the localization of the strain into major cracks is evident at 70% of the compressive strength. At the corresponding load level (0.7L state), a significant lower level of damage associated with microcracks and small cracks are seen in HSC. At 0.7L, visible cracking could not be identified in HSC. At 0.9L, there is significant cracking associated with large strains in NSC. A major crack is seen in HSC at 0.9L.
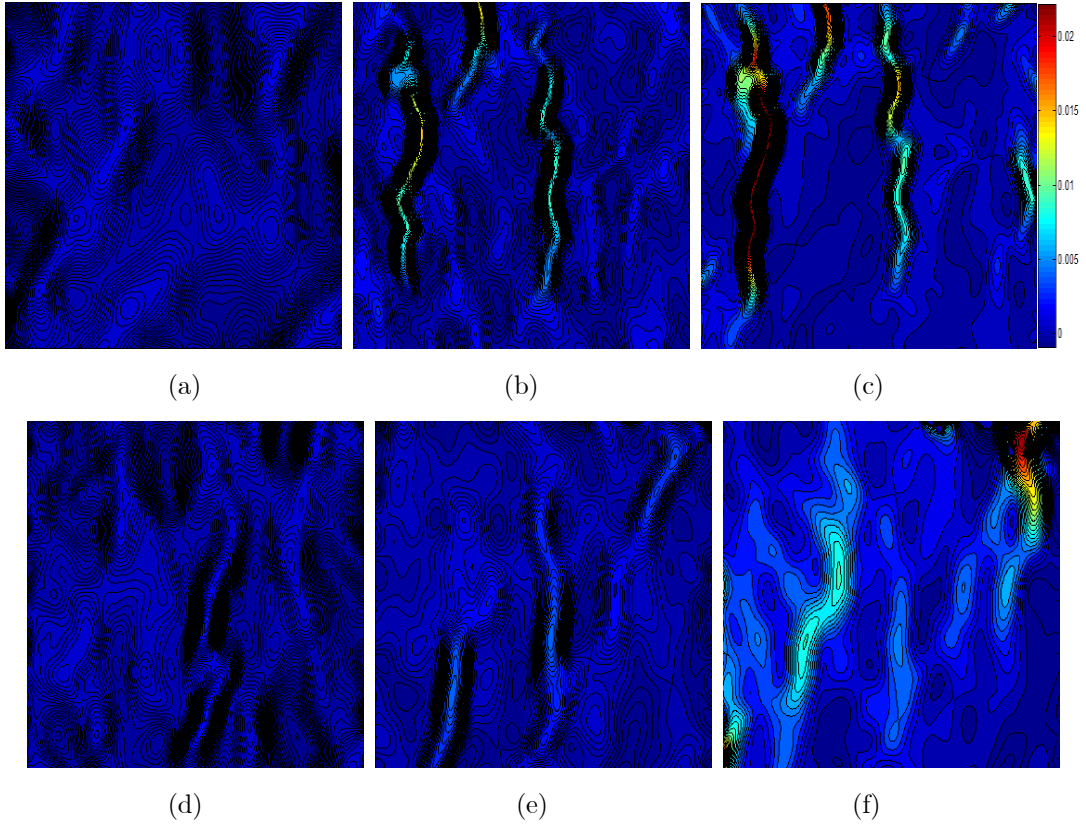
Figure 4.4: Strain contour $(\boldsymbol{\varepsilon_{xx}})$at different load levels obtained from DIC in different loaded states: NSC at (a) 0.4L (b) 0.7L (c) 0.9L; HSC at (d) 0.4L (e) 0.7L (f) 0.9L.

The average ε_{yy} (vertical strain) at the bottom and top of each load cycle obtained from DIC is shown in Fig. 4.5. The average ε_{yy} was obtained by averaging ε_{yy} from the DIC measurement across the entire front surface of the cube. The average strain at the top of a load cycle corresponds to strain due to load-induced stress and damage. The average strain at the bottom of the load cycle is indicative of plastic strain due to damage. There is no measurable plastic strain in both NSC and HSC up to 0.4L of the peak load (in the 0.4U state). As the loading increases, there is an increase in overall strain at the top of a load cycle and a steady accumulation of plastic strain upon unloading. The strain measures indicate a relatively larger plastic strain at corresponding load level (fraction of compressive strength) obtained from DIC measurements than from the surface mounted gages. This is due to the inclusion of localized

80

strains from cracking over the entire surface, which are accurately captured in the DIC measurements. After localization of damage, the surface gages may not detect the presence of the crack unless located over it, while it is reflected in the averaged surface measurement of DIC. The measurements indicate that NSC has a higher level of damage in the material when compared with HSC at the corresponding load level. In the 0.9U state, there is significant strain, on the order of 1000 $\mu\epsilon$ in the NSC. The strain in HSC in the 0.9U state is significantly smaller. Findings from DIC measurements suggest that the strain in the substrate is influenced by both the level of damage and the applied stress. Under applied loading, above 40% of the compressive strength, an increment in load would produce an increment of strain associated with both effects.
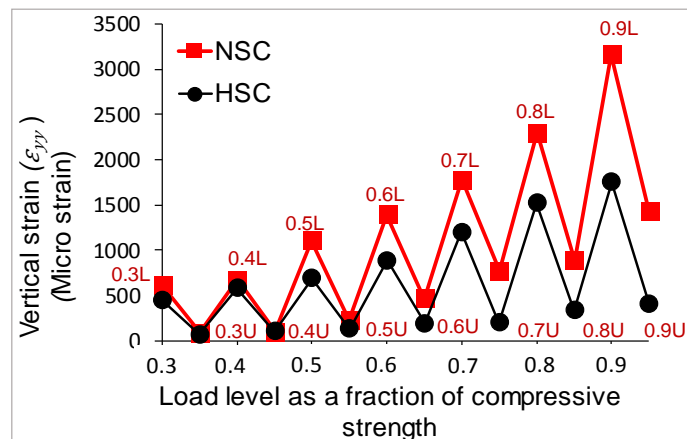
Figure 4.5: Average vertical strain ϵ_{yy} at different L and U states obtained from DIC

The level of damage in NSC and HSC can be assessed from LVDT and DIC measurements. The change in secant modulus (Fig. 4.3b) with incremental load at corresponding load levels with respect to the compressive strength is higher in NSC when compared with HSC. NSC exhibits significantly higher level of distributed microcracks at lower loads which coalesces to form visible cracks at 0.7L load level. In HSC, the overall level of damage was lower and

81

the failure was brittle with lower accumulation of plastic strains. Visible cracks do not appear till 0.9L load level.

The conductance signatures associated with the second resonant peak in the admittance response of PZT patch bonded to concrete cubes, for both NSC and HSC, at different levels of applied load are shown in Fig. 4.6. The conductance peak is associated with the second resonant peak is centred on 253 kHz and 255 kHz for NSC and HSC, respectively. Conductance spectra exhibit an increase in peak amplitude at successively higher load levels. There is also an overall increase in the amplitude at all frequencies. At corresponding load levels (fraction of compressive strength), larger shifts are observed in NSC when compared with HSC.

(a)   (b)
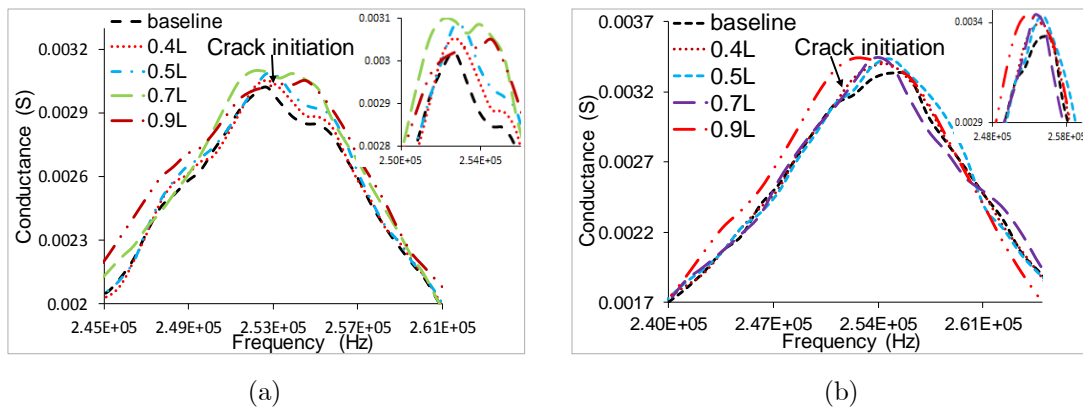
Figure 4.6: Conductance spectra close to second peak in the EI admittance response of PZT patch bonded to concrete cube at different levels of load (a) NSC cube (b) HSC cube

Changes in the second resonant peak in the conductance spectrum of the PZT patch bonded to concrete block after unloading from different load levels are shown in Fig. 4.7a and b for NSC and HSC, respectively. It can be seen that on unloading from successively higher load levels, consistently there is a leftward shift in the spectrum resulting from a larger relative decrease in amplitude at frequencies higher than the centreline frequency in the spectrum. The magnitude of shift and decrease in amplitude of the spectrum are

82

consistent with the level of damage indicated by the change in compliance and increase in substrate plastic strain obtained from mechanical measurements. For unloading from a given load level, the higher level of damage observed in NSC coincides with the larger shift in the spectrum and a larger decrease in amplitude of conductance. Visible crack appeared in NSC when the load level was 0.7L. There is correspondingly a larger shift in frequency to the left accompanied by a broadening of the peak. A slight flattening of the peak is also observed when the visible crack appeared. In NSC there is an abrupt change in the shape of the spectrum at 0.9L of the peak load, which produces significant peak broadening coinciding with significant localized damage in the form of visible cracking in the vicinity of the PZT. Visible cracking in HSC at 0.9L also produces significant decrease in amplitude and shift in the peak.

(a)   (b)
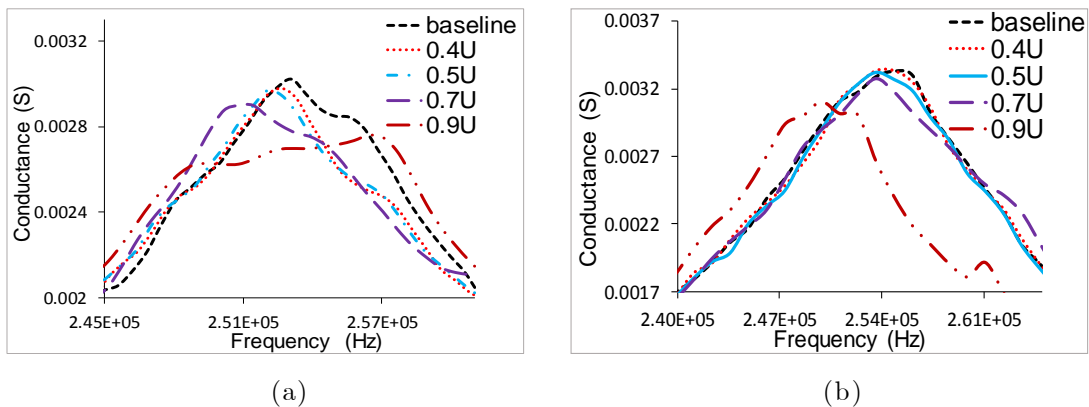
Figure 4.7: Conductance spectra close to second peak at different levels of damage (a) NSC cube (b) HSC cube

The susceptance part of the measured admittance spectrum obtained from an EI measurement of the bonded PZT patch in the U and L states is shown in Fig. 4.8a and b, respectively. The low frequency susceptance signature, which is related with the structural modes (or response) is also shown in the figure. The overall change in the slope of the low- frequency susceptance signature has previously been shown to be sensitive to stress under increasing loading

recorded from PZT patches bonded to thin aluminium specimens [27]. The slope of the low-frequency susceptance signature does not exhibit any significant or consistent variation with loading. Unlike the case of aluminium specimen, increasing stress level in concrete specimen is associated with an increase in the level of damage. The combined effect of increasing stress and damage in concrete may likely result in no change in the slope.
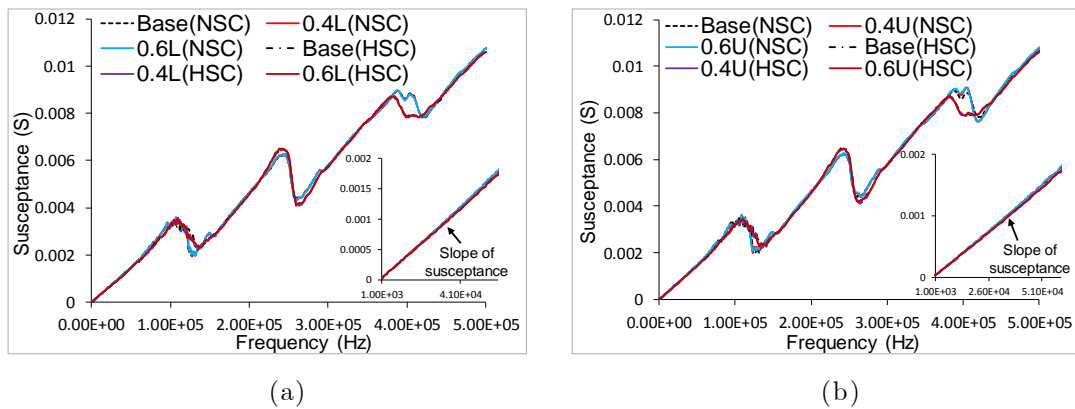
Figure 4.8: Susceptance signatures obtained from the admittance response from an EI measurement of bonded PZT in (a) L states; and (b) U states

The response of the PZT patch to an imposed strain was evaluated by applying small strains directly on the PZT patch. The PZT patch was subjected to an imposed strain using a digital micrometre. A photograph of the test setup is shown in Fig. 4.9a. The direction of applied strain in the PZT patch was kept the same as in the concrete specimen. The conductance signature of the second resonant mode of the bonded PZT patch for different levels of imposed strain is shown in Fig. 4.9b. The changes in peak of the conductance spectrum produced by imposed strains results in a shift in the central frequency to a higher value and an increase in the amplitude of the peak. The observed behaviour of the PZT patch confirms that an applied compressive strain influences the impedance response of a PZT patch resulting in a change in the resonant behaviour of the PZT patch. For a PZT patch bonded to a concrete

substrate, the incremental strain associated with an increment of load is expected to introduce an increase in the frequency and amplitude of the resonant peak in the electrical conductance response.
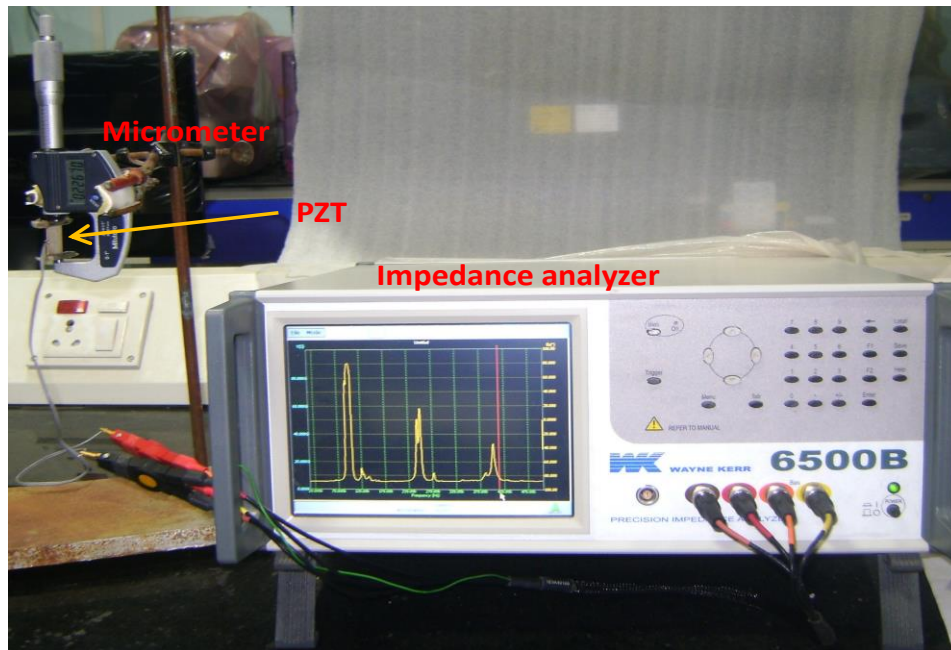
(a)
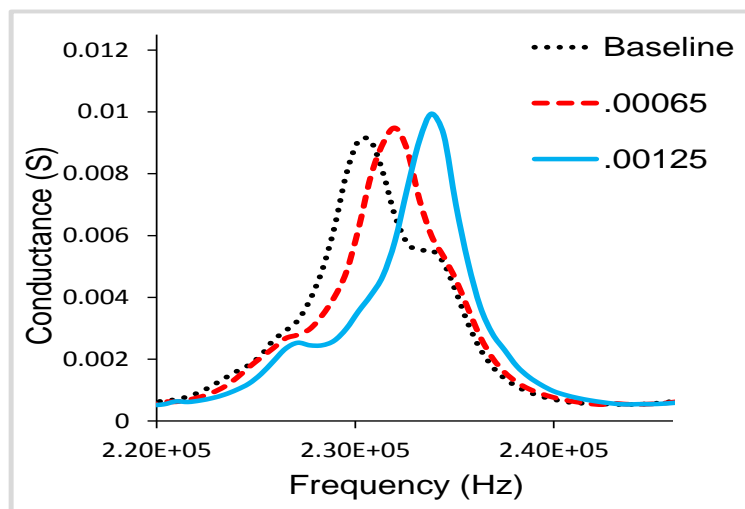
(b)

Figure 4.9: (a) Micrometer setup for imposed strain measurement; (b) Conductance spectra close to second peak of the PZT patch at different strain levels

85

Observations from the conductance signatures from all specimens were nominally similar. Some differences in the magnitudes of shifts in frequency and amplitude were observed, particularly in normal strength concrete at higher load levels. In the microcracking stages, prior to localization, the responses from the different specimens were consistent. After localization, the pattern of cracks is spatially heterogeneous. Proximity of the crack from the PZT patch had a significant influence on the observed behaviour. In some cases, the cracks formed directly under the PZT patch as shown in Fig. 4.10a. Cracking directly under the PZT patch impacts the bond between the PZT patch and the substrate resulting in reduction in the constraint from the substrate and hence resulting response is closer to the free response of PZT patch. This resulted in an increase in the amplitude and narrowing of the peaks in the conductance response as shown in Fig. 4.10b. Cracks passing under the PZT patch potentially produce splitting failure of the PZT patch as well.

(a)   (b)
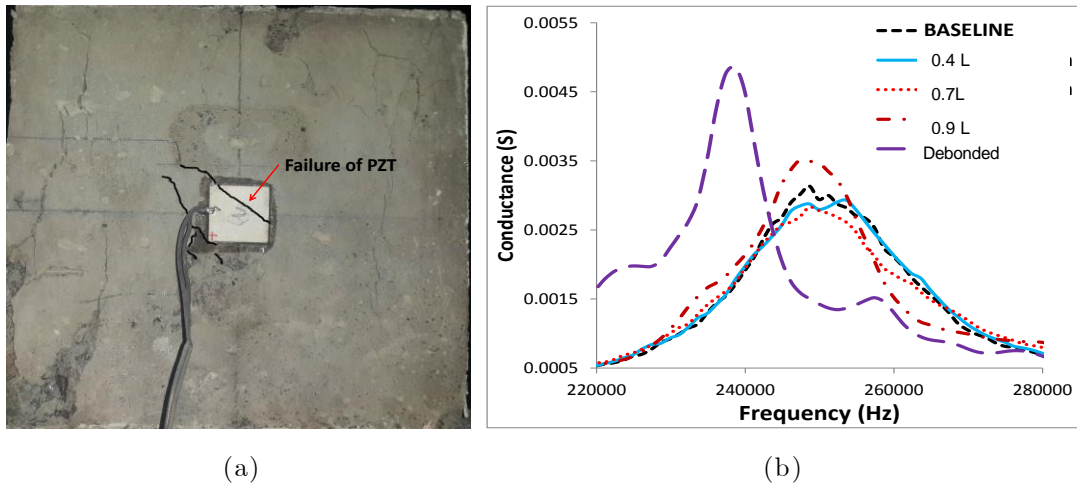
Figure 4.10: (a) Formation of crack in the proximity of the PZT patch (b) Increase in amplitude of the resonant peak in the EI conductance measurement.

4.5   Analysis of the results

The results of experimental program clearly indicate that the change in the measured conductance in the admittance response of a PZT patch bonded to a concrete substrate depends upon the level and type of damage and the stress in the substrate material. The observed changes in the PZT resonant peaks in the conductance spectrum can be interpreted in terms of considering the level of damage, stress in substrate material and strain in the PZT as shown schematically in Fig. 4.11. The increment in strain levels between two adjacent U levels is associated with an increment in the plastic strain. Between two adjacent U states, for a given change in the substrate plastic strain, the strain induced in the PZT depends on the material compliance of concrete. The compliance of the material also depends on the level of damage in the material. Further, the admittance spectrum from an EI measurement of the bonded PZT patch depends on the mechanical impedance of the substrate (and hence material compliance), which directly depends on the level of damage. Therefore, comparison of adjacent U states provides information about incremental levels of damage. A measure of the mechanical impedance of the substrate is obtained from the mechanical stiffness of the specimen. As the level of damage increases, there is an increase in the compliance of the material (and hence a decrease in its mechanical impedance). Consistently there is a downward shift in the resonant frequency to gather with an overall leftward shift in the spectrum recorded in the U states (shown in Fig. 4.7). The increase in the level of damage in the form of microcracks is associated with an increase in damping and an increase in compliance of the substrate, which produces a decrease in frequency of the peak. While the increase in material compliance produces an increase in amplitude, increase in damping results in a reduction in the amplitude of the peak. The amplitude variation in the resonant peak in

87

the conductance spectrum depends on the relative influence of damage on the elastic modulus and damping.

$d_n = n^{th}$ Damage state, n = 1,2,.. n
$\varepsilon_n = n^{th}$ Strain state, n = 1,2,.. n

(d_1, ε_1) 1L
(d_2, ε_2) 2L
(d_3, ε_3) 3L
1U $(d_1, \varepsilon_1 - \Delta\varepsilon_1)$
2U $(d_2, \varepsilon_2 - \Delta\varepsilon_2)$

Stress (GPa)
Time (S)
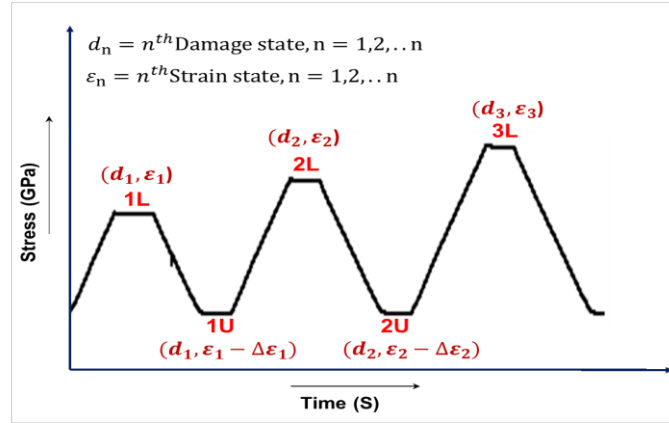
Figure 4.11: Schematic representation of strain and damage levels in substrate

On unloading the specimen from the L state to the U state, the stress in the substrate is reduced, while the level of damage is the same. In the L state, there is strain in the substrate associated with applied stress, in addition to the permanent strain produced by damage in the substrate. The strain in the substrate depends on the material compliance, which in turn depends on the level of damage. Since the level of damage is the same, comparing the L and the immediate U states allows for assessing the influence of stress in the substrate (and hence of strain in the PZT) on the EI response of a PZT patch for a given level of damage. A comparison of the conductance spectra from specimens at the top of the load cycle and after unloading from the load envelope is shown in Fig. 4.12. It can be seen that compared to the U state the corresponding L state exhibits an increase in the amplitude and a rightward shift in the spectrum. The results considering the increment in the PZT strain produced by applied stress in the substrate are consistent with the findings from direct application of strain on the PZT patch (shown in Fig. 4.9b). At the very high load level, corresponding to 0.9L, noticeable decreases in frequency and amplitude are observed in the unloaded state for both NSC

88

and HSC. The localized cracking in the vicinity of the PZT patch in NSC also produces a significant change in shape associated with broadening of the resonant peak. However, the level of damage is not that evident considering the response under load. The resonant peak in conductance spectrum from an EI measurement in the 0.9L state shows an increase in the amplitude and the observed changes are not so significant. The results indicate that the increment in the level of substrate stress has a dominant effect on the conductance of a bonded PZT patch.

(a)   (b)
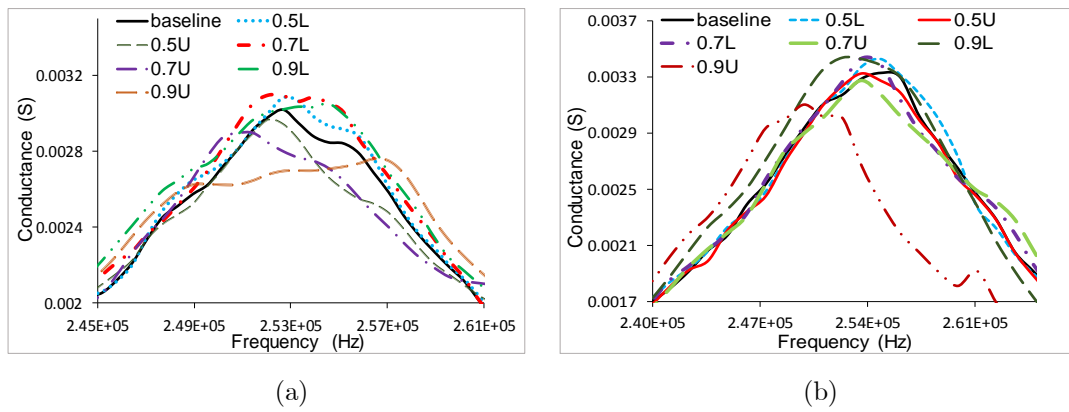
Figure 4.12: Conductance spectra close to second peak in the EI measurement of a bonded PZT patch from the L and the U states for: (a) NSC; (b) HSC.

The conductance spectra recorded at successively higher load levels correspond to the influence of change in mechanical compliance of substrate (produced by increasing material damage) and an increase in the induced strain in the PZT (produced by an increase in substrate stress). Strain induced in the PZT due to increasing stress in the substrate increases the amplitude of the conductance and produces a frequency shift to higher values. An increase in material compliance due to damage produces a leftward shift in frequencies, with a change in amplitude which depends on the relative influence of damping and increasing material compliance. The frequency shift in the EI spectrum is influenced by the counteracting effects produced by imposed strain and change

in material compliance. The shape of the spectrum is also influenced by level of damage and the imposed strain on the PZT.

4.5.1 Measures of quantification

A quantification of the observed frequency shifts and changes in the shape of the spectrum induced by applied stress and damage is now attempted. Measures of change include the shift in frequency, the change in bandwidth of the peak and the Root Mean Square Deviation (RMSD). A measure of the shift in frequency is obtained using the mean frequency measure of the resonant peak in the conductance spectrum.

$$f' = \frac{\int_{f_1}^{f_2} f Y_C df}{\int_{f_1}^{f_2} Y_C df} \tag{4.2}$$

Where Y_C is the conductance at a given frequency, f_1 and f_2 are fixed frequencies.

The mean frequency is the centroidal measure of the spectrum between two fixed frequencies. Shift in frequency, Δf is calculated using equation 4.3, where f_c' is the centroidal frequency of the spectrum and f_0' is the initial centroidal frequency.

$$\Delta f = |f_c' - f_0'| \tag{4.3}$$

The broadening effect of the peak at each damage level was quantified using bandwidth of the peak (BW). The bandwidth represents the distance between the two points in the frequency spectrum where the signal is $\frac{1}{\sqrt{2}}$ of the maximum amplitude (half power). The bandwidth is defined with respect to the full width at $\frac{Y}{\sqrt{2}}$ as shown in Fig. 4.13. Percentage change in bandwidth is calculated using equation 4.4.

$$\Delta BW(\%) = \frac{(BW_c - BW_0) * 100}{BW_0} \tag{4.4}$$
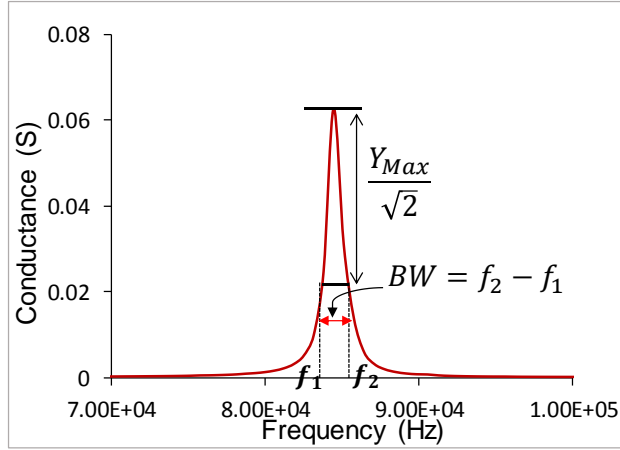
Figure 4.13: Bandwidth of resonant peak

The root-mean-square deviation (RMSD) is used to calculate the difference between values of baseline measurement of conductance signature and the signatures in the different L and U states. The RMSD for second resonant peak with respect to the baseline measurement were calculated in the frequency range (245 kHz-260 kHz) using equation 4.5, where.Y_{CB} and Y_{Ci} are the baseline and values of conductance at L or U states, respectively.

$$RMSD = \sqrt{\frac{\sum_{i=1}^{N}(Y_{Ci}-Y_{CB})^2}{\sum_{i=1}^{N}{Y_{CB}}^2}} \tag{4.5}$$

Fig. 4.14 shows the frequency shift of the conductance peak in the L and the U states. The frequency shift for the L and U states have been calculated with reference to the centroidal frequency recorded before initiating loading. While shifts are noticeable in the U states, there is no change in centroidal frequency in the L states. For both NSC and HSC there is a continuous frequency shift after 0.4U. There is a consistent increase in the centroidal frequency, with increasing damage level in the successive U states. The frequency shift in the U states follows a trend which is similar to the observed decrease in stiffness obtained from mechanical measurements; there is an exponential shift at higher load ratios in NSC, while the HSC exhibits a linear increase. At higher level of damage, the peak was flattened and there was no distinctive peak. The centroidal frequency therefore provides a good indication of damage level in

91

the U state. The insensitivity of resonance peak frequency shift in the L states is due to the combined influence of damage in the substrate and imposed strain on the PZT, which produce counteracting effects.
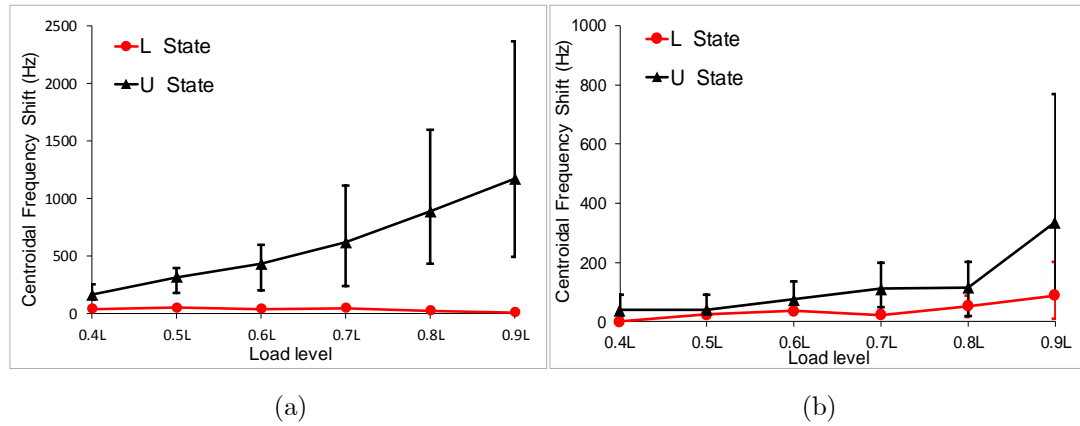
Figure 4.14: Frequency shift in resonant mode with unloading in the U states (a) NSC (b) HSC.

Change in the RMSD values for the L and U states in NSC and HSC are shown in Fig. 4.15. The RMSD values obtained in both the L and U states are generally in agreement for loads higher than after 70% of the compressive strength. While the RMSD values obtained from the L states are essentially constant up to 0.7L. The magnitude of change in the U states at any load level is higher in NSC than the corresponding change observed in HSC. The RMSD values in the U states have previously been shown to correlate well with the damage level. The RMSD value obtained in the L state is reflective of both damage and imposed strain. The observed trend in the RMSD indicates that the influence of imposed strain and damage produce counteracting effects. The influence of damage is evident after 0.7L. Thus it can be concluded in the presence of imposed strain, RMSD shows a change only at very high levels of damage in the material. At low stress levels, the counteracting influences of damage and stress produce little or no change in the RMSD.
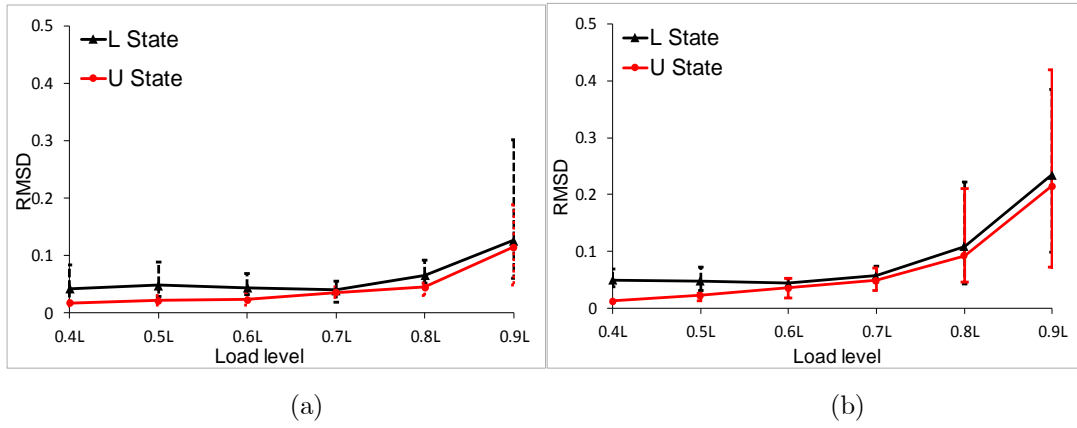
Figure 4.15: RMSD of resonance peak at L and U states: (a) NSC cube (b) HSC cube

The changes in bandwidth of the conductance spectrum in the U and L states for NSC cube are shown in Fig. 4.16. No change was obtained in the bandwidth for HSC cubes up to very high load levels. This suggests that the change in bandwidth is more related to localized damage as observed in NSC specimen. In NSC cubes, the bandwidth measured in the U states indicates a continuous increase with an increase in damage level. In the L states, the increase in bandwidth is minimal at low stress levels and an increasing trend can be observed under higher load ratios. Thus the strain dominant and damage dominant effect on conductance signature can be differentiated from the change in bandwidth.
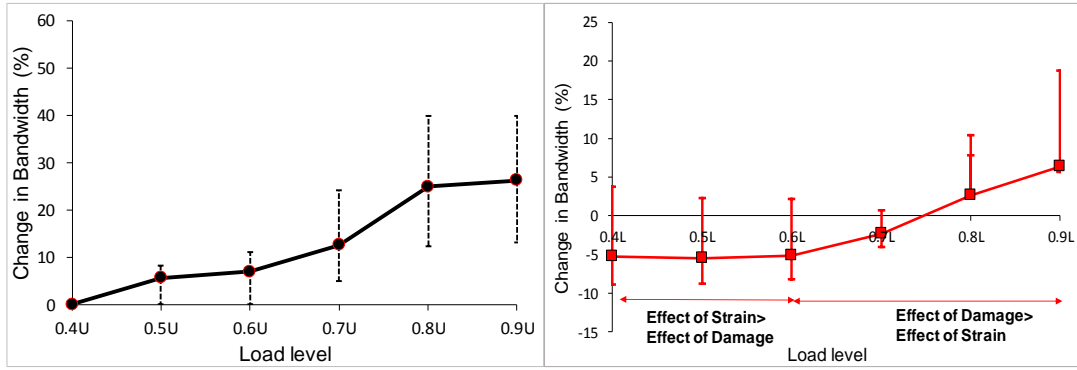
(a)   (b)

Figure 4.16: Percentage change in bandwidth in the (a) U states; and (b) L
states

4.5.2 Identification of Stress induced damage

A measure of normalized conductance given in equation 4.6 is introduced to
identify the amplitude shifts from the baseline signature produced by damage
and induced strain.

$$Normalized\ conductance\ signature\ (Y_{CN}) = \frac{Y_{Ci} - Y_{CB}}{Y_{CB}} \tag{4.6}$$

where Y_{Ci} is the conductance at a given frequency in the L or U states and Y_{CB}
is the corresponding baseline conductance. Fig. 4.17 shows the normalized
conductance signature at different load levels for NSC and HSC. The strain
induced conductance changes can be clearly identified from the normalized
conductance values. An upward shift can be seen qualitatively in the
normalized signature from the L states. Consistent shifts are produced with
increasing stress level in the substrate, irrespective of damage level. The
magnitude shift of normalized signature in the L states for HSC cube is lower
even than the shifts observed in the NSC cubes at the corresponding load
levels. This can be correlated with the overall lower strain in the L states in
HSC as seen in Fig. 4.5.
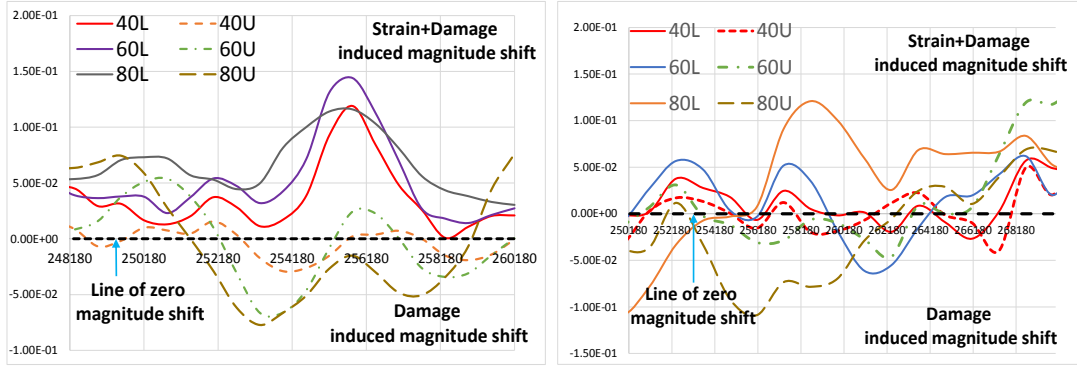
Figure 4.17: Conductance (Normalized) signature in the different L and U states: (a) NSC; (b) HSC

To quantify the observed shifts in the normalized conductance signature, the centroid of the normalized conductance, Y'_{CN} was computed as shown in equation 4.7.

$$Y'_{CN} = \frac{\int_{f_1}^{f_2} Y_N^2 df}{2 \int_{f_1}^{f_2} Y_N df} \tag{4.7}$$

where f_1 and f_2 are fixed frequencies

The trends in the values of Y'_{CN} in the L and U configurations are shown in Fig. 4.18a and b for NSC and HSC, respectively. The influence of strain in the substrate can be clearly identified with a positive shift (an upward movement) of the centroid. The magnitude of the shift in the L states corresponds with the level of stress in the substrate; a larger shift is observed in NSC when compared with HSC. With an increase in the substrate stress, up to 0.7L in NSC and 0.9L in HSC, there is an upward shift in Y'_{CN}. The values of Y'_{CN}, upon unloading to the U states show no change. The difference between the L and the immediate U state is the imposed strain in the PZT due to stress in the substrate. Comparing two U states, there is an increase in the level of damage, which produces additional plastic strain and an increase in material compliance. The counteracting influences of increase in material compliance

95

and increasing plastic strain (and hence imposed strain on PZT) result in no shift in the centroid of the normalized amplitude.

Localization of damage and the formation of a crack produces a downward shift in the Y'_{CN}, which occur close to 0.7L and 0.9L in NSC and HSC, respectively. The crack formation produces an overall downward shift in the centroid in both the L and U states. The downward movement of centroid in the L states shows that the influence of damage is more dominant on resonant peak behaviour after the localization into a visible crack.

(a)   (b)
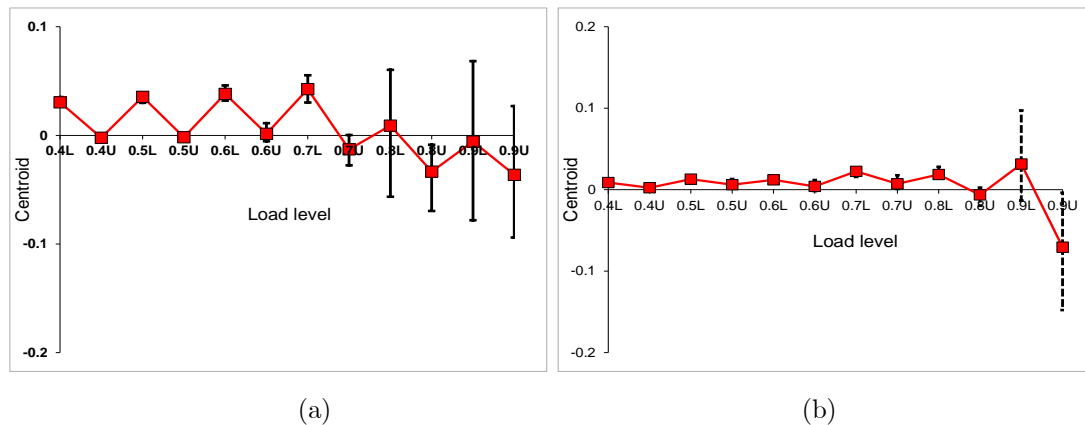
Figure 4.18: Position of centroid in the L and U states (a) for NSC; and (b) HSC

The effect of stress and microcrack damage can be decoupled using the normalized conductance signature as a quantitative measure. The absolute value of centroid of the normalized spectrum associated with the second resonant peak of a PZT bonded to a concrete substrate curve gives the identification of stress and microcrack damage induced change. The downward shift of the centroid can therefore be taken as indicator of localized damage in the form of cracks. The upward shift of the centroid is indicative of increasing stress in the substrate.

4.5.3 Identification of Damage and Strain

The results of the quantitative analysis can be assimilated to provide an understanding of the influence of damage and stress. The influence of increasing damage in the material substrate can be identified with three effects: (a) increase in material compliance; (b) increase in plastic strain; and (c) increase in material damping. While increase in material compliance effects a leftward shift in spectrum, the increase in plastic strain (increases the imposed strain on PZT) produces a rightward shift. In the absence of stress in the substrate, such as in the U states, while there are counteracting influences of the two effects, the influence of decrease in compliance is dominant producing a net shift in frequencies (as seen in Fig. 4.14). Considering the three effects of damage while (a) and (b) produce an increase in the amplitudes, damping produces a decrease in the amplitude. In the absence of stress, the influence of these counteracting effects is to produce no change in the amplitude centroid of the spectrum (as seen in Fig. 4.18).

Stress in the substrate produces an imposed strain in the PZT, which produces an increase in the frequency and the amplitude. For a given level of damage, on increasing the stress in the substrate, there is a net increase in the amplitude of the spectrum and no shift in the centroidal frequency of the spectrum.

4.6 Findings and Summary

The use of EI-based monitoring of concrete structures is evaluated in this study. Damage in concrete has been evaluated using full-field displacement measurements on the surface of a concrete cube obtained from digital image correlation. The evolution of micro- cracks, which coalesce leading to localization of damage in the form of cracks is shown to correlate with conductance obtained from EI measurements from a PZT patch bonded to the

concrete substrate. The results of the experimental program presented here clearly show that the conductance spectrum obtained from the EI measurement of a bonded PZT patch reflects changes in the local mechanical compliance of the substrate due to damage. Damage in the form of microcracking is found to influence the conductance through a change in substrate compliance. Increasing damage is shown to produce a decrease in the magnitude and frequency of the resonant peak of the PZT patch in the electrical conductance spectrum of the bonded PZT patch.

Imposed strain resulting from stress in the substrate is also shown to influence the conductance signature from an EI measurement of the bonded PZT patch. Increments in imposed strain in concrete are produced by increments of stress and level of damage in the material. Change in imposed strain on the PZT patch produces changes in the resonant peak which are counteracting to the influence of damage. In the presence of stress, the observed change in the resonant peak signature in the conductance spectrum did not show any significant changes for low levels of damage associated with microcracking. With an increase in stress, as the damage in the material increases in a non-linear manner, the influence of damage is reflected in most measures of damage such as the frequency shift, RMSD and band width calculated from the resonant peak. At low levels of damage, associated with distributed microcracking, the normalized conductance peak signature accurately reflects the level of stress in the substrate.

The use of EI measurements for evaluating damage in a concrete substrate requires careful consideration of the stress in the substrate in addition to the type and level of damage. An increment in the magnitude of stress is associated with an increment in the strain and also the level of damage. The presence of damage and the type of damage also influence the strain in the substrate for a given applied stress. Localization of damage in the form of cracks results in

a non-linear increase in strain in the substrate. The behaviour of the bonded PZT patch is influenced by the substrate compliance as influenced by the amount and type of damage. The localization of damage in the form of cracks is reflected in the non-linear decrease in the mechanical stiffness. Therefore, the extent and type of damage influence both the strain in the substrate and the mechanical compliance of the substrate.

In a real structure, the possibility of unloading to establish the true level of damage without the influence of applied stress does not exist. Features of the resonant peak in the conductance spectrum of a bonded PZT patch are indicative of the state of substrate in terms of the level of strain and the type and extent of damage. At low levels of damage, the increment in the substrate stress can be identified using the shifts in the normalized conductance signature. In a loaded state, localization of damage and formation of cracks can be identified using the shifts in the bandwidth of the resonant peak and the downward shift in the centroid of the normalized conductance signature.

Chapter 5

PZT Sensor Array for Local and Distributed Damage Measurements in Concrete

5.1   Introduction

PZT (Lead Zirconate Titanate) is a piezoelectric material, which is being used for developing economical methods for continuous damage assessment in structures. PZT exhibits a coupled electromechanical response; surface charges are produced when strained and strain when electrically excited. PZT-based sensors offer significant potential for continuously monitoring the development and progression of internal damage in concrete structures. Several damage detection strategies have been developed using PZT patches bonded to a substrate [32, 37, 52-54, 56, 72, 87, 88]. The use of PZTs has been primarily focused on metallic and composite structures with very limited application to concrete. The use of PZT patches in concrete structures is still evolving.

The EI measurements use the measured electrical response of a PZT patch bonded to a substrate. The EI response of each PZT to a given electrical input is influenced by the resistance to its motion offered by the substrate material, the mechanical impedance [3, 5, 25]. The use of a PZT patch to infer about the level of damage in the substrate requires interpreting the EI response of

the PZT patch bonded to the substrate. When a PZT patch is bonded to a substrate, the dynamic motion of the PZT patch in response to an applied electrical potential depends on the dynamic mechanical impedance to its motion provided by the substrate. Understanding the response of PZT patch bonded to a concrete substrate is still progressing. The application of EM impedance measurements to concrete structures has demonstrated that changes are registered due to formation of cracks well in advance of failure [18]. The EI -based measurements from concrete have been shown to be sensitively detect changes in the local material compliance produced by distributed damage in the vicinity of the sensor [Chapter 4]. For a PZT patch bonded to a concrete substrate, its motion at a given frequency is directly influenced by a zone of influence, which represent a finite volume of the material. The EM based measurements from a concrete substrate are shown to be sensitive to incipient distributed damage in the material within the zone of influence [Chapter 3]. A smaller zone of influence and higher sensitivity to local changes increases at higher frequencies. The EI measurements therefore provide a local measure of damage in the vicinity of the sensor.

The coupled constitutive electro-mechanical response of piezoelectric material allows a PZT patch to be used as an actuator for generating stress waves in the substrate material and as a receiver for sensing stress waves. The PZT patches are used as actuator/receiver (AR) pairs for generating and receiving stress waves. In the distributed sensing mode, damage in the material is inferred through changes in the elastic waves which propagate through the bulk material [44, 48, 55]. Presence of cracks in the wave propagation has been shown to significantly alter the wave characteristics [53, 89-91]. Most of the studies of PZT based distributed monitoring were reported on metallic structures. The condition monitoring of concrete infill in fiber reinforced polymer tubes and failure in concrete and composite structures has been

monitored using PZT sensor arrays [53, 56, 92, 93]. Most of the researchers used time of flight and decrease in wave energy to assess the change in material characteristics.

In concrete, damage initiation takes place in the form of distributed micro cracks, which eventually coalesce to form localized cracks. Cracks in concrete are associated with cohesive crack bridging stresses. By the time surface manifestation in the form of visible cracking appears there may be significant degradation of the capacity of the structure. Early detection of damage is essential to initiate early intervention measures, which can effectively increase the service life of a structure. Methods to detect incipient damage in the form of micro cracks are required to provide effective methods of monitoring structural health and service life performance of structures. Procedures for locating cracks in concrete and for assessing the depth of opening of these cracks is critical for evaluating the degradation of concrete structures.

Localized sensing methodology based on EM impedance technique provides information about changes in the local material, which produce changes in its compliance in the vicinity of PZT patch. Any damage located away from the sensing range of a PZT patch would not be detected in its EI signature. In concrete structures where large volume of material has to be monitored a large number of PZTs is required for local sensing. Sensing methodology using pairs of PZT patches for monitoring changes in the stress wave gives can be used for distributed sensing over a larger region. Local sensing technique (EI) can be employed to detect the damage in the vicinity of the PZT patches while distributed sensing using PZT sensor arrays can be used to monitor the location and the magnitude of damage in a region. The concept of array of sensors which combines both local and distributed sensing using minimum number of sensors provides detailed interpretation about the damage.

A sensing scheme using an array of PZT sensors for combined local and distributed damage monitoring is developed. Surface mounted PZT patches are used for continuous local monitoring of concrete and obtaining the information related to damage in the vicinity of the patch. Additionally, the PZT sensor array is used for monitoring damage in the actuator-receiver (AR) mode. The results of an experimental evaluation involving the use of a fracture test specimen are presented and issues related to the development of proposed system are evaluated for the case of localized damage in the form of a crack in concrete. The sensitivity of the EI -based local measurements and the through transmission measurements to a localized crack in concrete is evaluated.

5.2   Background

Piezoelectric materials exhibit electro-mechanical coupling characteristics; electric charges are produced when mechanically stressed and strain when electrically excited. PZT patches are piezoceramic materials which have high electro-mechanical coupling properties. The electrical admittance signature of the PZT patch can be measured when it is excited with a voltage of alternating frequency. The electrical admittance is a complex number consisting of real and imaginary parts and is determined as the ratio of the current to the applied voltage. The conductance response (real part of admittance) of the PZT patch (20x20x1 mm size) when excited with 10-500 kHz frequency of 1V amplitude is shown in Fig. 5.1. The peaks in the conductance response can be identified with the resonant modes of the PZT patch [3, 6]. The mechanical and the electromechanical resonances happen at the same frequency in a piezoelectric material because of the electro-mechanical coupling. The electro-mechanical resonance frequencies of the PZT patch depends on the mechanical resonances which in turn depend on geometry of the patch [94].
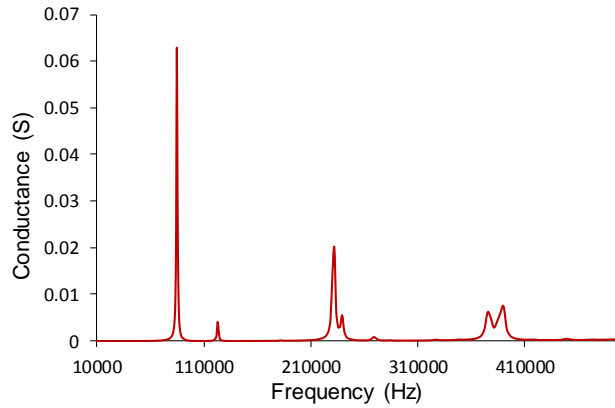
Figure 5. 1: Conductance spectrum of free PZT patch (patch size: 20mm x 20mm x 1mm)

The EI response of a PZT patch bonded to the substrate subjected to an applied electrical potential depends on the dynamic impedance to its motion from the substrate. The resistance to the motion of a PZT patch from the surrounding elastic medium is expressed as the mechanical impedance. Most approaches for modeling the PZT patch-structure interaction have varied in the degree of sophistication in representing the motion of the PZT patch and the structure. The first systematic attempt to model the PZT patch-structure interaction was presented by Liang et al. [3] using a PZT actuator driven one-degree-of-freedom spring-mass-damper system. Subsequently for a PZT patch, an effective 1-D approach was found to give a better representation of the dynamic response of the PZT considering in-plane motion of the PZT coupled to an elastic substrate [7].

A change in the mechanical impedance of the surrounding medium will change the electrical impedance response of the PZT patch. For a concrete substrate, the effective dynamic response of the PZT patch was shown to be influenced by the damping and the stress in the substrate. Considering high damping of concrete, the dynamic response of a PZT patch exhibits a frequency dependence. The vibratory motion of the PZT patch is influenced by the mechanical impedance derived from a zone of finite size. For a PZT patch

104

bonded to the concrete substrate, the dynamic response, which consists of distinct modes of vibration of the PZT patch is significantly influenced by the compliance of the material within a zone of influence. The zone of influence for the vibratory motion of a bonded PZT patch depends on the frequency of vibration; the zone of influence is smaller for higher frequencies [Chapter 3]. Any changes in the material compliance within the zone of influence, influences the vibratory motion of the PZT patch. Distributed damage produces an increase in the compliance and material damping of the material. Both these effects are known to produce a downward shift in frequency and decrease in amplitude of the resonant mode.

In this study, an array of surface mounted PZT patches were used in a substrate. EI-based measurement method is used as local measure of damage detection as shown in Fig. 5.2. An array of PZT patch sensors is deployed in a structural element, where impedance response of the PZT patch is used for local monitoring while the through transmission measurements are used for distributed sensing. Each PZT patch is used as an actuator and a sensor in the through-transmission measurements. A schematic representation of the methodology is given in Fig. 5.2. A received signal undergoes the losses due to signal propagation path and in epoxy at the concrete-beam interfaces. Measures for quantifying changes in the EI and the received waves due to damage in the form of stress-induced crack are developed for the level of material discontinuity produced by a stress-induced crack of a given opening.
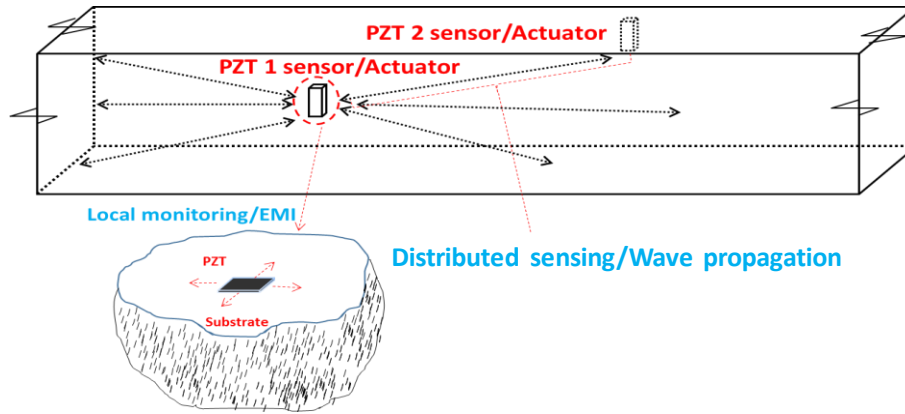
Figure 5. 2: Schematic representation of local-distributed monitoring system.

5.3   Materials and Methods

Concrete used in this study had a composition by mass given as cement: water: fine aggregate: coarse aggregate = 1.0: 0.45: 1.85: 2.9. Coarse aggregate consisted of 20 mm and 10 mm crushed gravel in a 1:1 proportion and river sand was used as fine aggregate. Cement conforming to the requirements of OPC grade 53 as per the Indian code of practice, IS 12269:2013 was used. The 28-day compressive strength and modulus of rupture obtained by testing standard 150 mm cubes and 500 mm x 150 mm x 150 mm sized beams were 50 MPa and 3.6 MPa, respectively.

The experimental program consisted of using PZT patches in the distributed (AR) mode and for local impedance-based measurements on beams where the damage is induced in the form of a localized crack. A fracture beam was used to produce a crack under flexure loading. The experiments were conducted using six beams of size 500 mm x 150 mm x 150 mm. All the beams were made with plain cement concrete. A notch, 25 mm in depth was introduced in the middle and fracture tests were performed using a computer-controlled, servo–hydraulic testing machine in crack mouth opening displacement (CMOD) control. The test setup consisted of third point loading as per the requirements of UNI 11039-2:2003 standard [97]. The flexure test was conducted with a span equal to 450 mm in four-point bending configuration

where the CMOD was increased at rate of 30 µm/minute. During the test, the crack tip opening displacement (CTOD) was also measured using a clip gauge mounted at the tip of the notch. The complete test set up along with sensor locations is shown in Fig. 5.3a. Six square 20 mm PZT patches of 1 mm thickness were used in the study. Properties of the PZT are given in Table 3.2. Two PZT patches were bonded on front face and two on back face, remaining two were bonded to the soffit of the beam. The PZT patches labelled PZT5 and PZT6 were positioned at the bottom of the beam 50mm away from the notch while all other PZT patches were bonded at mid-height of the beam. The PZT patches labelled PZT2 and PZT4 were bonded at a mid-height location, 75 mm from the bottom of the beam and 50mm from the center. The PZT patches labelled PZT1 and PZT3 were bonded at the mid-depth location on opposite faces of the beam at a distance 50 mm away from the opposite side face of the beam. All the PZT patches were bonded to concrete using a two component epoxy. The properties of the epoxy are given in Table 3.1. The detailed configuration of the PZTs is given in Fig. 5.3a.

The test program consisted of incremental loading to larger crack opening; the beam was progressively loaded to predefined increasing values of CMOD. The loading program is shown schematically in Fig. 5.3b. Initially the beam was loaded up to a CMOD equal to 50µm and unloaded. In subsequent load cycle, the specimen was loaded to CMOD values equal to 100 µm relative to the CMOD in the unloaded configuration. In subsequent load cycles, the CMOD was increased to values equal to 250µm and 450µm with respect to the residual crack opening from the previous load cycle. In the following text, the load cycles are referred to by the maximum relative CMOD in each cycle. The first, second, third and fourth load cycles are referred to by the maximum relative CMOD values equal to 50µm, 100µm, 250µm and 450µm, respectively.
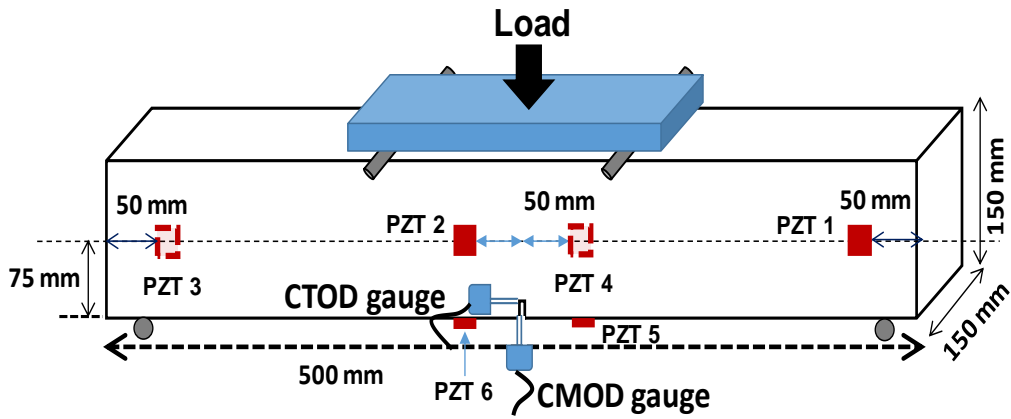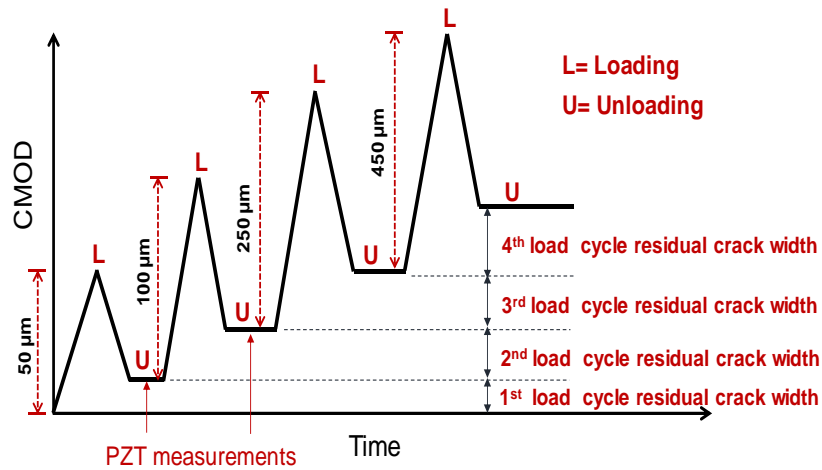
Figure 5. 3: (a) Test set up along with configuration of PZT patches (b) Cyclic
loading to increasing CMOD.

The measurements from the PZT patches consisted of EI measurements from
the individual PZT patches and through transmission measurements from
pairs of PZT patches in the AR mode. A schematic sketch of the test setup is
shown in Fig. 5.4. The impedance and wave propagation measurements were
taken after unloading from the predetermined value of CMOD. The
experimental set up for EI and the AR measurements consisted of an
impedance analyzer, function generator, amplifier, digital storage oscilloscope
and a computer. In the AR mode, the waveform generated by the function

generator was amplified and sent to the actuator PZT. Then, the response signal of the remaining five PZTs were logged by the computer through computer controlled digital storage oscilloscope. After acquiring wave propagation data from all the PZTs, the actuator PZT is switched to the impedance analyzer through switching unit and the admittance measurements were recorded. Electrical admittance measurements were performed on all the PZTs before attaching to the beam. The electrical admittance measurements of the PZTs were measured at an applied voltage of 1 V at 800 discrete frequencies varying between 10 kHz and 500 kHz using a 6500B series impedance analyzer of Wayne Kerr make. A typical conductance (real part of admittance) signature of the a PZT patch bonded to beam is shown in Fig. 5.4. This measurement procedure was followed when the specimen is in unloaded state after each load cycle (unloading from CMOD openings equal to 50µm, 100µm, 250µm and 450µm, relative to the previous unloaded configuration).
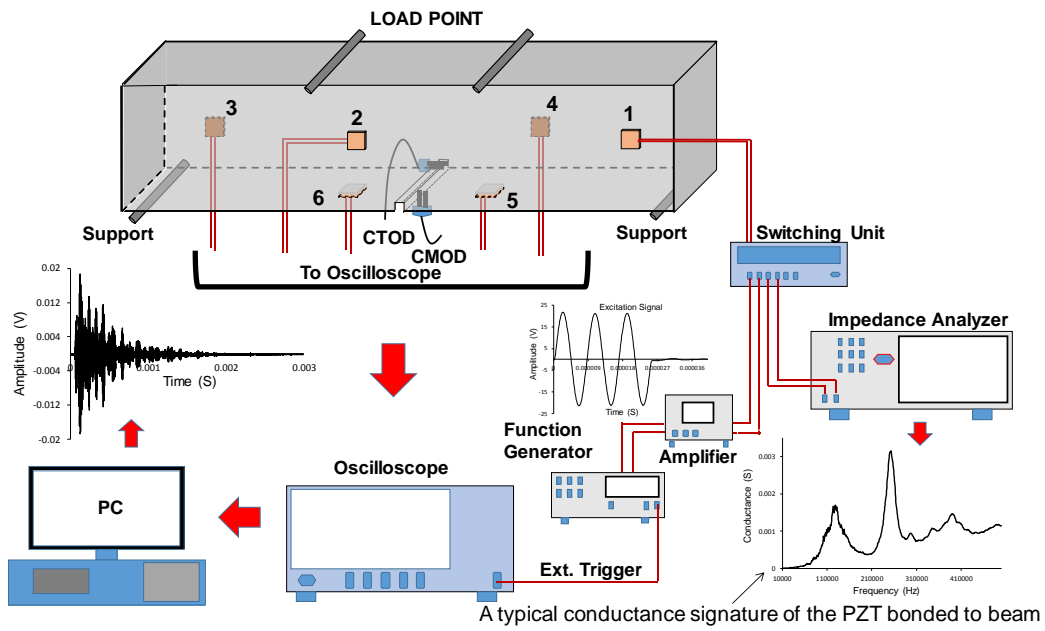
Figure 5. 4: Experimental setups for EI from individual PZT patches and through transmission measurements from pairs of PZT patches in the AR mode. In the AR mode, wave propagation measurements, the excitation applied to the PZT patches consisted of a 3-cycle tone burst sine signal with center frequency of 120 kHz with a 45 V peak-to-peak voltage at a pulse repeating frequency equal to 100 Hz (Fig. 5.5a). A typical received signal when actuating PZT 1 and received at PZT 2 (A_1R_2) is shown in Fig. 5.5b. All the six PZT patches were individually excited and the response from the all other PZT patches were collected at a sampling frequency of 6.25 MHz.

(a)   (b)
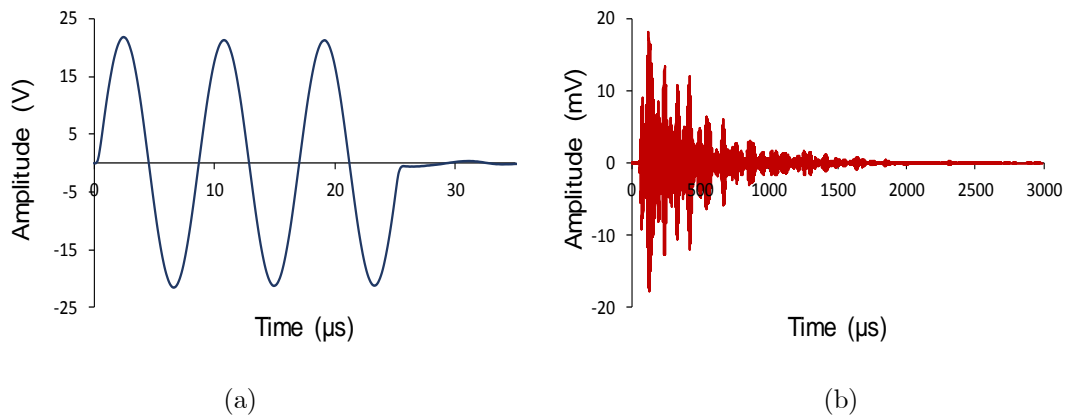
Figure 5. 5: Signals from a through-transmission measurement in the AR mode:
(a) The excitation signal applied to the actuator (b) The received signal at
PZT2 when actuating PZT1 (A_1R_2)

During the loading cycles, the surface displacements from the beam were
obtained using the full-field optical technique based on digital image
correlation (DIC). DIC measurements were performed on notched specimens
to monitor the localization of damage and the subsequent propagation of a
crack. A detailed description of DIC measurement system is discussed in
section 4.3 of Chapter 4. A schematic representation of the DIC setup is shown
in Fig. 5.6.
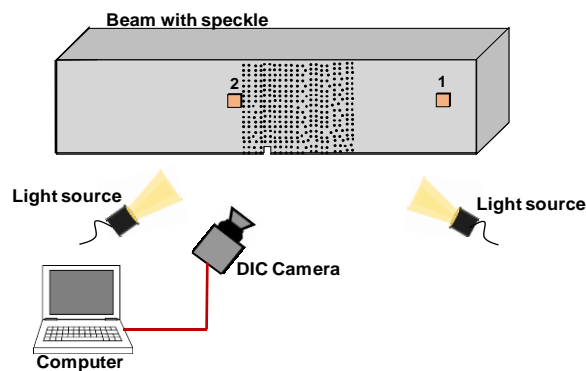
Figure 5. 6: Schematic representation of the DIC setup

5.4   Experimental Results

The load-CMOD responses of the three beam specimens are shown in Fig. 5.7a and a typical load-CMOD responses of the beam is shown in Fig. 5.7b for clarity. The beam was tested in four stages. In each stage, the beam was loaded in CMOD control to a predetermined crack opening relative to the beginning of load cycle and then unloaded to zero load. The EI and wave propagation measurements were taken in the unloaded configuration. The quasi-static load response can be readily identified with the load envelope obtained from the load cycles. The peak load of the envelope load response is attained in the first load cycle. CMOD equal to 50µm is in the post-peak part of the softening load response. There is a continuous increase in the residual CMOD on unloading after each loading cycle. There is also correspondingly a decrease in the stiffness of the load-CMOD response. With every subsequent load cycle, the peak load attained is also smaller.
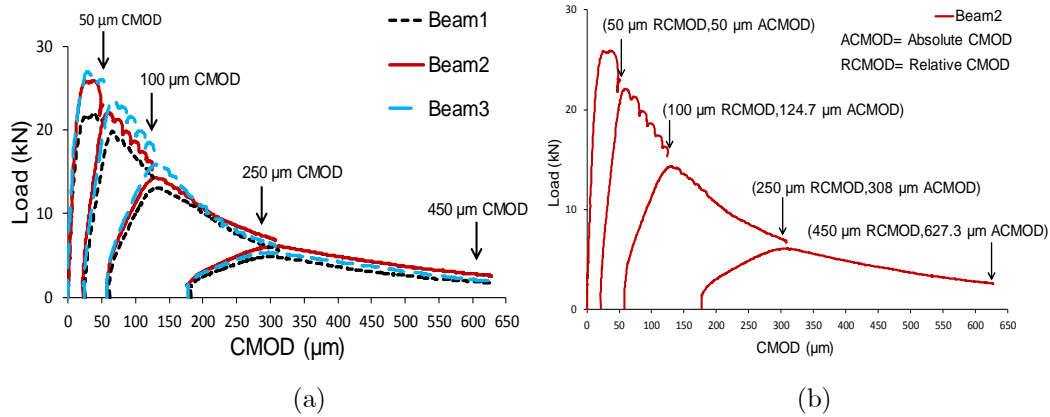
Figure 5. 7: (a) Load-CMOD responses of beams; (b) Load-CMOD of Specimen Beam 2. The CMOD relative to the residual CMOD for each cycle are shown. The absolute value of CMOD at the end of each cycle is also indicated in the bracket.

Contours of horizontal strain (ε_{xx}) from the beam specimen 2 at different CMOD values obtained using DIC are plotted in Fig. 5.8. The contours of

strain are plotted at the top of the load cycle, just prior to unloading. Localization of the strain can be identified in all the contour plots. The location of the crack can be clearly identified even at a small CMOD equal to 50µm. The localized zone propagates along the depth of the beam with increasing CMOD. While the crack could be identified in the contours of ε_{xx} even at a small CMOD of 50µm, the crack could not be delineated visually up to a CMOD of 124µm. There is a sharp gradient in strain within a small region centered on the crack. In the region in the immediate vicinity of the PZT patch, the magnitude of strain is very small and there is no visible damage which produces variation in the measured strain. There is also no visible damage in the form of micro cracking in the region away from the crack.

(a)　　　　　　　(b)　　　　　　　(c)　　　　　　　(d)
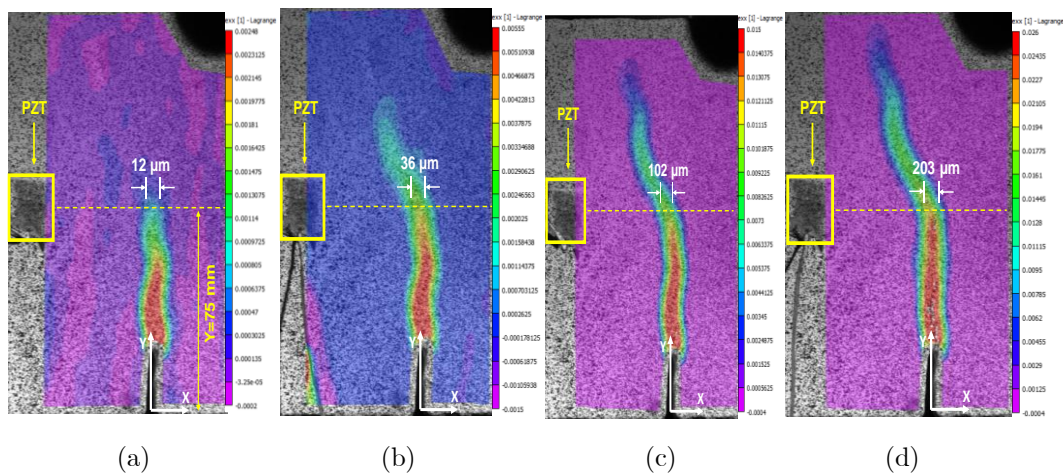
Figure 5. 8: Strain contour ($\boldsymbol{\varepsilon_{xx}}$) at different CMOD levels (a) 50 µm (b) 100 µm relative to unloading after first load cycle (up to an absolute CMOD equal to 124.7 µm) (d) 250 µm relative to unloading after second load cycle (up to an absolute CMOD equal to 308 µm) (e) 450 µm relative to unloading after third load cycle (up to an absolute CMOD equal to 627 µm)

The horizontal strain (ε_{xx}) along length of the beam at the mid-height location along a line with Y coordinate fixed at 75 mm above the bottom face and 50 mm above the notch for various CMOD levels are shown in Fig. 5.9. The variation of ε_{xx} along the length shows a sharp increase in the magnitude of

113

strain indicating localization of strain. It is observed that the width of the localization remains relatively constant with increasing crack opening. There is however an increase in the magnitude of strain and there is also a sharper strain gradient within the region of localization with increasing CMOD.
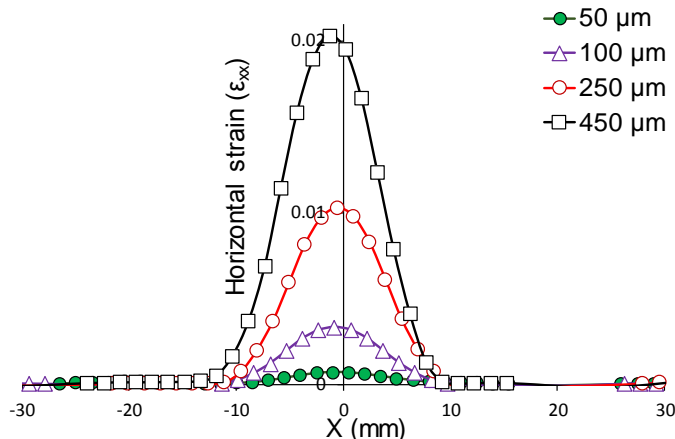
Figure 5. 9: Variation in the horizontal strain (ε_{xx}) with X coordinate for a line located at Y = 75 mm from the bottom of the beam at different values of relative CMOD after each unloading.

The 3D contours of horizontal displacement (U_x) obtained at the end of the last load cycle when the CMOD was increased to 450 µm is shown in Fig. 5.10a. The crack in the medium is identified by the displacement discontinuity emanating from the notch. The profile of the crack is identified by the sudden increase in the U_x over a small region. The discontinuity in U_x introduced by the crack emanating from the notch is evident in the jump in the U_x. For increasing CMOD, the physical opening produced by the crack originating from the notch resulted in a loss of correlation within a region corresponding to the subset size used for correlation overlapping with the opening. A procedure for obtaining the crack opening precisely, free from the error introduced by the finite subset size was developed using the asymptote matching procedure [95, 96]. The crack opening widths along the depth of the beam at different values of CMOD obtained using the asymptote matching

114

procedure and are shown in Fig. 5.10b for beam specimen 2. The CMOD corresponds to the displacement measured across the notch at Y=0, using the CMOD gauge located at the bottom of the beam. The CMOD is also shown marked in the figure at the location corresponding to Y=0. The crack opening widths were determined from the U_x measured using DIC. Corresponding to the CMOD value, the crack opening width exhibits a decreasing profile with increasing height above the notch (increasing Y coordinate). The zero crack opening along the depth of the beam indicates the physical location of the tip of the propagating crack. The observed crack opening as a function of depth for different values of CMOD indicates that the crack tip progresses along the depth of the beam with increasing CMOD. For a CMOD of 50µm, the crack has propagated along the depth and the tip of the crack can be identified at 86 mm from bottom of the beam and the corresponding crack opening at the mid-height location is 12µm. At a CMOD equal to 100µm relative to unloaded configuration at the end of the first load cycle (absolute CMOD equal to 124.7µm), the tip of the crack is located at Y= 119 mm and the crack opening at the mid-height location is 36µm. In the subsequent load cycles when the CMOD is increased to 250µm and 450µm relative to the unloaded CMOD from the previous cycles, the crack advances to a depth of 124 mm and 135 mm respectively. The corresponding crack openings at the mid-height are 102µm and 203µm, respectively.

(a)   (b)
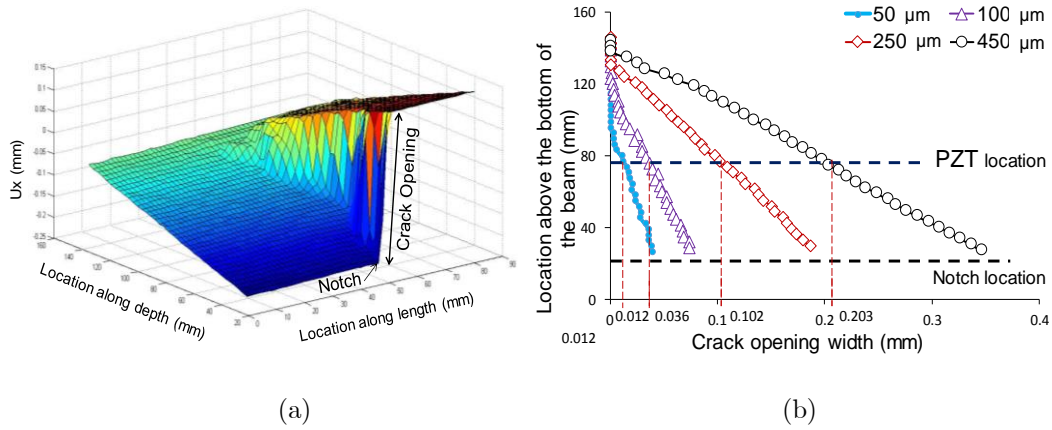
Figure 5. 10: (a) Contours of correlation coefficient at the relative value of CMOD = 450µm after the third cycle; (b) Crack opening width as a function of depth of the beam at different crack mouth opening displacements.

5.4.1 Measurements from PZT patches

The stress wave attenuation measurements were performed in the unloaded state, where the removal of the load results in closing of the crack. The measured changes recorded by the PZT patches therefore correspond to the physical discontinuity in the medium produced by the stress-induced crack. PZT patches were individually actuated with a 3-cycle tone burst sine signal with center frequency of 120 kHz and 45 V peak-to-peak voltage (Fig. 5.11b) and response of all the other PZT patches were taken when one PZT patch was actuated. This measurement procedure was repeated when the specimen was in the unloaded state after pre-determined crack opening indicated by different relative values of CMOD (50µm, 100µm, 250µm and 450µm). The level of noise obtained from the standard deviation of the initial part of the signal was on the order of 0.1 mV. All the received signals were conditioned with a linear phase, band-pass filter. A comparison of actual received signal and filtered received signal is shown in Fig. 5.11a. Fig. 5.11b shows a typical signal received by PZT2 using PZT1 as the actuator (A_1R_2) at the seating load, prior to initiation of the first cycle of loading. The received signal is significantly smaller in magnitude when compared with the excitation. The

116

decrease in the magnitude of the received signal is attributed to losses in the path of the wave produced by the geometric spreading of the wave and the material attenuation in the wave path in the epoxy and in the concrete. There is also a significant increase in the length of the received wave when compared with the excitation applied, which is due to several effects such as, the ringing of the PZT patch, geometric spreading and multiple reflections, mode conversions and from inhomogeneity of the beam specimen [48].
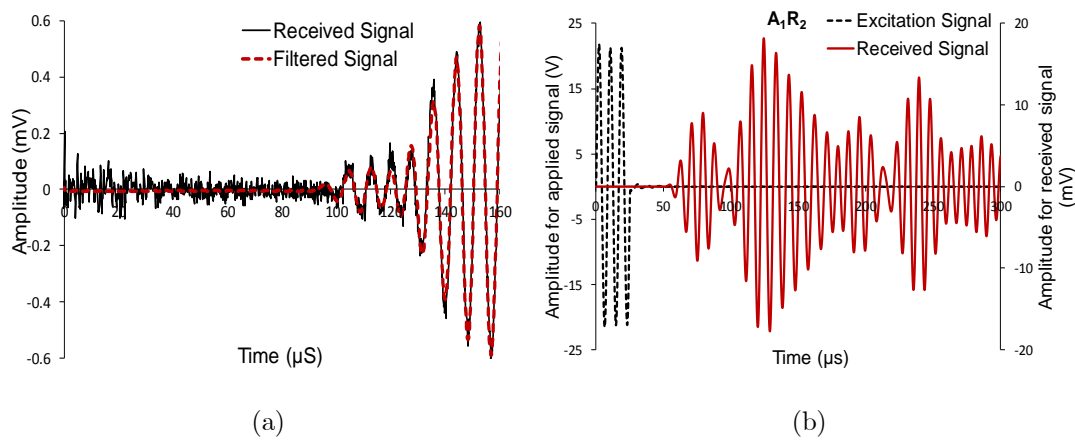
Figure 5. 11: (a) Comparison of actual received and filtered received signal (b) Comparison of actuating signal with sensor signal prior to loading.

Figure 5.12 shows the signals recorded from different PZT sensors (PZT2, PZT4, PZT6) when PZT1 was actuated. The received signals at PZT6 have a smaller amplitude when compared with the signals recorded by PZT2 and by PZT4 even in the pristine stage. The amplitude of the signal is influenced by the material and geometric attenuation in path of the transmission. Each subfigure in Fig. 5.12 shows the variation in the received signal in the unloaded state after each cycle. The changes recorded at the different PZT patches however vary depending on the positions of the PZT patches relative to the notch. With increasing CMOD, there was a decrease in the amplitude and an increase in the time of arrival of the stress waves received at PZT2 and PZT6 when compared with the corresponding baseline signatures. The changes in

117

the received waves are produced by the presence of the crack in the path of stress wave propagation. The received signals of PZT4 are not significantly altered since the wave path does not intersect the crack. The received signals at PZT4 exhibit a small change which may be attributed to stress wave reflection from the crack surface.

(a)

(b)

(c)
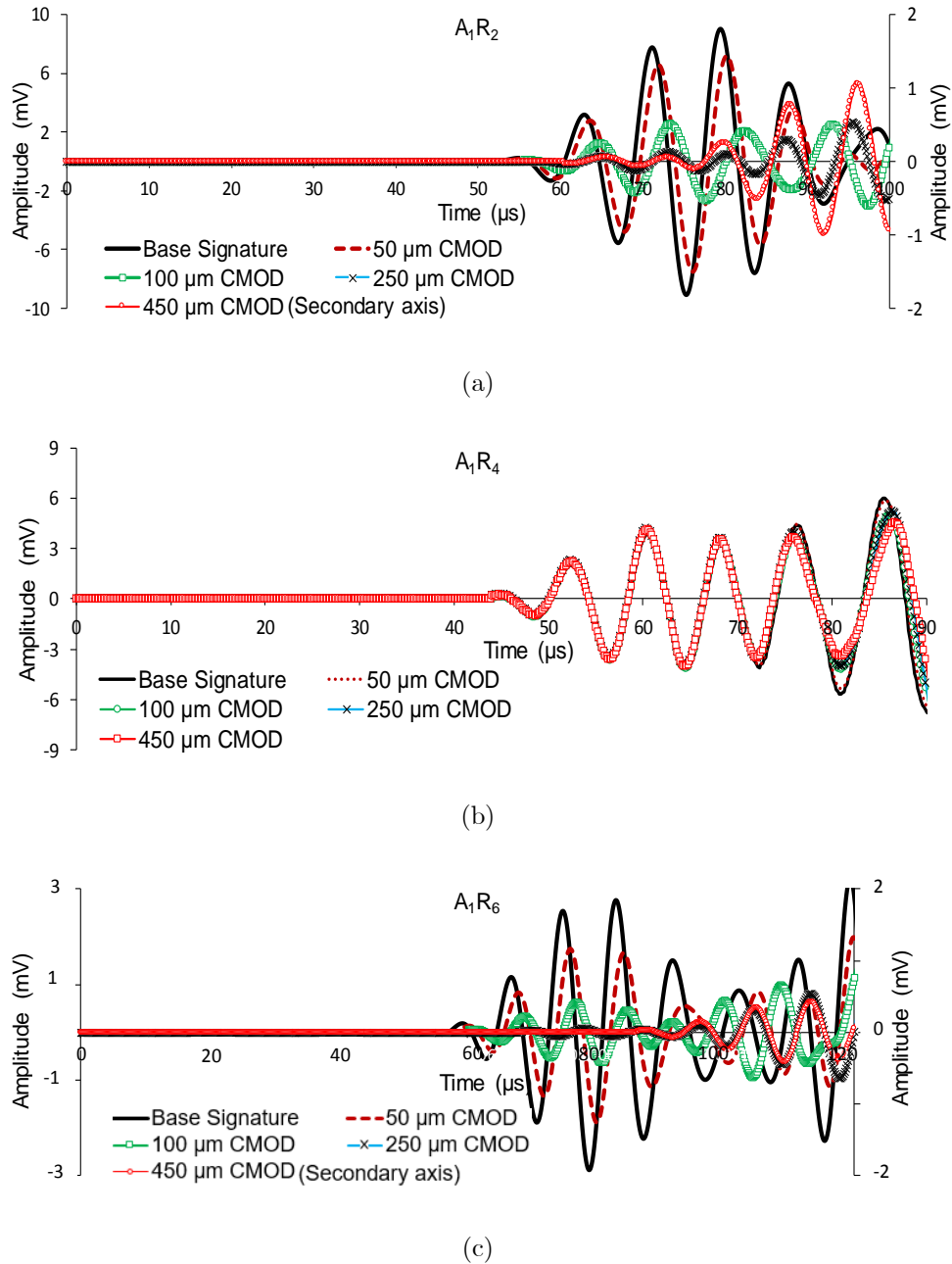
Figure 5. 12: Sensor signals when PZT1 is actuated and received at: (a) PZT2 (b) PZT4 (c) PZT6

118

When PZT1 is actuated, the stress wave signals received at the other PZT patches depend on the stress wave transmission path. Any changes in the received signal characteristics are produced by changes in the signal transmission path. When comparing the sensor signals after each load cycle with base line signature, the signals received at PZT 2 and PZT6 undergo changes in the time of arrival and the energy content. The contours of ε_{xx} shown in Fig. 5.9 also show that there was ε_{xx} concentration beyond the mid height of the beam in the A_1R_2 transmission path for all four CMOD levels. There is an increasing level of material discontinuity in the propagation path produced by the crack after each load cycle. Correspondingly, there is a larger decrease in the amplitude and a larger increase in the arrival time in the received signals. After the first load cycle, the crack was not visually apparent and was only detected from the displacement discontinuity recorded using DIC. From the crack opening width as a function of height shown in Fig. 5.10b, for a CMOD equal to 50 µm, the crack propagating depth was 86 mm from bottom of the beam and the crack opening displacement at the mid-height in the loaded configuration was 12µm. The crack propagated beyond the direct wave path of A_1R2 (actuating PZT1 and receiving PZT2) even at the CMOD equal to 50µm.

Typical electrical conductance spectra recorded from the six PZT patches bonded at different locations on the beam specimen 2 are shown in Fig. 5.13. Distinct resonance modes are clearly identified with peaks in the spectra. The relative locations and amplitudes of the peaks in the conductance spectra are relatively constant. The variations in the absolute values of amplitudes and the center frequencies of the individual peaks are due to variations in the properties of the individual PZT patches and the thickness of the epoxy used for bonding the PZT patch to the concrete substrate. The first and the second resonance peaks are centered on 120 kHz and 250 kHz, respectively. The peaks

of resonance have previously been shown to be sensitive to changes in substrate compliance within their respective zones of influence [Chapter 4]. The zones of influence for the first and the second resonant peaks for 1 mm thick, 20 mm square patches have been shown to be 100 mm and 75 mm, respectively. The local peaks on the first resonant peak are identified with the influence of the boundary of the specimen, which is within its zone of influence [Chapter 3]. The presence of distributed damage, which influences the mechanical impedance of the substrate in the zone of influence has been shown to produce changes in the amplitude and center frequency of the resonant peak.
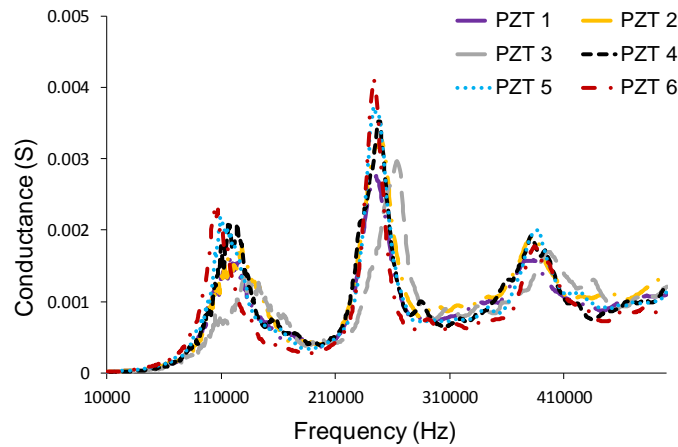
Figure 5. 13: Conductance spectra recorded from the PZT patches

The electrical admittance measurements were recorded from the PZT patches in the unloaded state. The electrical conductance spectra over frequencies centered on the first and second peaks for PZT2 and PZT5 (50mm away from notch) and PZT3 (180mm away from notch) are shown in Fig. 5.14. The electrical conductance obtained from the PZTs centered on the first resonant peak are shown in Fig. 5.14 a, b, c. A change is noticed in the EI response of all the PZTs. As the crack is located away from the zone of influence of first peak for PZT 3, the changes are minimal. For PZT 2 and PZT5, there are irregular changes identified in the local peaks due to the presence of the

material discontinuity within the zone of influence of the first peak of the PZTs.

The electrical conductance obtained from the PZTs centered on the second peak are shown in Fig. 5.14 d, e, f. There were no changes in the second peak of EI response of PZT 3 since the crack lies outside its zone of influence [Chapter 3]. There are small changes in conductance signatures centered on the second resonant peak for PZT2 and PZT5 at the different levels of CMOD as the crack passes through the zones of influence. The measurements from DIC indicated that the crack was very localized while the material away from the localized zone had no damage. Considering no visible distributed damage, the presence of localized damage within the zone of influence does not appear to significantly influence the mechanical impedance offered by the concrete medium to the motion of the PZT in the second resonant mode. The second resonant mode is therefore not sensitive to the presence of a localized material discontinuity produced by a stress-induced crack in concrete.
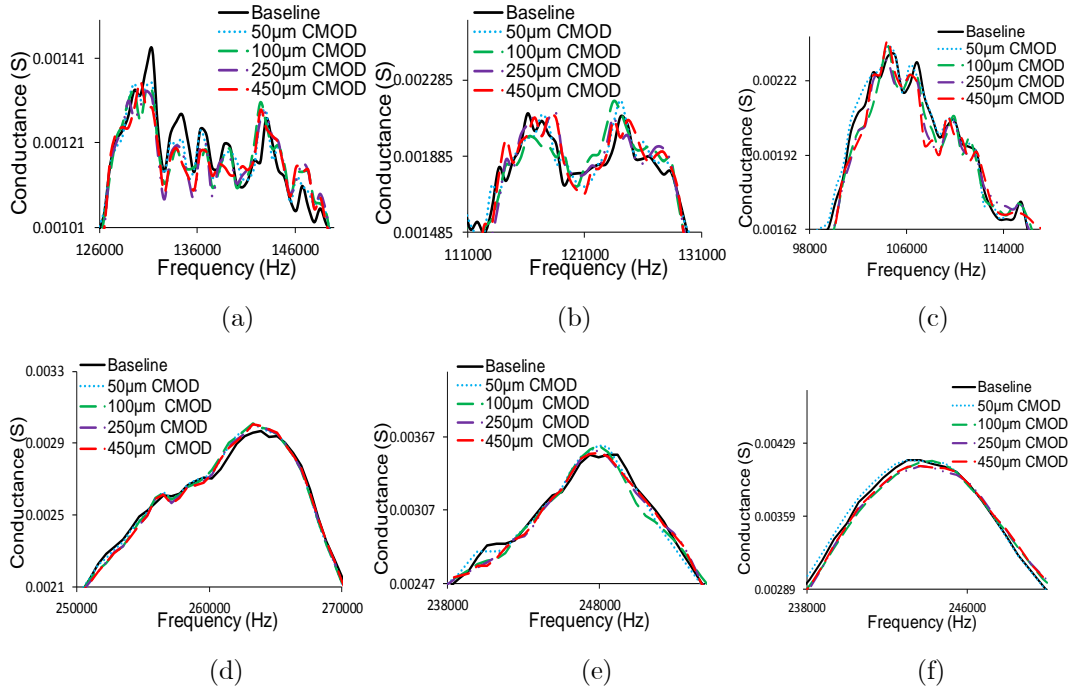
Figure 5. 14: Conductance spectra close to first peak at different CMOD levels of (a) PZT 3 (b) PZT 2 (c) PZT 5. Conductance spectra close to second peak at different CMOD levels of (d) PZT 3 (e) PZT 2 (f) PZT 5.

5.5   Analysis of Results

The experimental studies conducted on the beam at different levels of CMOD indicate that there is a consistent change in the recorded parameters induced by the localized crack. A quantification of the observed changes is performed to identify the changes in the wave characteristics and the EI measurements produced by the presence of the localized crack in the medium. In the AR measurements, the changes are observed in the time of flight of stress wave arrival and in the amplitude of stress wave. Percentage changes in the time of flight (TOF) and the attenuation factor (A(f)) were used to quantify the changes in the received signal. Changes in the conductance signature at the resonance peaks of the EI response were quantified using the root mean square deviation (RMSD).

The changes in propagation path of stress wave due to material discontinuity produce changes in the time of flight (TOF) of the received signal. The percentage (%) change in the time of light (TOF) at each levels of CMOD was calculated using equation 5.2, where $(TOF)_d$ is the TOF at different CMOD and $(TOF)_0$ is the TOF at zero CMOD. Time of flight of the signals were calculated using voltage thresholding technique where a threshold value (5 µV) was set for the signal and the time at which the received signal crosses threshold is taken as TOF. The threshold voltage was set based on maximum voltage of noise present in the signal.

$$\Delta TOF(\%) = \frac{[(TOF)_d - (TOF)_0]}{(TOF)_0} * 100 \qquad (5.2)$$

The percentage change in the time of flight (ΔTOF%) for the different AR pairs are plotted as a function of the different stress-induced crack opening at the mid-height of the beam in Fig. 5.15. The physical crack opening at the mid-height location of the beam determined using DIC are used for the plot. The values corresponding to reverse excitation of PZTs are avoided since there was no change in the TOF. After the first cycle of loading, for unloading from a CMOD equal to 50µm, there is a change in TOF in the received signals at the different PZTs. In the AR pairs, where the wave path did not intersect the crack registered no change in TOF. From the DIC measurements it was established that even at a CMOD equal to 50µm, the crack had propagated to a depth of 86mm above the notch. The physical opening at the mid-height was determined to be 12µm. In the subsequent load cycle when the relative value of CMOD was equal to 100µm, 250µm and 450µm there is a further increase in the TOF for in the AR pairs with signal path crossing the crack (A_6R_5, A_1R_3, A_3R_4. A_4R_6, A_3R_5 and A_1R_6).

Percentage change in TOF for transmission paths A_3R_2- A_2R_4- A_4R_1, which connect PZTs located at mid-height, are plotted for the different stress-induced crack opening in the stress wave path in Fig. 5.15b. There is no change

on the TOF measured in the signal path A_3R_2, A_4R_1. In the path A_2R_4 there is consistent increase in TOF with an increase in the stress induced crack opening. The stress induced crack in concrete produces a material discontinuity in the material, which is associated with a physical opening under applied loading. The discrete crack present in the concrete is also very localized and does not produce any additional strain or damage in the bulk of the medium. Changes in the time of flight of the received signal are therefore attributed to the changes in propagation path produced by the crack. The percentage (%) change in the time of light (TOF) therefore provides a reliable parameter for detecting changes in the transmission of the stress wave due to the discontinuity in the material medium produced by a localized crack in concrete.

(a)   (b)
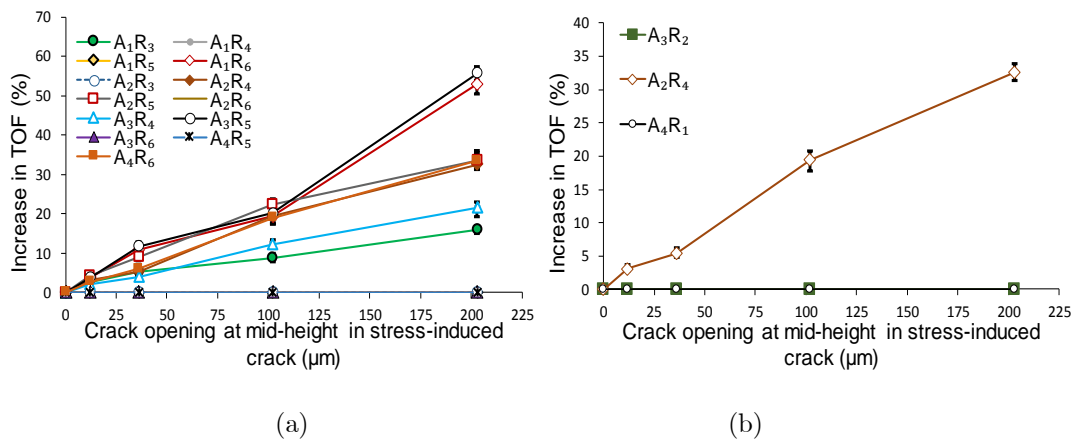
Figure 5. 15: (a) Percentage Change in TOF at different CMOD values. (b) TOF for transmission paths A_3R_2, A_2R_4 and A_4R_1

A comparison between the actuated signal and the received signal prior to initiation of loading indicates that there is significant attenuation in the path of wave. When one PZT pair is used in the AR mode it is of interest to determine the additional attenuation produced by the material damage. The influence of attenuation produced by the materials, concrete and epoxy, have

to be separated to determine the effect of a crack in the wave path. In the case of array of sensors, the changes in the received signals due to the propagation of crack are nonlinear in nature and the degree of non-linearity varies in between the PZTs depending on the distance between actuator and sensor, depth and width of crack. In an array of sensors where comparison among different transmission paths are necessary to identify the location and the severity of the crack, a new damage index known as Attenuation factor $(A(f))$ was introduced in the analysis which can self-compensate all the intervening effects such as properties of PZTs, amplitude of the resonance frequencies of PZTs, epoxy concrete interface losses and length of propagation path by normalizing them in frequency domain. The signal processing in the AR mode consisted of determining the attenuation factor, $A(f)$. Attenuation factor $(A(f))$ was calculated by using the conversion of non-reflected time domain signal obtained from sensor to the corresponding frequency domain. The initial 26 µs (length of actuating signal) signal starting from time of flight of the received signal was taken as the non-reflected signal as shown in the Fig. 5.16a. The typical FFT of non-reflected time domain signal with the corresponding half power bandwidth was shown in Fig. 5.16b.

The sensor signal in the time domain can be expressed as,

$$r_s = a_s * l_{ea} * l_{sp} * l_{es} \tag{5.3}$$

where r_s is the received signal, a_s is the actuating signal, l_{ea}, l_{es} are the signal losses due to epoxy at concrete-beam interfaces for actuator and sensor, l_{sp} is the loss due to signal path, and '$*$' is the convolution operator.

Since the computation of $A(f)$ is performed in the frequency domain, the sensor signal at zero CMOD $(r_s(f)_0)$ and at different CMOD levels $(r_s(f)_d)$ can be expressed as,

$$r_s(f)_0 = a_s(f).l_{ea}(f).l_{sp}(f).l_{es}(f) \tag{5.4}$$

$$r_s(f)_d = a_s(f).l_{ea}(f).l_{sp}(f).l_{es}(f).L_d(f) \tag{5.5}$$

where $L_d(f)$ is signal loss due to crack. $L_d(f)$ is calculated from equation 5.4 and 5.5 as,

$$L_d(f) = \left(\frac{r_s(f)_d}{r_s(f)_0}\right)_{f_1, f_2} \tag{5.6}$$

$$A(f) = Avg.\left(L_d(f)\right)_{f_1, f_2} \tag{5.7}$$

$r_s(f)_0$, $r_s(f)_d$ are the magnitude of FFT corresponding to a frequency in the bandwidth of the of the received non-reflected time domain signals (26 µs) FFT peak which is ranging from f_1 to f_2 (Fig. 5.16b). $A(f)$ is calculated as the average of $L_d(f)$.
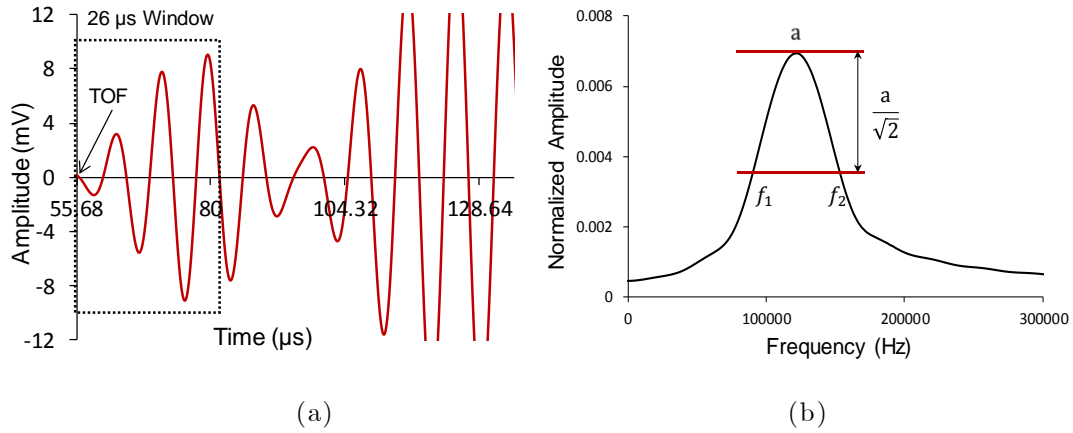
Figure 5. 16: (a) Non-reflected signal (26 µs) (b) FFT of the received non-reflected time domain signal (26 µs)

Attenuation factor $(A(f))$ is calculated for all the received signals using equation 7 and is shown in Fig. 5.17a. There is a considerable decrease in the $A(f)$ for the transmission paths which encounters the crack, even at the stress-induced physical opening of 12µm at the mid-height of the beam. The decrease in the attenuation factor values were high for signals received from PZTs placed at the soffit of the beam when compared with values of the signals received at the PZTs place at the center of the beam. This is can be explained considering the crack opening in the direct stress wave propagation between an AR pair. The crack width opening along the depth of a specimen at different

126

values of CMOD is shown in Fig. 5.10b. The signals received at the PZTs placed at the soffit of the beam experienced a higher attenuation because of a larger physical discontinuity in the direct path connecting the actuator to the receiver. There is a complete attenuation of direct stress wave when the physical discontinuity reaches a value of 200µm. This indicates that when the physical separation between the crack faces is on the order of 0.2mm, there is no direct transmission of direct stress waves centered on 120 kHz. There is no change in the attenuation factor even at very large crack openings for the transmission paths which do not encounter crack.

The changes in $A(f)$ are only due to the changes in characteristics of discrete crack such as depth and width of crack, irrespective of length of signal transmission path. The changes in attenuation factor corresponding to the transmission paths which encounter a physical opening produced by a stress-induced crack and pass through center line of beam (actuator and receiver located in the mid height of the beam) are shown in Fig. 5.17b. For the PZTs mounted at the mid-height, the stress wave paths linking the AR pair which cross the crack plane the $A(f)$ is identical. It can therefore be concluded that the observed $A(f)$ in these cases is only due to the magnitude of the physical discontinuity produced by the crack. The similarity in the trends of changes in attenuation factor irrespective of length of signal transmission path also suggests that the attenuation factor only depends on the severity of crack irrespective of all other intervening effects. The $A(f)$, therefore provides an effective way to analyze the received signals to detect changes introduced by material discontinuity in the stress wave path. The opening displacement produced by a stress induced crack creates a physical discontinuity in the material medium. The $A(f)$ is sensitive to a physical discontinuity in the concrete medium even in the unloaded state associated with a stress induced crack opening on the order of 10µm. The physical discontinuity in the concrete

associated with a stress-induced crack opening on the order of 200μm produces a complete attenuation of the stress wave.
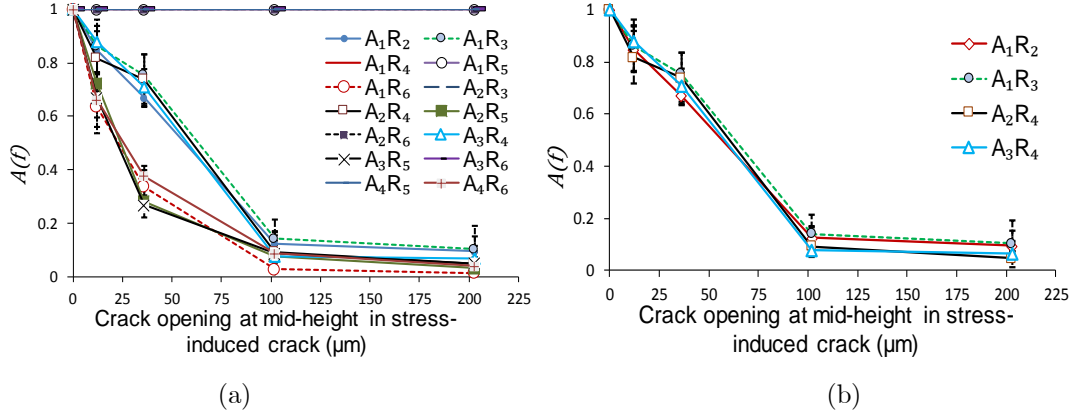
Figure 5. 17: (a) Attenuation factor ($A(f)$) at different CMOD values (b) $A(f)$ at different transmission paths

A damage index derived from the RMSD is used to calculate the difference between the conductance signatures recorded for different crack openings. The RMSD with respect to the baseline measurement (zero CMOD) were calculated in the frequency range of the bandwidth for first and second resonant peaks using equation 5.8, where, x_i and y_i are the values of baseline conductance and conductance at different CMOD levels and N is total number of frequencies in the bandwidth of the corresponding peak.

$$\text{RMSD} = \sqrt{\frac{\sum_{i=1}^{N}(y_i - x_i)^2}{\sum_{i=1}^{N}(x_i)^2}} \qquad (5.8)$$

Damage index based on RMSD for PZTs of different positions is shown in Fig. 5.18a. The damage index was calculated using the frequency range of the bandwidth for second resonant peak. PZT3, which located 180 mm from the crack location registered a small change in the RMSD with increasing crack opening. PZT2 and PZT5, which are bonded on the face and the soffit, respectively at the distances of 50 mm from the beam centerline show an increase in the RMSD with increasing CMOD. Fig. 5.18b shows the RMSD

calculated using first resonance peak in the frequency range of bandwidth. PZT3 is showing same RMSD trend as for second peak. There is a larger increase in value for RMSD at all CMOD values for PZT2 and PZT5 when comparing with RMSD of the second peak. The scatter in the RMSD values may be attributed to the irregular trend in the local peaks present on first resonance peak of the PZT.
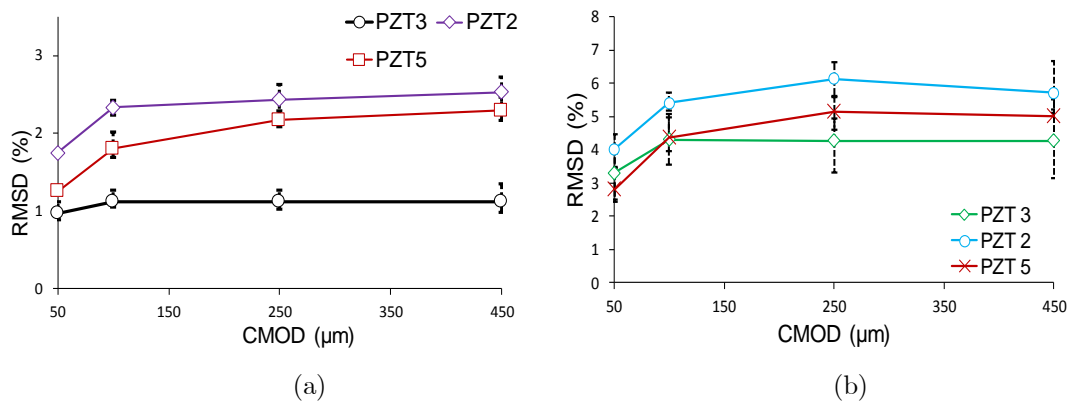
Figure 5. 18: RMSD (%) (a) second resonance peak (b) First resonance peak

The measured RMSD detects changes in the first cycle while the changes in the subsequent load cycles are not significant. The measurements indicate changes in the material medium within the zone of influence produced by the discontinuity introduced by the crack. The discontinuity in the unloaded state represents the physical separation introduced in the material due to the stress-induced crack opening. The RMSD values indicate that the EI measurement is very sensitive in detecting the discontinuity more than the magnitude of the discontinuity. EI measurement would therefore provide a very sensitive measure of crack initiation in concrete.

5.6   Summary and Findings

A combined local and distributed monitoring system for concrete structures using an array of surface mounted PZT patches is presented. EI measurements from individual PZT patches are used for local monitoring while the through-

transmission stress wave propagation technique is used for distributed sensing. Progression of discrete crack in concrete was evaluated using a full-field displacements measured on the surface of the beam obtained with the use digital image correlation and was correlated with measurements obtained from the PZT patches. The crack opening is mapped from a very small value on the order to 10µm to 200µm. The material away from the localized discontinuity produced by the crack is shown to relatively free from any damage.

Both the EI and the stress-wave propagation techniques are shown to be influenced by discontinuity in the concrete substrate produced by a stress-induced crack. The impedance measure is not very sensitive to localized damage in the form of a load induced crack. The very localized material discontinuity does not affect the mechanical driving point impedance experienced by the PZT. A new damage index known as attenuation factor is introduced for the wave propagation technique. The attenuation factor is shown to be an effective damage index for detecting the severity of discontinuity produced by a crack. The attenuation factor is shown to determine attenuation of the wave produced by the discontinuity encountered by the direct stress wave, independent of the length of propagation. The attenuation measurements were performed in the unloaded state, where the removal of the load results in closing of the crack. The through transmission of direct stress wave through the medium is very sensitive to the presence of a discontinuity left in the medium resulting from a stress-induced crack in its path. There is an attenuation of the wave even for a physical discontinuity in the concrete in the stress free state associated with a small stress-induced crack opening on the order of 10µm. There is a complete attenuation of the direct stress wave transmission at 120 kHz for physical discontinuity in the concrete associated with a stress-induced crack opening on the order of 200µm.

The measurements from the PZT patches indicate that the localized discontinuity in concrete produced by a stress induced crack is easily detected using the attenuation factor from the direct stress wave transmission path. The stress-induced crack has considerable crack closing stresses provided by aggregates bridging the crack. The discontinuity in the unloaded state represents the physical separation introduced in the material due to the stress-induced crack opening. The cracks which would have propagated due to overloads, but are closed due to removal of the loads can therefore be easily be detected using attenuation factor measurements. This provides a very convenient measure for monitoring increment of damage due in the material. Further, crack opening on the order of 200µm under service loads is often stipulated for durable design. The attenuation factor from distributed sensing provides for monitoring discontinuity in the material medium even in the unloaded state, when the crack is not visually detectable. The creating of the discontinuity would also be reflected in the EI signature if the discontinuity lies within its zone of influence. Service load condition of the concrete structure can therefore be monitored conveniently using combined EI and AR modes of an array of PZT patches.

Chapter 6

Conclusions and Future Work

A systematic approach is developed for local and distributed health monitoring for concrete structures using an array of surface mounted PZT patches. A combined damage monitoring approach where the Electrical Impedance measurement from individual PZT patches are used for local monitoring while the through-transmission stress wave propagation technique is used for distributed sensing is presented. The main contributions of this work are: (a) A methodology for assessing the zone of influence of surface mounted PZTs in Electro Mechanical response of a PZT patch obtained using the EI measurement is developed; (b) A theoretical frame work is developed to decouple the effect of stress and damage from the EI response of the bonded PZT; (c) Development of a procedure for accurately monitoring physical discontinuity on the order of 10 μm using stress-wave propagation; (d) Development of an integrated methodology for monitoring concrete structures using an array of PZT sensors for local and distributed sensing.

6.1   Key findings and conclusions

Coupled Electromechanical Response of a PZT Patch Bonded to Concrete

A study on the influence of the material properties and substrate size on the Electrical Impedance response of a PZT patch bonded to concrete is conducted. The electrical measurement obtained from the coupled dynamic electromechanical (EM) response of the PZT patch bonded to a concrete

substrate is derived using an approach which combines experimentation with numerical simulations. A fundamental understanding of the electrical conductance spectrum is obtained and the resonant behaviour in the dynamic electromechanical response of the PZT patch is established. The resonant modes in the dynamic electromechanical response of the bonded PZT patch exhibit a dependence on the size of the substrate. The resonant peaks in the dynamic response of the structure are superimposed on the resonant response of the PZT. For each resonant mode of the bonded PZT patch, a finite zone of influence where there is an influence of the boundary on the resonant behaviour of the bonded PZT patch, is identified. The zone of influence is larger for lower frequency modes and smaller for high frequency modes. If the size of the substrate is larger than the zone of influence at a given frequency of measurement, the dynamic response of the PZT patch would depend only on the material properties of the concrete medium.

Effect of substrate stress and damage on EI response of coupled PZT

The effect of substrate stress and damage on the coupled response of the bonded PZT was evaluated using tests conducted on concrete specimens under loading-unloading conditions. Damage in concrete is associated with a decrease in the mechanical impedance of the substrate. Increasing damage is shown to produce decrease in the mechanical impedance and an associated increase in the material damping. Both effects result in a decrease in the magnitude and the frequency of the resonant peak of the PZT in the electrical conductance spectrum of the bonded PZT. Imposed strain resulting from stress in the substrate produces changes in the resonant peak which are counteracting to the influence of damage. At low levels of damage, the counteracting effects of stress and damage do not show any significant changes in coupled resonance frequency of the bonded PZT. The centroidal shifts of the normalized electrical conductance spectrum of a bonded PZT allows to decouple the effect of

imposed strain on PZT and change in compliance of the substrate due to damage induced changes in the electrical conductance spectrum of bonded PZT patch.

PZT sensor array for continuous monitoring of concrete structures

A combined local and distributed monitoring system for concrete structures using an array of surface mounted PZT patches is investigated. The EI measurements from individual PZT patches are used for local monitoring while the through-transmission stress wave propagation technique is used for distributed sensing. The electrical impedance measure was found to be not very sensitive to localized damage in the form of a load induced crack since the material away from the localized material discontinuity is not effected. The mechanical driving point impedance experienced by the PZT is not significantly influenced by a localized tension crack in the medium. A frequency domain based damage index known as attenuation factor which is independent of wave transmission paths is developed to interpret the stress wave data collected from different actuator and receiver pairs of PZT. The attenuation factor is shown to be an effective damage index for detecting the severity of the discontinuity produced by a crack. The physical discontinuity produced in the material due to a stress-induced crack of 10μm on unloading is sensitively detected.

6.2   Future Work

The findings presented in previous section sets the basis for future work on developing theoretical and experimental methodology for effective health monitoring system for concrete structures. The directions of future work which arise from this work are listed below.

1. A relation between the elastic constants and level of damage of the substrate for surface mounted PZT can be established using the concept of zone of influence developed here.

134

2. The non-linear part of the transmitted stress waves has to be further analyzed to infer more details about damage in concrete structures.

3. The methodology developed here can be extended to investigate the effect of embedded PZT sensors for stress and damage monitoring in concrete structures.

4. Studying the environmental effects on the coupled EI response for implementing the presented monitoring methodology to real structures.

5. Changing the baseline based damage index to baseline free damage index method for quantifying damage.

References

[1] IEEE Standard on Piezoelectricity. ANSI/IEEE, Std. 176-1987.

[2] J. Sirohi, and I. Chopra. Fundamental understanding of piezoelectric strain sensors. Journal of intelligent material systems and structures 11, (2000) 246-257.

[3] C. Liang, F. P. Sun, and C. A. Rogers. An impedance method for dynamic analysis of active material systems. Journal of Vibration and Acoustics 116, (1994) 120-128.

[4] S.W. Zhou, C. Liang, and C. A. Rogers. An impedance-based system modeling approach for induced strain actuator-driven structures. Journal of Vibration and Acoustics 118, (1996) 323-331.

[5] V. Giurgiutiu and C. A. Rogers. Modeling of the electro-mechanical (E/M) impedance response of a damaged composite beam. Adaptive Structures and Material Systems Symposium 87, (1999) 39-46.

[6] Y. G. Xu, and G. R. Liu. A modified electro-mechanical impedance model of piezoelectric actuator-sensors for debonding detection of composite patches. Journal of Intelligent Material Systems and Structures 13, (2002) 389-396.

[7] S. Bhalla and C. K. Soh. Structural health monitoring by piezo-impedance transducers. I: Modeling. Journal of Aerospace Engineering 17, (2004) 154-165.

[8] S. Bhalla and C. K. Soh. Structural health monitoring by piezo–impedance transducers. II: applications. Journal of Aerospace Engineering 17, (2004) 166-175.

[9] Y. Yang, J. Xu, and C.K Soh. Generic impedance-based model for structure-piezoceramic interacting system. Journal of Aerospace Engineering 18, (2005) 93-101.

[10] V. G. M. Annamdas, and C.K Soh. Three-dimensional electromechanical impedance model for multiple piezoceramic transducers—structure interaction. Journal of Aerospace Engineering 21, (2008) 35-44.

[11] S. Bhalla, P. Kumar, A. Gupta, and T. K. Datta. Simplified impedance model for adhesively bonded piezo-impedance transducers. Journal of Aerospace Engineering 22, (2009) 373-382.

[12] H. Song, H. J. Lim, and H. Sohn. Electromechanical impedance measurement from large structures using a dual piezoelectric transducer. Journal of Sound and Vibration 332, (2013) 6580-6595.

[13] D. Wang, H. Song, and H. Zhu. Numerical and experimental studies on damage detection of a concrete beam based on PZT admittances and correlation coefficient. Construction and Building Materials 49, (2013) 564-574.

[14] D. Wang, H. Song, and H. Zhu. Embedded 3D electromechanical impedance model for strength monitoring of concrete using a PZT transducer. Smart Materials and Structures 23, (2014) 115019.

[15] X. Zhu, and F. L. Scalea. Sensitivity to axial stress of electro-mechanical impedance measurements. Experimental Mechanics 56, (2016) 1599-1610.

[16] J.W. Ayres, F. Lalande, Z. Chaudhry, and C. A. Rogers. Qualitative impedance-based health monitoring of civil infrastructures. Smart Materials and Structures 7, (1998) 599.

[17] V. Giurgiutiu, A. Reynolds, and C. A. Rogers. Experimental investigation of E/M impedance health monitoring for spot-welded

structural joints. Journal of Intelligent Material Systems and Structures 10, (1999) 802-812.

[18] G. Park, H. H. Cudney, and D.J. Inman. Impedance-based health monitoring of civil structural components. Journal of infrastructure systems 6, (2000) 153-160.

[19] C. K. Soh, K. KH. Tseng, S. Bhalla, and A. Gupta. Performance of smart piezoceramic patches in health monitoring of a RC bridge. Smart materials and Structures 9, (2000) 533.

[20] C-W. Ong, Y. Yang, A. S. K. Naidu, Y. Lu, and C. K. Soh. Application of the electro-mechanical impedance method for the identification of in-situ stress in structures. In Smart Structures, Devices, and Systems 4935, (2002) 503-515.

[21] K. KH. Tseng, and A. S. K. Naidu. Non-parametric damage detection and characterization using smart piezoceramic material. Smart Materials and Structures 11, (2002) 317.

[22] S. Bhalla, and C. K Soh. Structural impedance based damage diagnosis by piezo-transducers. Earthquake Engineering & Structural Dynamics 32, (2003) 1897-1916.

[23] K. K. Tseng, and L. S. Wang. Smart piezoelectric transducers for in situ health monitoring of concrete. Smart Materials and Structures 13, (2004) 1017.

[24] C. K. Soh, and S. Bhalla. Calibration of piezo-impedance transducers for strength prediction and damage assessment of concrete. Smart materials and structures 14, (2005) 671.

[25] S. Park, S. Ahmad, CB. Yun, and Y. Roh. Multiple crack detection of concrete structures using impedance-based structural health monitoring techniques. Experimental Mechanics 46, (2006) 609-618.

[26] Y. Y. Lim, S. Bhalla, and C. K. Soh. Structural identification and damage diagnosis using self-sensing piezo-impedance transducers. Smart Materials and Structures 15, (2006) 987.

[27] V. G. M. Annamdas, Y. Yang, and C. K Soh. Influence of loading on the electromechanical admittance of piezoceramic transducers. Smart Materials and Structures 16, (2007) 1888.

[28] B. S. Divsholi and Y. Yang. Application of PZT sensors for detection of damage severity and location in concrete. In Smart Structures, Devices, and Systems IV 7268, (2008) 726813.

[29] D. Wang, H. Zhu, D. Shen, and D. Ge. Health monitoring of reinforced concrete structures based on PZT admittance signal. In Second International Conference on Smart Materials and Nanotechnology in Engineering 7493, (2009) 74931H.

[30] D. Xu, X. Cheng, S. Huang, and M. Jiang. Identifying technology for structural damage based on the impedance analysis of piezoelectric sensor. Construction and Building Materials 24, (2010) 2522-2527.

[31] S. Park, JW. Kim, C. Lee, and SK. Park. Impedance-based wireless debonding condition monitoring of CFRP laminated concrete structures. NDT & E International 44, (2011) 232-238.

[32] Y. Y. Lim and C. K. Soh. Effect of varying axial load under fixed boundary condition on admittance signatures of electromechanical impedance technique. Journal of Intelligent Material Systems and Structures 23, (2012) 815-826.

[33] D. Wang, H. Song, and H. Zhu. Numerical and experimental studies on damage detection of a concrete beam based on PZT admittances and correlation coefficient. Construction and Building Materials 49, (2013) 564-574.

[34] E.L.M. Ribolla, P. Rizzo, and V. Gulizzi. On the use of the electromechanical impedance technique for the assessment of dental implant stability: Modeling and experimentation. Journal of Intelligent Material Systems and Structures 26, (2015) 2266-2280.

[35] V. G. M. Annamdas, Y. Chew, J. H. L. Pang, H. J. Hoh, K. Zhou, and B. Song. Fatigue growth analysis of pre induced surface defects using piezoelectric wafer based impedance method and digital image correlation system. Journal of Nondestructive Evaluation 33, (2014) 413-426.

[36] P. Negi, T. Chakraborty, and S. Bhalla. Damage monitoring of dry and saturated rocks using piezo transducers. Journal of Testing and Evaluation 45, (2016) 169-181.

[37] D. Ai, H. Luo, C. Wang, and H. Zhu. Monitoring of the load-induced RC beam structural tension/compression stress and damage using piezoelectric transducers. Engineering Structures 154, (2018) 38-51.

[38] W. Suaris and V. Fernando. Ultrasonic pulse attenuation as a measure of damage growth during cyclic loading of concrete. ACI Materials Journal 84, (1987) 185-193.

[39] Y. Berthaud. Damage measurements in concrete via an ultrasonic technique. Part I experiment. Cement and concrete research 21, (1991) 73-82.

[40] S. F. Selleck, E. N. Landis, M. L. Peterson, S. P. Shah, and J. D. Achenbach. Ultrasonic investigation of concrete with distributed damage. ACI Materials Journal 95, (1998) 27-36.

[41] N. M. Akhras. Detecting freezing and thawing damage in concrete using signal energy. Cement and concrete research 28, (1998) 1275-1280.

[42] W. Yeih and R. Huang. Detection of the corrosion damage in reinforced concrete members by ultrasonic testing. Cement and concrete research 28, (1998) 1071-1083.

[43] C. L. Nogueira and K. J. Willam. Ultrasonic testing of damage in concrete under uniaxial compression. Materials Journal 98, (2001) 265-275.

[44] Yc. Jung, T. Kundu and M. R. Ehsani. A New Nondestructive Inspection Technique for Reinforced Concrete Beams. ACI Materials Journal 99, (2002).

[45] JF. Chaix, V. Garnier and G. Corneloup. Concrete damage evolution analysis by backscattered ultrasonic waves. NDT & E International 36, (2003) 461-469.

[46] K. Warnemuende and HC. Wu. Actively modulated acoustic nondestructive evaluation of concrete. Cement and Concrete Research 34, (2004) 563-570.

[47] J. D. Stauffer, C. B. Woodward and K. R. White. Nonlinear ultrasonic testing with resonant and pulse velocity parameters for early damage in concrete. ACI materials journal 102, (2005) 118.

[48] D. G. Aggelis and T. Shiotani. Repair evaluation of concrete cracks using surface and through-transmission wave measurements. Cement and Concrete Composites 29, (2007) 700-711.

[49] M. Sun, W. J. Staszewski, R. N. Swamy and Z. Li. Application of low-profile piezoceramic transducers for health monitoring of concrete structures. NDT & E International 41, (2008) 589-595.

[50] T. Shiotani and D. G. Aggelis. Wave propagation in cementitious material containing artificial distributed damage. Materials and Structures 42, (2009) 377-384.

[51] P. Antonaci, C. L. E. Bruno, A. S. Gliozzi and Marco Scalerandi. Monitoring evolution of compressive damage in concrete with linear and nonlinear ultrasonic methods. Cement and Concrete Research 40, (2010) 1106-1113.

[52] J. Zhu and L. He. Study on piezoelectric wave propagation based nondestructive monitoring method of concrete. International Conference on Electric Technology and Civil Engineering (ICETCE) IEEE (2011) 764-767.

[53] Y. Lu, J. Li, L. Ye and D. Wang. Guided waves for damage detection in rebar-reinforced concrete beams. Construction and Building Materials 47, (2013) 370-378.

[54] M. Rucka and K. Wilde. Experimental study on ultrasonic monitoring of splitting failure in reinforced concrete. Journal of Nondestructive Evaluation 32, (2013) 372-383.

[55] F. Moradi-Marani, P. Rivard, CP. Lamarche and S. A. Kodjo. Evaluating the damage in reinforced concrete slabs under bending test with the energy of ultrasonic waves. Construction and Building Materials 73, (2014) 663-673.

[56] B. S. Divsholi and Y. Yang. Combined embedded and surface-bonded piezoelectric transducers for monitoring of concrete structures. NDT & E International 65, (2014) 28-34.

[57] J. Chen, J. Ren and T. Yin. Nondestructive evaluation of notched cracks in mortars by nonlinear ultrasonic technique. Nondestructive Testing and Evaluation 31, (2016) 109-121.

[58] P. Fröjd and P. Ulriksen. Amplitude and phase measurements of continuous diffuse fields for structural health monitoring of concrete structures. NDT & E International 77, (2016) 35-41.

[59] T. Ju, J. D. Achenbach, L. J. Jacobs, M. Guimaraes and J Qu. Ultrasonic nondestructive evaluation of alkali–silica reaction damage in concrete prism samples. Materials and Structures 50, (2017) 60.

[60] Y. Yang, Y. Hu and Y. Lu. Sensitivity of PZT impedance sensors for damage detection of concrete structures. Sensors 8, (2008) 327-346.

[61] X. Hu, H. Zhu and D. Wang. A study of concrete slab damage detection based on the electromechanical impedance method. Sensors 14, (2014) 19897-19909.

[62] D. Xu, S. Banerjee, Y. Wang, S. Huang and X. Cheng. Temperature and loading effects of embedded smart piezoelectric sensor for health monitoring of concrete structures. Construction and Building Materials 76, (2015) 187-193.

[63] Y. Liang, D. Li, S. M. Parvasi, Q. Kong and G. Song. Bond-slip detection of concrete-encased composite structure using electro-mechanical impedance technique. Smart Materials and Structures 25, (2016) 095003.

[64] Y.Y Lim, K. Z. Kwong, W. Y. H. Liew and C. K. Soh. Non-destructive concrete strength evaluation using smart piezoelectric transducer—A comparative study. Smart Materials and Structures 25, (2016) 085021.

[65] P. Liu, W. Wang, Y. Chen, X. Feng and L. Miao. Concrete damage diagnosis using electromechanical impedance technique. Construction and Building Materials 136, (2017) 450-455.

[66] A. N. Zagrai and V. Giurgiutiu. Electro-mechanical impedance method for crack detection in thin plates. Journal of Intelligent Material Systems and Structures 12, (2001) 709-718.

[67] V. Giurgiutiu, A. N. Zagrai and J. Bao. Damage identification in aging aircraft structures with piezoelectric wafer active sensors. Journal of Intelligent Material Systems and Structures 15, (2004) 673-687.

[68] Y. Yang and Y. Hu. Electromechanical impedance modeling of PZT transducers for health monitoring of cylindrical shell structures. Smart materials and structures 17, (2007) 015005.

[69] M. Gresil, L. Yu, V. Giurgiutiu and M. Sutton. Predictive modeling of electromechanical impedance spectroscopy for composite materials. Structural Health Monitoring 11, (2012) 671-683.

[70] Y. Y. Lim and C. K. Soh. Towards more accurate numerical modeling of impedance based high frequency harmonic vibration. Smart Materials and Structures 23, (2014) 035017.

[71] T. Kamas, V. Giurgiutiu and B. Lin. Thickness mode EMIS of constrained proof-mass piezoelectric wafer active sensors. Smart Materials and Structures 24, (2015) 115035.

[72] M. Rebillat, M. Guskov, E. Balmes and N. Mechbal. Simultaneous influence of static load and temperature on the electromechanical signature of piezoelectric elements bonded to composite aeronautic structures. Journal of Vibration and Acoustics 138, (2016) 064504.

[73] V. G. M. Annamdas and M. A. Radhika. Electromechanical impedance of piezoelectric transducers for monitoring metallic and non-metallic structures: A review of wired, wireless and energy-harvesting methods. Journal of Intelligent Material Systems and Structures 24, (2013) 1021-1042.

[74] COMSOL 4.3b. Structural Mechanics Module User's Guide, 2013.

[75] S. E. Stein. An integrated method for spectrum extraction and compound identification from gas chromatography/mass spectrometry data. Journal of the American Society for Mass Spectrometry 10, (1999) 770-781.

[76] Origin 8 User Guide, First edition, (2007).

[77] V. Giurgiutiu and A. N. Zagrai. Characterization of piezoelectric wafer active sensors. Journal of Intelligent Material Systems and Structures 11, (2000) 959-976.

[78] S. Moharana and S. Bhalla. Numerical investigations of shear lag effect on PZT-structure interaction: review and application. Current Science, (2012) 685-696.

[79] G. Park and D. J. Inman. Structural health monitoring using piezoelectric impedance measurements. Philosophical Transactions of the Royal Society of London A: Mathematical, Physical and Engineering Sciences 365, (2007) 373-392.

[80] S. P. Shah and S. Chandra. Critical stress, volume change, and microcracking of concrete. ACI Journal Proceedings 65, (1968) 770-780.

[81] V. S. Gopalaratnam and S. P. Shah. Softening response of plain concrete in direct tension. ACI Journal Proceedings 82, (1985) 310-323.

[82] Y.Y. Lim and C. K. Soh. Damage detection and characterization using EMI technique under varying axial load. Smart Structures and Systems 11, (2013) 349-364.

[83] T. J. Saravanan, K. Balamonica, C. B. Priya, A. L. Reddy and N. Gopalakrishnan. Comparative performance of various smart aggregates during strength gain and damage states of concrete. Smart Materials and Structures 24, (2015) 085016.

[84] VIC-2D^{TM} Reference manual. Correlated Solutions (2009).

[85] H. A. Bruck, S. R. McNeill, M. Ae Sutton and W. H. Peters. Digital image correlation using Newton-Raphson method of partial differential correction. Experimental mechanics 29, (1989) 261-267.

[86] H. W. Schreier, and M. A. Sutton. Systematic errors in digital image correlation due to undermatched subset shape functions. Experimental Mechanics 42, (2002) 303-310.

[87] F. Song, G. L. Huang, J. H. Kim and S. Haran. On the study of surface wave propagation in concrete structures using a piezoelectric actuator/sensor system. Smart materials and Structures 17, (2008) 055024.

[88] D.D.S Rabelo, J.D. Hobeck, D. J. Inman, R. M. F. Neto and V. Steffen Jr. Real-time structural health monitoring of fatigue crack on aluminum beam using an impedance-based portable device. Journal of Intelligent Material Systems and Structures 28, (2017) 3152-3162.

[89] T. Watanabe, H. T. H. Trang, K. Harada and C. Hashimoto. Evaluation of corrosion-induced crack and rebar corrosion by ultrasonic testing. Construction and Building Materials 67, (2014) 197-201.

[90] S-H. Kee and B. Nam. Automated surface wave measurements for evaluating the depth of surface-breaking cracks in concrete. International Journal of Concrete Structures and Materials 9, (2015) 307-321.

[91] M. Luo, W. Li, C. Hei and G. Song. Concrete infill monitoring in concrete-filled FRP tubes using a PZT-based ultrasonic time-of-flight method. Sensors 16, (2016) 2083.

[92] B. Xu, H. Chen and S. Xia. Numerical study on the mechanism of active interfacial debonding detection for rectangular CFSTs based on wavelet packet analysis with piezoceramics. Mechanical Systems and Signal Processing 86, (2017) 108-121.

[93] V. Memmolo, L. Maio, N. D. Boffa, E. Monaco and F. Ricci. Damage detection tomography based on guided waves in composite structures using a distributed sensor network. Optical Engineering 55, (2015) 011007.

[94] V. Giurgiutiu. Structural Health Monitoring with Piezoelectric Active Sensors. Academic Press, Oxford, UK, 2001.

[95] K. C. Reddy and K. V. L. Subramaniam. Analysis for multi-linear stress-crack opening cohesive relationship: Application to macro-synthetic fiber reinforced concrete. Engineering Fracture Mechanics 169, (2017) 128-145.

[96] S. Gali and K. V. L. Subramaniam. Multi-linear stress-crack separation relationship for steel fiber reinforced concrete: Analytical framework and experimental evaluation. Theoretical and Applied Fracture Mechanics 93, (2018) 33-43.

[97] UNI 11039-2. Steel Fibre Reinforced Concrete - Test Method for Determination of First Crack Strength and Ductility Indexes. National Italian Unification centre Italy. (2003).

List of Publications

Journal Papers

1. Narayanan, A., and Subramaniam, K V L., (2016), "Experimental evaluation of load-induced damage in concrete from distributed microcracks to localized cracking on electro-mechanical impedance response of bonded PZT", *Construction and Building Materials*, Vol.105, pp. 536-544.

2. Narayanan, A., and Subramaniam, K V L., (2016), "Sensing of damage and substrate stress in concrete using electro-mechanical impedance measurements of bonded PZT patches", *Smart Materials and Structures*, Vol. 25, No. 9, p.095011

3. Narayanan, A., Kocherla, A., and Subramaniam, K. V. (2017). Embedded PZT Sensor for Monitoring Mechanical Impedance of Hydrating Cementitious Materials. *Journal of Nondestructive Evaluation*, Vol.36, No. 4, p.64.

4. Narayanan, A., Kocherla, A., and Subramaniam, K V L., (2018), "Understanding the Coupled Electromechanical response of a PZT Patch bonded to Concrete: Influence of Substrate size", Measurement, Vol. 124, pp. 505-514

5. Narayanan, A., Subramaniam, K V L., (2017). "Damage assessment in concrete structures using piezoelectric based sensors", *Revista ALCONPAT*, Vol. 7, No.1, pp. 25-35.

6. Narayanan, A., Kocherla, A., and Subramaniam, K V L., (2018), "PZT Sensor Array for Local and Distributed Measurements of Localized Cracking in Concrete". *Smart Materials and Structures*, Vol. 27, No.7, p.075049

Conference Papers

1. Narayanan, A., and Subramaniam, K V L., (2016), "Early age monitoring of cement mortar using embedded piezoelectric sensors", Proc. *SPIE* 9805, Health Monitoring of Structural and Biological Systems 2016, 98052W (April 1, 2016); doi:10.1117/12.2219655.

2. Kocherla, A., Narayanan, A., and Subramaniam, K V L., (2017), "Monitoring progressive changes in cementitious materials using embedded piezo-sensors", Proc. *SPIE* 10170, Health Monitoring of Structural and Biological Systems; 101702I (2017); doi: 10.1117/12.2259842

3. Narayanan, A., Kocherla, A., and Subramaniam, K V L., (2017), "Development of an Embedded PZT Sensor for Monitoring Mechanical Impedance of a Cementitious Material through Setting and Early Strength Gain", Proceedings of *RILEM* Annual Week; Vol.118, pp. 497-505.

4. Narayanan, A., and Subramaniam, K V L., (2015), "Damage Assessment in Concrete Structures using PZT patches", *RN Raikar Memorial Intl. Conference, Mumbai, India*